Directed Evolution of Stabilized Peptides with Bacterial Display

Tejas A. Navaratna

A dissertation submitted in partial fulfillment
of the requirements for the degree of
Doctor of Philosophy
(Chemical Engineering)
in the University of Michigan
2020

Doctoral Committee:

Associate Professor Greg Thurber, Chair
Professor James Bardwell
Professor Erdogan Gulari
Associate Professor Xiaoxia Nina Lin
Associate Professor Fei Wen

Tejas Navaratna

tejasn@umich.edu

ORCID iD: 0000-0003-2976-0137

Acknowledgments

I deeply thank Professor Greg Thurber for his guidance, trust, and support in me. I cannot count the number of times I came into his office unsure of future research paths and came away inspired and eager to probe new directions. He gave me the opportunity and freedom to explore my ideas, while also being an excellent mentor and advisor in this journey. I also thank my other committee members, Professors Jim Bardwell, Erdogan Gulari, Nina Lin, and Fei Wen for their support and productive discussions. I also would like to thank Professor Jim Van Deventer, Professor Cathy Fromen, Professor Kevin Solomon, and Dr. Marco Jost for helpful career advice.

I would also like to acknowledge Andrew Min and Liz Goulston, two undergraduate students I have had the pleasure of mentoring. Working with them led me to realize my passion for mentorship. Other Thurber Lab members that I closely worked with are Lydia Atangcho, Liang Zhang, Marshall Case, and Mukesh Mahajan – I am deeply grateful for your advice and support. Finally, I would also like to thank Sumit Bhatnagar, Cornelius Cilliers, Bruna Menezes, Eshita Khera, Ian Nessler, Reggie Evans, Anna Kopp, Celia Dong, Haolong Huang, and Yinuo Chen for fostering a social, friendly, and wonderfully collaborative lab environment, even through the COVID-19 shutdown– I couldn't have asked for better labmates.

I am thankful for the generous support of the National Science Foundation and National Institutes of Health.

I feel extremely lucky to have such great friends, both new connections made in Ann Arbor and old ones from Cambridge and San Jose. From rock climbing cliffs in Kentucky to scaling mountains in Washington, to virtual get togethers in these trying times, I will cherish these connections and memories for decades to come. You made me laugh when I needed it and I cannot thank you enough for your support.

Finally, I am grateful to mom and dad and my sister for their support leading up to this point, and I could not have done it without you all. You encouraged me from childhood to pursue my curiosity – and this has led me to this point.

Table of Contents

List of Figures

List of Tables

List of Appendices

Abstract

Interactions between proteins govern cellular and the body's states, including aberrant interactions found in diseases such as in cancers and infections. Small molecule drugs are not ideal in targeting these interactions as their size generally prevents efficient blocking of contacts over large surface areas. Antibodies and related biologics have seen clinical success in the past few decades and can block large surfaces but are typically limited to extracellular targets. Intermediate-size peptides have the potential to bridge this gap, with the ability to target large surface areas inside the cell. Peptide stapling, by chemically linking two or more amino acid residues, can confer affinity improvements, resistance to degradation, and better biological transport properties. As such, stapled peptides show promise as next-generation therapeutics. Unfortunately, existing methods to screen sequence and stapling locations suffer from numerous disadvantages including limited search space, lack of real-time monitoring of selections, and difficulty in incorporating the non-canonical amino acids used for amino acid stapling.

In this dissertation, I describe my research on stapled peptide discovery with bacterial incorporation of non-canonical amino acids. To screen stapled peptides of the type desired, we incorporated azidohomoalanine (AHA) into surface displayed peptides, enabling an in situ 'click' chemistry reaction to bridge two turns of an alpha helical (i, i+7) amino acid library for directed evolution. Using the p53-MDM2 interaction as a model target, we developed peptides that block MDM2 degradation of the tumor suppressor

protein p53, an interaction that is dysregulated in a sizeable fraction of cancers. We generated and displayed a stapled peptide library on the bacterial cell surface with fixed residues for stabilization and binding requirements, while randomizing the remaining amino acids. After multiple rounds of selection, clones were sequenced and characterized. The dissociation constants of the peptide-MDM2 interaction were measured on both the bacterial cell surface by flow cytometry and in solution by bio-layer interferometry. The highest affinity variant, named SPD-M6-V1 with sequence VCDFXCYWNDLXGY (dissociation constant = 1.8 nM; X = azidohomoalanine) was selected for structural characterization by NMR spectroscopy, revealing a bicyclic disulfide and double click-constrained peptide. Sequencing showed that peptides with two cysteines were highly enriched, further suggesting that the MDM2-binding conformation was enforced with a disulfide bond. In addition, SPD-M6-V1 was the most protease-resistant peptide from the library that we tested.

Next, we stapled the displayed peptide library with chemically distinct linkers and screened each library separately. We performed deep sequencing to better understand the relationship between amino acid sequence and linker identity in contributing to high affinity MDM2 binding. We found that both linker-specific and linker-agnostic (i.e. MDM2-specific) mutations were enhanced. Finally, we developed a dual-channel, sequential labeling selection strategy to discriminate between high-display, low-affinity peptides and low-display, high-affinity peptides, two categories that would ordinarily overlap in a typical one-color screen in the absence of an independent display marker. In summary, this thesis develops the chemical tools to screen libraries of stabilized peptides on the

bacterial cell surface and applies these techniques to select stabilized alpha helices that disrupt the p53-MDM2 interaction.

Chapter I: Introduction and Background

Abstract

Proteins are the workhorses of the cell, and in the course of carrying out their functions, will generally interact with one or more of the same or different proteins. The variety in the twenty naturally occurring amino acids endows proteins with diverse structures, leading to a massive range of functions ranging from biological signal transduction, chemical transformations, and genetic material manipulation (and these non-exhaustive categories often overlap). Because of their role in nearly all cellular activities, protein-protein interactions are viewed as attractive drug targets as the blocking or enhancing of these can in theory result in therapeutic effects for a range of different diseases, such as Spike1-ACE2 in viral entry and p53-MDM2 and Her2/Her family in cancers, among others. In practice however, even after decades of developing small molecule drugs, protein-protein interactions remain elusive drug targets. Binding interfaces between proteins often lack deep pockets, precluding targeting by traditional small molecules whereas large proteins, such as antibodies, suffer from poor intracellular uptake due to their size. In between these two categories, stabilized alpha helical peptides can enter cells but can also disrupt large protein-protein interfaces. Additionally, over the past two decades, researchers have developed ways to incorporate additional chemical functionality into proteins by incorporating noncanonical amino acids (NCAAs). These additional reactivities can be used bio-orthogonally to site-specifically modify NCAA-incorporated

peptides for stabilization. Displaying these peptides on the surface of bacteria offers a potent strategy for evolving stapled peptides against a variety of interactions, including the p53-MDM2 interaction which we focus on in this dissertation.

Stapled Peptides

The majority of interfaces between interacting proteins include an alpha helix, the most common protein secondary structure motif[1]. An alpha helix consists of a right-handed spiral of amino acids maintained by backbone hydrogen bonding interactions and outward-facing side chains. Such interfaces have posed attractive drug targets due to their importance in virtually all diseases, in which inhibition, by blocking interactions, or activation, by triggering function, can result in therapeutic effects[2]. However, due to the large size of protein-protein interaction surface areas, small molecules have seen little success in drug development to target protein-protein interactions[3]. Small molecules are better suited towards targeting catalytic sites or deep (generally hydrophobic) pockets, whereas protein-protein interfaces are generally characterized by shallow grooves and many intermolecular interactions.

Despite these difficulties, the past two decades have yielded some success with small molecule inhibitors of PPI with more than 40 PPIs having been targeted with small molecules[4]; however, only two molecules have seen FDA approval (the integrin binder tirofiban[4] and the BCL-2 binder Venotoclax[5]). These developments have led to an understanding that binding to the full surface area of a PPI is not typically necessary and targeting an important hotspot of a few amino acids is sufficient. Approaches like

fragment-based discovery have been developed to target PPIs by screening a small library of diverse molecules smaller than 300 Da for any affinity at all (typically 0.1 – 10 mM). These initial hits are improved by introducing functional groups to yield more potent inhibitors[6]. However, most small molecules that have entered clinical testing still only target smaller interfaces (250 – 900 $Å^2$) in which the biological interaction involves amino acid sidechain interaction with a deep pocket. These include so-called inhibitors of apoptosis proteins (IAPs), several of which mimic the caspase-activating domain tetrapeptide motif of Smac (Ala-Val-Pro-Ile) and have shown single-digit nM potency[7]. Venetoclax (developed as ABT-199), a BH3 mimic that binds to BCL2, has been approved by the FDA for chronic lymphocytic leukemia (CLL)[5]. The previous iteration of this drug, navitoclax (ABT-263) caused dose-limiting thrombocytopenia in patients due to BCL-xL engagement, and developing of ABT-199 required rational structure-enabled design to bias binding against BCL-xL (K_d < 0.01 nM for BCL-2, 48 nM for BCL-xL)[8]. Venetoclax so far is the only example of an alpha-helix-in-groove small molecule mimic that has received FDA approval. While there have been several examples of deep pocket PPI inhibition (e.g. the integrin antagonists tirofiban and lifitegrast), interactions involving secondary and tertiary structures have been more recalcitrant to small molecule inhibition due to their large surface area[9].

Antibodies and antibody-based molecules have seen great success in today's oncology and autoimmune disease drug landscape in binding to proteins to alter function. They can be developed against virtually any protein target with high specificity and affinity but their use in the laboratory is restricted to extracellular proteins or intracellular proteins

inside permeabilized cells[10]. Clinical use has been limited to extracellular targets like Her2, integrins, EGFR, interleukins, and immune checkpoint proteins as these very large biomolecules are unable to cross plasma membranes without significant modifications. Antibody-drug conjugates (ADCs), which consist of potent, small molecule drugs attached to antibodies, rely on the antibody portion for binding and internalization[11] and have seen recent success in the clinic for both liquid and solid tumors[12]. Once internalized, the small molecule payload can cross endosomal or lysosomal membranes to engage with their targets, typically microtubules or DNA, to achieve tumor cell killing. Usage of ADCs is restricted to tumors containing extracellular target-expressing cells. Approaches to directly target cytoplasmic proteins with antibodies involve attachment of cell-penetrating peptides[13] or DNA transfection[14], both which have limited clinical utility at this point. A potent, G12D mutation-specific (K_d = 6 nM) inhibitor of the KRAS-BRAF interaction was developed, but as this was based on a Sso7d protein scaffold (7 KDa), transfection was required for cellular activity[14].

Smaller peptides, of the length of 10 to 30 amino acids, are more capable of entering cells and inhibiting protein-protein interactions[15]. A given candidate peptide, when unmodified, will generally show poorly defined secondary structure and thus exhibit weak binding to its target. Binding to a protein interface requires the peptide to adopt a particular configuration, which can contribute to an entropic penalty, as the need for pre-organization reduces the number of possible states. This entropic penalty is often accompanied by a kinetic enthalpic penalty as well, as a disordered peptide in solution contains a large number of water-side chain and water-backbone hydrogen bonds, which

need to be broken in order to adopt the binding configuration[16]. The formation of intramolecular and peptide-protein hydrogen bonds and other intermolecular bonds can reduce the thermodynamic enthalpic cost of desolvation, but kinetic effects can dominate formation of the complex in vivo. Indeed, simulations by Bairy and Wong showed that for targeting the extracellular receptor EGFR, a faster on-rate drug was more efficacious than a slower off-rate drug at the same K_d[17]. In contrast, lower off-rates will increase target engagement time, which is important for slower signaling complexes[18]. Thus, optimization of both on and off rates is dependent on the signaling kinetics of the target, location, and safety considerations. When the peptide is unbound, it can undergo loss of effectiveness, such as through protease degradation and pharmacokinetic clearance, and therefore tuning kinetic rates for maximum efficacy and safety profiles is important.

Within the last decade or so, the field of chemical biology has developed stapled peptides between 10 and 40 amino acids in length that contain a covalent link between two side chains (Figure I - 1).

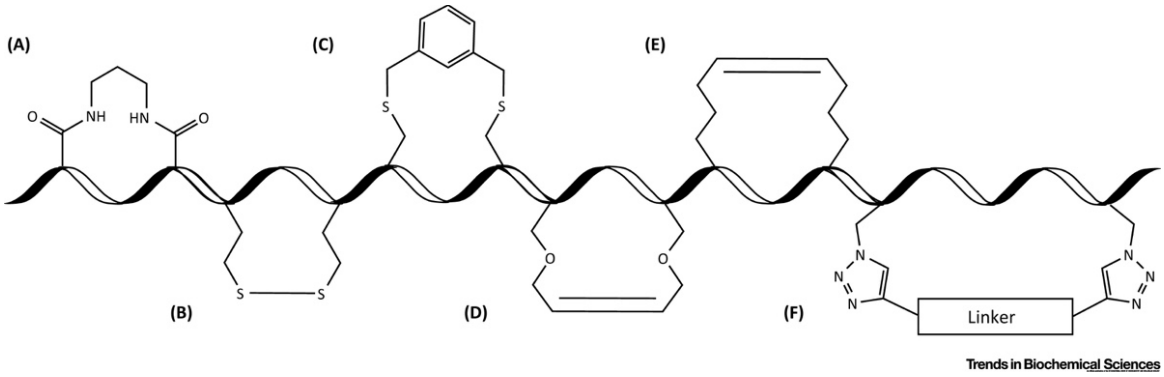

Figure I - 1. Common chemistries used in peptide stapling approaches.
A) amide bond formation between a bis-amine linker and two acidic side chains. B) disulfide bond C) thiol bridging with a bis-alkylating linker D) ring-closing metathesis of two O-allylserine residues E) ring-closing metathesis of two all-hydrocarbon side chains F) double-click stapling between a bis-alkyne linker and two azido side chains. Figure adapted from Atangcho et al. (2018)[16].

Stapled peptides have demonstrated greatly improved stability in the presence of proteases and higher binding affinities, enabling longer circulation times and considerable therapeutic potential. They have been developed for a range of protein targets, including KRAS[19], the transcription factor NOTCH[20], the plasma protease kallikrein[21], and MDM2[22]. In the last case, the stapled peptide inhibitor ALRN-6924 is in clinical trials[23] at the time of this writing.

Despite all the progress in the field, intracellular entry continues to be challenging and is the rate-limiting step for peptide efficacy. The sub-nanomolar binding affinity (K_d) of the related ALRN-related ATSP-7041[2] molecule can be contrasted with the much higher hundreds-of-nanomolar cellular toxicity[24] (K_i), which may indicate a significant barrier to entry for this molecule. Along with direct confirmation that stapled peptides exhibit sequence- and staple-dependent uptake[25,26], the discrepancy between potent K_d values and modest cellular efficacy have motivated major efforts to understand and

improve uptake. Early cell culture efficacy studies with hydrocarbon-stapled peptides involved the use of serum-free media[27], and it is now appreciated that serum can interfere with cellular entry and efficacy in a sequence and staple-specific manner[2,25]. Bird et al. developed a medium-throughput microscopy assay to test a few dozen point mutants and staple locations of a BIM-mimic helix for cellular entry. They found that the presence of too many hydrophobic and cationic residues in a stapled peptide led to off-target toxicity due to membrane disruption, and that staple placement and helicity were key to cellular uptake[25]. Microscopy, however, has its drawbacks, as it is often difficult to differentiate among endosomal, membrane-bound, and cytoplasmic localized peptide[28]. Hydrophilic molecules generally lack the ability to cross the lipophilic core of cell membranes, and rapid endocytosis and endosomal/lysosomal residualization can resemble cytoplasmic signal especially in low-resolution imaging. The HaloTag-based chloroalkane penetration assay (CAPA) involves treating HaloTag-transfected cells with a chloroalkane-derivatized molecule of interest[26]. A covalent bond is formed between the HaloTag protein and chloroalkane-tagged molecule and this can be assayed with a chase with a dye-chloroalkane and quantified by microscopy or flow cytometry. When HaloTag is localized to the cytoplasm via a mitochondria-outer membrane anchoring peptide, CAPA measures cytoplasmic access. Nuclear and other localization sequences can be employed to measure molecule entry to various compartments[26]. In order to engage intracellular targets, the majority of which are cytoplasmic, the stapled peptide must cross the cellular membrane. CAPA, cytoplasmic fluorescence-correlation spectroscopy[28], and cellular thermal shift assays[29] can be used to measure peptide entry into the cytoplasm.

Double-click stabilized peptides (Figure I - 1) were developed to expand the peptide stapling repertoire[30] and has permitted modular, bifunctional strategies to not only improve stability through covalent cross-linking but also other properties using chemically diverse linkers[31], such as ones containing polyarginine motifs to improve cell permeability[32] and fluorophore-conjugated ones for imaging applications[33]. Unlike cysteine bridging or lysine/carboxylic acid lactamization, double-click chemistry through incorporation of azide or alkyne bearing residues is bio-orthogonal: side-reactions with other residues on the same peptide do not readily occur, and in the case of peptide stabilization on the protein and other macromolecule-dense bacterial outer membrane[34], interference is less likely. As discussed below, azide-containing amino acids can be readily incorporated into induced proteins in E. coli, unlike the olefin-bearing amino acids used in all hydrocarbon stapling. Antibody fragments have been successfully displayed and reacted on the surface of E. coli with noncanonical amino acids[35], exhibiting fast kinetics amenable for a directed evolution approach. The necessity of Cu(I) catalysis in standard azide-alkyne cycloaddition results in high levels of toxicity in bacteria[36], and regrowth of bacteria following screening can be challenging[37]. The strain-promoted Cu-free methodology[38] has the potential to be much less toxic, but requires a bulky cyclooctyne reaction partner. The dearth of reports of successful protein-protein inhibitors using a strain-promoted reaction (one good example has been reported by Lau et al[39]) led us to focus on the Cu(I) catalyzed reaction in this dissertation.

Noncanonical amino acid incorporation

Solid phase peptide synthesis (SPPS), which involves the stepwise C- to N-terminal conjugation of amino acids, has long been used to incorporate noncanonical amino acids[40] (NCAAs). The length of peptides amenable to SPPS is typically limited to 50 amino acids, as small yield losses per step compound to result in large losses and low efficiencies. Native chemical ligation has been used to connect two peptides in vitro, potentially extending the range of SPPS to hundreds of amino acids[41], but this can also be low-yielding and results in a cysteine residue at the junction, which many proteins cannot tolerate. Furthermore, many applications of NCAAs require ribosomal translation, such as for intracellular activity, directed evolution screens, and metabolism studies[35,42,43]. Thus, there has been a multi-decade effort to expand the protein code outside the 20 ribosomally-incorporated canonical amino acids to facilitate non-native intermolecular interactions, reactivity, and structure.

Selenomethionine (SeMet), a naturally occurring amino acid typically incorporated into proteins at methionine codons (AUG), has been used in quantitative replacement of methionine residues in recombinant proteins[44,45], aiding in x-ray crystallographic applications and reportedly improving crystal diffraction resolution[46]. Incorporation of SeMet is typically accomplished in a methionine-auxotrophic strain of E. coli in minimal media containing SeMet[44] and induced proteins purified similarly to the unmodified protein. More recent developments in NCAA applications involve the incorporation of azide-containing amino acids for translational labeling in a cell- and species- specific

manner to analyze protein expression by reaction, selective pull-down, and mass spectrometry[47].

Ribosomal NCAA incorporation efforts can be broadly categorized into two approaches: 1. Codon replacement or reassignment and 2. The NCAA as a canonical amino acid surrogate. In the codon replacement strategy, amber suppression, in which the amber stop codon (UAG) on mRNA is translated to incorporate a NCAA in the ribosome is the most commonly used approach. UAG is the most rare stop codon in E. coli, being used in only 7% of genes and only 2-3% of essential genes[48], making global reassignment of UAG codons feasible without severe growth impairment[48]. For desired "mistranslation" by the endogenous ribosome, the cell must have a cognate AUC tRNA and corresponding tRNA synthetase reactive with the NCAA. An exogenous tRNA/aminoacyl tRNA synthetase pair (tRNA-aaRS) has to be artificially evolved to be both highly efficient and have low cross-reactivity with undesired amino acids[49]. The Schultz group has developed several such tRNA/aaRS pairs using parts from the archaea M. jannaschii with directed evolution for specificity and reactivity[50]. In this scheme, a randomized library of aaRS mutants go through both positive and negative sorts to ensure that the aaRS acylates the cognate tRNA with the NCAA but does not acylate the tRNA with endogenous amino acids. This approach has been used to introduce a wide range of functionalities into proteins, including fluorescence[51], glycosylation[52], and reactive azide groups for directed evolution in phages[53].

In the surrogate-replacement strategy, similar to SeMet incorporation, other NCAAs can be introduced into ribosomally synthesized proteins in auxotrophic bacteria.

A methionine-replacement strategy was used to incorporate azidohomoalanine (AHA) in methionine auxotrophic E. coli by Link, Tirrell, and coworkers[54] (Figure I - 2). Other met-replacement NCAAs include azidoalanine, azidonorvaline, and azidonorleucine[54], with AHA having by far the highest efficiency with >95% incorporation at AUG codons[55]. Directed evolution and mutation of methionyl-tRNA synthetases and aaRS overexpression can be used to improve protein yields and incorporation efficiency, especially of more recalcitrant amino acids like azidonorleucine[56,57] and the NMR-active trifluoronorleucine[58]. Design and evolution of phenyl and tyrosyl synthetases have been carried out for the incorporation of aryl amino acids[59], and these various mutant synthetases represent a versatile toolkit for the incorporation of NCAAs into proteins.

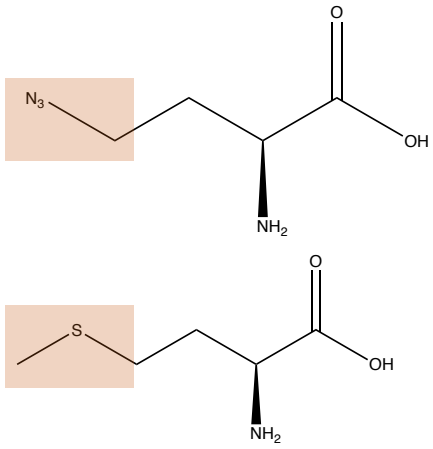

Figure I - 2. Structures of azidohomoalanine (AHA), and methionine (met), top and bottom respectively showing structural similarity. In met auxotrophic E. coli, AHA can be incorporated at high efficiency at AUG codons by endogenous met tRNA synthetase.

Directed evolution and bacterial surface display

Adaptation to environments, including inter- and intra-species competition, has led to the diversity of all life on earth[60]. Evolutionary forces have been observed and harnessed in

the lab, both in organisms to evolve novel metabolic pathways[61] and in the round-bottom flask to yield powerful new enzymes[62]. In the past few decades, random mutagenesis paired with x-ray and NMR structural data have been powerful tools for engineering proteins with improved and novel activities[63]. A homology modeling approach, followed by multiple rounds of computational docking, evolution, and testing led to the engineering of a transaminase for industrial production of sitagliptin at Codexis and Merck[64].

Display techniques have greatly advanced the development of therapeutics and research proteins, especially antibodies and antibody derivatives, with combinatorial library screening enabled by diverse display methods coupling genetic information to phenotype, allowing rapid selection of favorable DNA sequences. Surface display techniques have been used successfully for the development of very high affinity antibodies, ScFvs evolved against whole cells, epitope mapping[65] or for immune presentation of antigens for vaccination[66]. This has been recently recognized by the Nobel Prize in Chemistry in 2018 awarded partially for phage display, in which proteins are fused to bacteriophages capable of infecting E. coli. This permits various selection schemes, such as biopanning. In this, phage particles, containing displaying diverse and randomized protein sequences fused to phage coat proteins, are passed over a surface that is functionalized with the target, usually another protein[65], but can also be inorganic materials[67]. Unbound or weakly bound phages are washed away, and bound phages are re-screened and eventually used to infect E. coli or directly sequenced[68].

In yeast and bacterial systems, surface display broadly involves cloning a randomized sequence as a fusion to an outer membrane-localizing display scaffold,

typically Aga2 in yeast[69], or an outer membrane protein in bacteria[70]. The randomized sequence can be generated by a variety of methods, commonly error-prone PCR for larger proteins and DNA assembly using randomized primers for shorter peptides. In the yeast Aga2 system and in bacteria outer membrane fusions, induction causes localization of the random library to the cell exterior, where derivatized target protein is added[71,72]. Cell surface techniques have several advantages over phage-based display as the cells' larger size allows for fluorescence-activated cell sorting (FACS) for excellent control over sorting parameters like sorted numbers and stringency.

Selection takes place by enrichment for cells bound to target protein, identified by fluorescence if the derivatization is a fluorophore, and carried out using FACS. For larger library sizes, where FACS is intractable, bead-based sorting methods can be carried out for a preliminary round of sorting, using streptavidin coated beads and a biotinylated target[71]. After several rounds of selection, tightly binding clones are sequenced, and consensus sequences identified. Further affinity maturation is often carried out involving random mutagenesis of specific residues to sample sequences not present in the original library[73]. This is beneficial, as even for libraries of small peptides of length 12 amino acids, the theoretical diversity is greater than 10^{15}, which cannot be achieved in phage, bacterial or yeast display systems. Whereas yeast surface display is very flexible in the type of protein to be displayed, in that the Aga2 system can display small peptides as well as large mammalian proteins[72], using a bacterial display system has advantages that make it preferable for the stabilized peptide display presented in this dissertation. As discussed in the preceding section, NCAA incorporation into E. coli proteins is facile[54]. The higher

transformation efficiency in E. coli enables library sizes approaching 10^{11} members, whereas yeast methods are limited to around 10^7 sequences [71]. The cellular nature of bacteria enables quantitative, real-time sorting by flow (i.e., FACS), unlike phage systems, which use panning. Cytometry allows for cell-based methods to rapidly quantify and compare the binding affinities of many clones without resorting to time-consuming solid-phase peptide synthesis, enabling initial affinity characterization of many more clones than phage or bead-based methods.

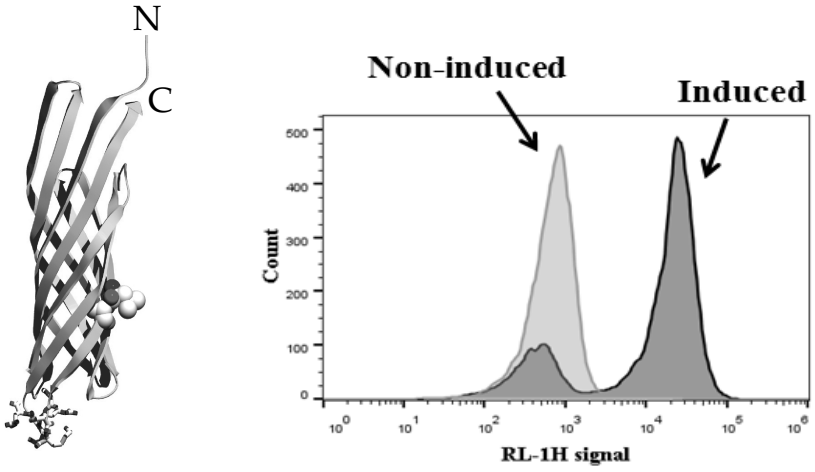

Figure I - 3. Beta barrel structure of eCPX (left) and histograms of expression.
The structure shows free N- and C- termini, adapted from Rice et al. (2008)[74]. Flow cytometry histograms of non-induced vs. arabinose-induced E. coli expressing exenatide-4 using the eCPX scaffold (right). Peptides were detected by anti-exendin-4 labeling followed by AlexaFluor647 anti-mouse secondary staining. Even the relatively tightly regulated araBAD promoter results in a more than order of magnitude spread in detected signal (10^4 – 10^5).

The eCPX scaffold used in this research permits simultaneous display of both C- and N- terminal fusion peptides[74] (Figure I - 3, left). Previous directed evolution work with bacterial surface display used loop insertion fusions, where randomized peptides were incorporated within an extracellular loop in a bacterial outer membrane protein (e.g.

OmpA, FliTrx). However these peptides showed poor binding outside the loop context, as the binding peptide conformation required the framework of the display scaffold[71]. The eCPX and related OmpX-based systems have been used for a wide range of bacterial applications, including as effectors for light-induced expression[75] and to engineer protease resistant affinity scaffolds[76]. In an interesting variation of a typical evolution screen, Pantazes, Daugherty, and coworkers displayed a randomized peptide library with eCPX on the E. coli surface and incubated with the serum antibody repertoire[77]. Antibody-bound peptides were sorted with MACS or FACS, and the resulting libraries deep sequenced. Peptide sequences that bound to antibodies from patients with autoimmune diseases could be compared with those from healthy control subjects to identify significant motifs. Patients with celiac disease had much higher levels of antibody specific to the QPEQPFXE sequence, which appears in wheat, barley, and rye antigens. The pairing of surface display and deep sequencing has the potential to uncover exciting new directions in peptide engineering and antibody epitope discovery.

The ability to display peptides both on the C- and N- terminus in eCPX permits the use of a second epitope to enable quantitation of display level. Randomized peptide display at the N terminus of eCPX and tag display at the C-terminus (e.g. HA tag) should, in theory, enable display normalization. Even with robust promoter and expression systems, a population of bacteria can display varying numbers of peptide per cell spanning as much as an order of magnitude (Figure I - 3, right). One round of FACS selection could then potentially exclude a tightly binding clone that stochastically displays a lower number of peptides and include a weaker binder with a higher displayed number

of peptides. The tighter binding cell would have a higher ratio of target signal to scaffold signal than a weaker binding cell, and the gate for sorting can be drawn to capture tight binding sequences, regardless of display level. In summary, bacteria display libraries have enabled the directed evolution of peptide sequences as binders to various disease-relevant targets.

The MDM2-p53 interaction

Due to its widespread dysregulation in many cancers, MDM2 (mouse double minute 2 protein) has posed as an attractive target for drug development. Despite this, no MDM2-targeting drug has seen FDA approval[78]. The p53 protein, encoded by Trp53, is involved in critical tumor suppressor pathways and is involved in an autoregulatory loop with MDM2, where MDM2 negatively regulates p53 through proteasome targeted degradation and transcriptional regulation, and p53 target expression upregulates MDM2 (Figure I - 4). MDM2 overexpression leading to p53 dysregulation is found in 7% of all cancers, and is more common in soft tissue tumors such as esophageal carcinomas[79]. Crystallization of the N-terminal region of p53 with MDM2 revealed a p53 alpha helix engaging with a deep groove of MDM2[80] with critical hydrophobic interactions mediated by F19, W23, and L26 of the p53 helix. Phage display has been used to find more potent inhibitors of the MDM2-p53 interaction than the p53 native sequence[81,82] but these studies did not screen peptides in the context of stapling.

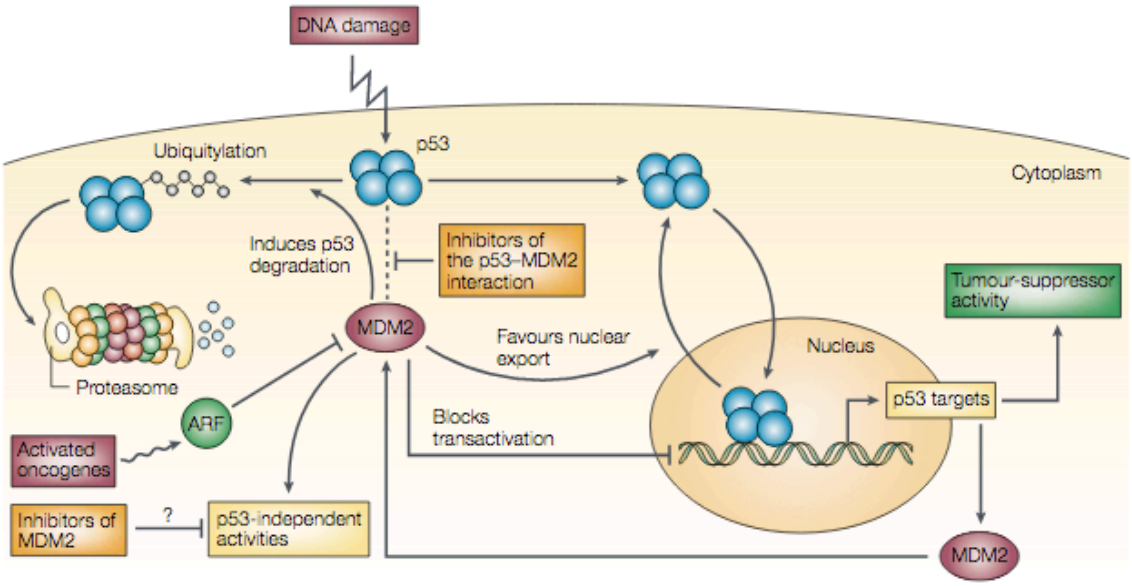

Figure I - 4. Partial map of signaling pathways involving the p53-MDM2 interaction. P53 functions as a tumor-suppressor gene, triggering transcription of downstream targets following DNA damage. MDM2 functions as a ubiquitin ligase of p53, targeting it for degradation, and also inhibiting p53 nuclear localization. Figure adapted from Chéne et al. (2003)[79].

The Nutlin family of small molecules, discovered by Vassilev and colleagues was found to bind MDM2 and block p53, activating the p53 pathway in tumor cells[83]. They were discovered through small molecule screens revealing cis-imidazoline analogs and exhibited 100-300 nM binding affinity values. Unfortunately, despite exciting preclinical and early stage clinical results, a derivative of Nutlin 3a, RG7112, exhibited poor pharmacokinetics and toxicity. Along with other small molecule MDM2 binders, RG7112 also exhibited a lack of strong binding to MDMX (a related p53 suppressor), which likely contributed to its modest efficacy during clinical trials. The lack of engagement of Nutlin and Nutlin derivatives to MDMX, despite extensive structural similarities between MDM2 and MDMX, is well documented in the literature. In one example, Hu and coworkers

overexpressed MDMX in a stably transfected U2OS osteosarcoma cell line and found lack of p53 activation in cells even when treated with Nutlin[84]. While MDMX does not participate in direct ubiquitination of p53, it forms a heterocomplex with MDM2 and is critical for p53 suppression in embryonic development[85]. Gene or protein alterations of MDMX are found in many cancers and the frequency is higher in tumors with wild-type p53[85]. Because of their larger surface area, alpha helical stapled peptides have shown to be capable of targeting both MDM2 and MDMX[2]. Aileron Therapeutics' lead compound ALRN-6924 is currently being evaluated in phase 2 clinical trials[23].

Summary

The design of stapled peptides has largely been limited to targeting interactions with a solved X-ray crystal structure, to which an inhibitor can be rationally designed. Even in this case, stabilization requires time consuming trial-and-error optimization of linker location (Figure I - 5) as stabilization is a major structural modification and so can also reduce or completely abrogate binding if the covalent bridge is made between inappropriate residues. Researchers routinely test multiple variants in search for optimum biological activity[86]. In one case, hydrocarbon stapling of a Bim-derived peptide exhibited weaker binding to Bcl-xL than the unstapled peptide[87]. In the complex landscape of protein-protein interactions, there are many such pairs in which no crystal structure exists.

Compound	Sequence * = R_8 * = S_5	Charge at pH 7.4	α helicity	K_d (nM)	Cell permeable	Cell death
WT	Ac-LSQETFSDLWKLLPEN-NH_2	-2	11%	410±19	no	–
SAH-p53-1	Ac-LSQETFSD*WKLLPE*-NH_2	-2	25%	100±8	no	–
SAH-p53-2	Ac-LSQE*FSDLWK*LPEN-NH_2	-2	10%	400±50	no	–
SAH-p53-3	Ac-LSQ*TFSDLW*LLPEN-NH_2	-2	12%	1200±89	no	–
SAH-p53-4	Ac-LSQETF*DLWKLL*EN-NH_2	-2	59%	0.92±0.11	no	–
SAH-p53-5	Ac-LSQETF*NLWKLL*QN-NH_2	0	20%	0.80±0.05	yes	–
SAH-p53-6	Ac-LSQQTF*NLWRLL*QN-NH_2	+1	14%	56±11	yes	–
SAH-p53-7	Ac-QSQQTF*NLWKLL*QN-NH_2	+1	36%	50±10	yes	–
SAH-p53-8	Ac-QSQQTF*NLWRLL*QN-NH_2	+1	85%	55±11	yes	+
SAH-p53-8$_{F19A}$	Ac-QSQQTA*NLWRLL*QN-NH_2	+1	39%	>4000	yes	–
UAH-p53-8	Ac-QSQQTF*NLWRKK*QN-NH_2	+1	36%	100±10	yes	–

Figure I - 5. Development of a p53 mimic for MDM2 inhibition
Trial-and-error optimization of staple locations and amino acid sequence, adapted from Bernal et al. (2007)[22]

Solid phase peptide synthesis (SPPS), today's method of choice for producing peptides, has been used to generate and screen libraries of stapled molecules containing non-canonical amino acids[88,89]. The one-bead-one-compound method (OBOC) has significant advantages due to the vast accessible chemical space. Virtually any type of side chain can be incorporated by SPPS, but care must be taken to avoid generating peptides of different sequence but same molecular weight due to decoding accomplished by mass spectrometry. Because of this constraint, and also because screening for binders typically involves manually selecting beads in fluorescence microscopy, the library size is limited to about 10^4 members[90] and thus is not tractable as a method for screening large libraries of stabilized peptides. Screening two residues on the outside of the stabilized residues and 6 residues between the stabilized residues requires a library size of about 10^{10} molecules, and so OBOC screening approaches significantly undersample this space. Bacterial surface display enables large library sizes, to numbers not typically achievable by yeast, mammalian, and OBOC methods. Furthermore, the relatively facile

incorporation of non-canonical acids in the genetically tractable E. coli host, as well as ability to use quantitative FACS for sorting and analysis confers powerful advantages compared to phage and mRNA/ribosomal display systems. This dissertation addresses the need for a high throughput, combinatorial-driven method to screen large numbers of stabilized peptides for activity.

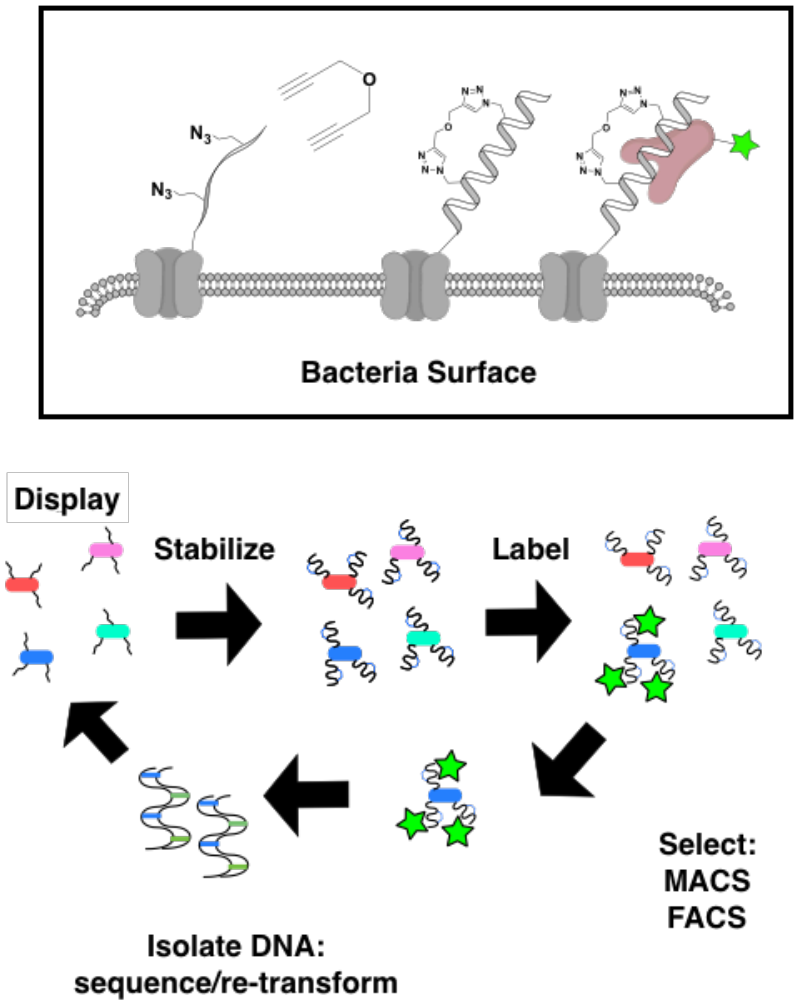

Figure I - 6. Putting the pieces together
We used bacterial surface display to expose libraries of peptides containing the non-canonical amino acid azidohomoalanine. We stabilized the displayed peptides and screened with magnetic and fluorescent methods to discover new sequences.
.

References

(1) Pace, C. N.; Scholtz, J. M. A Helix Propensity Scale Based on Experimental Studies of Peptides and Proteins. Biophys. J. **1998**, 75 (1), 422–427. https://doi.org/10.1016/S0006-3495(98)77529-0.

(2) Chang, Y. S.; Graves, B.; Guerlavais, V.; Tovar, C.; Packman, K.; To, K.-H.; Olson, K. A.; Kesavan, K.; Gangurde, P.; Mukherjee, A.; et al. Stapled A–helical Peptide Drug Development: A Potent Dual Inhibitor of MDM2 and MDMX for P53-Dependent Cancer Therapy. Proc. Natl. Acad. Sci. **2013**, 110 (36), E3445–E3454. https://doi.org/10.1073/pnas.1303002110.

(3) Arkin, M.; Wells, J. Small-Molecule Inhibitors of Protein-Protein Interactions: Progressing towards the Dream. Nat. Rev. Drug Discov. **2004**, 3 (4), 301–317. https://doi.org/10.1038/nrd1343.

(4) Arkin, M. R.; Tang, Y.; Wells, J. A. Small-Molecule Inhibitors of Protein-Protein Interactions: Progressing toward the Reality. Chemistry and Biology. 2014. https://doi.org/10.1016/j.chembiol.2014.09.001.

(5) Cang, S.; Iragavarapu, C.; Savooji, J.; Song, Y.; Liu, D. ABT-199 (Venetoclax) and BCL-2 Inhibitors in Clinical Development. Journal of Hematology and Oncology. 2015. https://doi.org/10.1186/s13045-015-0224-3.

(6) Winter, A.; Higueruelo, A. P.; Marsh, M.; Sigurdardottir, A.; Pitt, W. R.; Blundell, T. L. Biophysical and Computational Fragment-Based Approaches to Targeting Protein-Protein Interactions: Applications in Structure-Guided Drug Discovery. Quarterly Reviews of Biophysics. 2012. https://doi.org/10.1017/S0033583512000108.

(7) Condon, S. M.; Mitsuuchi, Y.; Deng, Y.; Laporte, M. G.; Rippin, S. R.; Haimowitz, T.; Alexander, M. D.; Kumar, P. T.; Hendi, M. S.; Lee, Y. H.; et al. Birinapant, a Smac-Mimetic with Improved Tolerability for the Treatment of Solid Tumors and Hematological Malignancies. J. Med. Chem. **2014**. https://doi.org/10.1021/jm500176w.

(8) Souers, A. J.; Leverson, J. D.; Boghaert, E. R.; Ackler, S. L.; Catron, N. D.; Chen, J.; Dayton, B. D.; Ding, H.; Enschede, S. H.; Fairbrother, W. J.; et al. ABT-199, a Potent and Selective BCL-2 Inhibitor, Achieves Antitumor Activity While Sparing Platelets. Nat. Med. **2013**. https://doi.org/10.1038/nm.3048.

(9) Smith, M. C.; Gestwicki, J. E. Features of Protein–Protein Interactions That Translate into Potent Inhibitors: Topology, Surface Area and Affinity. Expert Rev. Mol. Med. **2012**. https://doi.org/10.1017/erm.2012.10.

(10) Slastnikova, T. A.; Ulasov, A. V.; Rosenkranz, A. A.; Sobolev, A. S. Targeted

Intracellular Delivery of Antibodies: The State of the Art. Front. Pharmacol. **2018**. https://doi.org/10.3389/fphar.2018.01208.

(11) Cilliers, C.; Guo, H.; Liao, J.; Christodolu, N.; Thurber, G. M. Multiscale Modeling of Antibody-Drug Conjugates: Connecting Tissue and Cellular Distribution to Whole Animal Pharmacokinetics and Potential Implications for Efficacy. AAPS J. **2016**. https://doi.org/10.1208/s12248-016-9940-z.

(12) Coats, S.; Williams, M.; Kebble, B.; Dixit, R.; Tseng, L.; Yao, N. S.; Tice, D. A.; Soria, J. C. Antibody-Drug Conjugates: Future Directions in Clinical and Translational Strategies to Improve the Therapeutic Index. Clinical Cancer Research. 2019. https://doi.org/10.1158/1078-0432.CCR-19-0272.

(13) Marschall, A. L. J.; Frenzel, A.; Schirrmann, T.; Schüngel, M.; Dübel, S. Targeting Antibodies to the Cytoplasm. **2011**, No. February, 3–16. https://doi.org/10.4161/mabs.3.1.14110.

(14) Kauke, M. J.; Traxlmayr, M. W.; Parker, J. A.; Kiefer, J. D.; Knihtila, R.; McGee, J.; Verdine, G.; Mattos, C.; Dane Wittrup, K. An Engineered Protein Antagonist of K-Ras/B-Raf Interaction. Sci. Rep. **2017**. https://doi.org/10.1038/s41598-017-05889-7.

(15) Sawyer, T. K.; Partridge, A. W.; Kaan, H. Y. K.; Juang, Y.-C.; Lim, S.; Johannes, C.; Yuen, T. Y.; Verma, C.; Kannan, S.; Aronica, P.; et al. Macrocyclic α Helical Peptide Therapeutic Modality: A Perspective of Learnings and Challenges. Bioorg. Med. Chem. **2018**, 26 (10), 2807–2815. https://doi.org/10.1016/J.BMC.2018.03.008.

(16) Atangcho, L.; Navaratna, T.; Thurber, G. M. Hitting Undruggable Targets: Viewing Stabilized Peptide Development through the Lens of Quantitative Systems Pharmacology. Trends Biochem. Sci. **2018**. https://doi.org/10.1016/j.tibs.2018.11.008.

(17) Bairy, S.; Wong, C. F. Influence of Kinetics of Drug Binding on EGFR Signaling: A Comparative Study of Three EGFR Signaling Pathway Models. Proteins Struct. Funct. Bioinforma. **2011**. https://doi.org/10.1002/prot.23072.

(18) Schoop, A.; Dey, F. On-Rate Based Optimization of Structure-Kinetic Relationship - Surfing the Kinetic Map. Drug Discovery Today: Technologies. 2015. https://doi.org/10.1016/j.ddtec.2015.08.003.

(19) Leshchiner, E. S.; Parkhitko, A.; Bird, G. H.; Luccarelli, J.; Bellairs, J. A.; Escudero, S.; Opoku-Nsiah, K.; Godes, M.; Perrimon, N.; Walensky, L. D. Direct Inhibition of Oncogenic KRAS by Hydrocarbon-Stapled SOS1 Helices. Proc. Natl. Acad. Sci. **2015**, 112 (6), 1761–1766. https://doi.org/10.1073/pnas.1413185112.

(20) Moellering, R. E.; Cornejo, M.; Davis, T. N.; Bianco, C. Del; Aster, J. C.; Blacklow, S. C.; Kung, A. L.; Gilliland, D. G.; Verdine, G. L.; Bradner, J. E. Direct Inhibition of the NOTCH Transcription Factor Complex. Nature **2009**, 462 (7270), 182–188. https://doi.org/10.1038/nature08543.

(21) Heinis, C.; Rutherford, T.; Freund, S.; Winter, G. Phage-Encoded Combinatorial Chemical Libraries Based on Bicyclic Peptides. Nat. Chem. Biol. **2009**, 5 (7), 502–507. https://doi.org/10.1038/nchembio.184.

(22) Bernal, F.; Tyler, A. F.; Korsmeyer, S. J.; Walensky, L. D.; Verdine, G. L. Reactivation of the P53 Tumor Suppressor Pathway by a Stapled P53 Peptide. J. Am. Chem. Soc. **2007**, 129 (9), 2456–2457. https://doi.org/10.1021/ja0693587.

(23) Shustov, A. R.; Horwitz, S. M.; Zain, J.; Patel, M. R.; Goel, S.; Sokol, L.; Meric-Bernstam, F.; Shapiro, G.; Nasta, S. D.; Janakiram, M.; et al. Preliminary Results of the Stapled Peptide ALRN-6924, a Dual Inhibitor of MDMX and MDM2, in Two Phase IIa Dose Expansion Cohorts in Relapsed/Refractory TP53 Wild-Type Peripheral T-Cell Lymphoma. Blood **2018**, 132 (Suppl 1), 1623–1623. https://doi.org/10.1182/BLOOD-2018-99-116780.

(24) Thean, D.; Ebo, J. S.; Luxton, T.; Lee, X. C.; Yuen, T. Y.; Ferrer, F. J.; Johannes, C. W.; Lane, D. P.; Brown, C. J. Enhancing Specific Disruption of Intracellular Protein Complexes by Hydrocarbon Stapled Peptides Using Lipid Based Delivery. Sci. Rep. **2017**. https://doi.org/10.1038/s41598-017-01712-5.

(25) Bird, G. H.; Mazzola, E.; Opoku-Nsiah, K.; Lammert, M. A.; Godes, M.; Neuberg, D. S.; Walensky, L. D. Biophysical Determinants for Cellular Uptake of Hydrocarbon-Stapled Peptide Helices. Nat. Chem. Biol. **2016**, 12 (10), 845–852. https://doi.org/10.1038/nchembio.2153.

(26) Peraro, L.; Deprey, K. L.; Moser, M. K.; Zou, Z.; Ball, H. L.; Levine, B.; Kritzer, J. A. Cell Penetration Profiling Using the Chloroalkane Penetration Assay. J. Am. Chem. Soc. **2018**. https://doi.org/10.1021/jacs.8b06144.

(27) Walensky, L. D.; Kung, A. L.; Escher, I.; Malia, T. J.; Barbuto, S.; Wright, R. D.; Wagner, G.; Verdine, G. L.; Korsmeyer, S. J. Activation of Apoptosis in Vivo by a Hydrocarbon-Stapled BH3 Helix. Science **2004**, 305 (5689), 1466–1470. https://doi.org/10.1126/science.1099191.

(28) LaRochelle, J. R.; Cobb, G. B.; Steinauer, A.; Rhoades, E.; Schepartz, A. Fluorescence Correlation Spectroscopy Reveals Highly Efficient Cytosolic Delivery of Certain Penta-Arg Proteins and Stapled Peptides. J. Am. Chem. Soc. **2015**, 3 (Figure 1), 150213085027009. https://doi.org/10.1021/ja510391n.

(29) Molina, D. M.; Jafari, R.; Ignatushchenko, M.; Seki, T.; Larsson, E. A.; Dan, C.; Sreekumar, L.; Cao, Y.; Nordlund, P. Monitoring Drug Target Engagement in Cells

and Tissues Using the Cellular Thermal Shift Assay. Science (80-.). **2013**. https://doi.org/10.1126/science.1233606.

(30) Torres, O.; Yüksel, D.; Bernardina, M.; Kumar, K.; Bong, D. Peptide Tertiary Structure Nucleation by Side-Chain Crosslinking with Metal Complexation and Double "Click" Cycloaddition. ChemBioChem **2008**, 9 (11), 1701–1705. https://doi.org/10.1002/cbic.200800040.

(31) Lau, Y. H.; de Andrade, P.; Quah, S.-T.; Rossmann, M.; Laraia, L.; Skold, N.; Sum, T. J.; Rowling, P. J. E.; Joseph, T. L.; Verma, C.; et al. Functionalised Staple Linkages for Modulating the Cellular Activity of Stapled Peptides. Chem. Sci. **2014**, 5 (5), 1804–1809. https://doi.org/10.1039/C4SC00045E.

(32) Lau, Y. H.; Wu, Y.; Andrade, P. De; Galloway, W. R. J. D.; Spring, D. R. A Two-Component ' Double-Click ' Approach to Peptide Stapling. Nat. Protoc. **2015**, 10 (4), 585–594. https://doi.org/10.1038/nprot.2015-033.

(33) Zhang, L.; Navaratna, T.; Liao, J.; Thurber, G. M. Dual-Purpose Linker for Alpha Helix Stabilization and Imaging Agent Conjugation to Glucagon-like Peptide-1 Receptor Ligands. Bioconjug. Chem. **2015**, 26 (2), 329–337. https://doi.org/10.1021/bc500584t.

(34) Patel, D. S.; Qi, Y.; Im, W. Modeling and Simulation of Bacterial Outer Membranes and Interactions with Membrane Proteins. Curr. Opin. Struct. Biol. **2017**, 43, 131–140. https://doi.org/10.1016/J.SBI.2017.01.003.

(35) Van Deventer, J. a.; Yuet, K. P.; Yoo, T. H.; Tirrell, D. a. Cell Surface Display Yields Evolvable, Clickable Antibody Fragments. ChemBioChem **2014**, 15 (12), 1777–1781. https://doi.org/10.1002/cbic.201402184.

(36) Dupont, C. L.; Grass, G.; Rensing, C. Copper Toxicity and the Origin of Bacterial Resistance—New Insights and Applications. Metallomics **2011**, 3 (11), 1109. https://doi.org/10.1039/c1mt00107h.

(37) Navaratna, T.; Atangcho, L.; Mahajan, M.; Subramanian, V.; Case, M.; Min, A.; Tresnak, D.; Thurber, G. M. Directed Evolution Using Stabilized Bacterial Peptide Display. J. Am. Chem. Soc. **2020**. https://doi.org/10.1021/jacs.9b10716.

(38) Agard, N. J.; Prescher, J. A.; Bertozzi, C. R. A Strain-Promoted [3 + 2] Azide-Alkyne Cycloaddition for Covalent Modification of Biomolecules in Living Systems. J. Am. Chem. Soc. **2004**. https://doi.org/10.1021/ja044996f.

(39) Lau, Y. H.; Wu, Y.; Rossmann, M.; Tan, B. X.; De Andrade, P.; Tan, Y. S.; Verma, C.; McKenzie, G. J.; Venkitaraman, A. R.; Hyvönen, M.; et al. Double Strain-Promoted Macrocyclization for the Rapid Selection of Cell-Active Stapled Peptides. Angew. Chemie - Int. Ed. **2015**. https://doi.org/10.1002/anie.201508416.

(40) Cudic, M.; Fields, G. B. Solid-Phase Peptide Synthesis. In Molecular Biomethods Handbook: Second Edition; 2008. https://doi.org/10.1007/978-1-60327-375-6_32.

(41) Dawson, P. E.; Muir, T. W.; Clark-Lewis, I.; Kent, S. B. H. Synthesis of Proteins by Native Chemical Ligation. Science (80-.). **1994**. https://doi.org/10.1126/science.7973629.

(42) Yuet, K. P.; Doma, M. K.; Ngo, J. T.; Sweredoski, M. J.; Graham, R. L. J.; Moradian, A.; Hess, S.; Schuman, E. M.; Sternberg, P. W.; Tirrell, D. a. Cell-Specific Proteomic Analysis in Caenorhabditis Elegans. Proc. Natl. Acad. Sci. **2015**, 112 (9), 201421567. https://doi.org/10.1073/pnas.1421567112.

(43) Ngo, J. T.; Champion, J. a; Mahdavi, A.; Tanrikulu, I. C.; Beatty, K. E.; Connor, R. E.; Yoo, T. H.; Dieterich, D. C.; Schuman, E. M.; Tirrell, D. a. Cell-Selective Metabolic Labeling of Proteins. Nat. Chem. Biol. **2009**, 5 (10), 715–717. https://doi.org/10.1038/nchembio.200.

(44) Hendrickson, W. A.; Horton, J. R.; LeMaster, D. M. Selenomethionyl Proteins Produced for Analysis by Multiwavelength Anomalous Diffraction (MAD): A Vehicle for Direct Determination of Three-Dimensional Structure. EMBO J. **1990**. https://doi.org/10.1002/j.1460-2075.1990.tb08287.x.

(45) Cowie, D. B.; Cohen, G. N. Biosynthesis by Escherichia Coli of Active Altered Proteins Containing Selenium Instead of Sulfur. BBA - Biochim. Biophys. Acta **1957**. https://doi.org/10.1016/0006-3002(57)90003-3.

(46) Walden, H. Selenium Incorporation Using Recombinant Techniques. Acta Crystallogr. Sect. D Biol. Crystallogr. **2010**. https://doi.org/10.1107/S0907444909038207.

(47) Ngo, J. T.; Tirrell, D. A. Noncanonical Amino Acids in the Interrogation of Cellular Protein Synthesis. Acc. Chem. Res. **2011**. https://doi.org/10.1021/ar200144y.

(48) Mukai, T.; Lajoie, M. J.; Englert, M.; Söll, D. Rewriting the Genetic Code. Annu. Rev. Microbiol. **2017**. https://doi.org/10.1146/annurev-micro-090816-093247.

(49) Wang, L.; Schultz, P. G. A General Approach for the Generation of Orthogonal TRNAs. Chem. Biol. **2001**. https://doi.org/10.1016/S1074-5521(01)00063-1.

(50) Wang, L.; Xie, J.; Schultz, P. G. Expanding the Genetic Code. Annual Review of Biophysics and Biomolecular Structure. 2006. https://doi.org/10.1146/annurev.biophys.35.101105.121507.

(51) Wang, J.; Xie, J.; Schultz, P. G. A Genetically Encoded Fluorescent Amino Acid. J. Am. Chem. Soc. **2006**. https://doi.org/10.1021/ja062666k.

(52) Zhang, Z.; Gildersleeve, J.; Yang, Y. Y.; Xu, R.; Loo, J. A.; Uryu, S.; Wong, C. H.; Schultz, P. G. A New Strategy for the Synthesis of Glycoproteins. Science (80-.). **2004**. https://doi.org/10.1126/science.1089509.

(53) Tian, F.; Tsao, M. L.; Schultz, P. G. A Phage Display System with Unnatural Amino Acids. J. Am. Chem. Soc. **2004**. https://doi.org/10.1021/ja045673m.

(54) Link, A. J.; Vink, M. K. S.; Tirrell, D. A. Presentation and Detection of Azide Functionality in Bacterial Cell Surface Proteins Presentation and Detection of Azide Functionality in Bacterial. J. Am. Chem. Soc. **2004**, 126 (34), 10598–10602. https://doi.org/10.1021/ja047629c.

(55) Strable, E.; Prasuhn, D. E.; Udit, A. K.; Brown, S.; Link, A. J.; Ngo, J. T.; Lander, G.; Quispe, J.; Potter, C. S.; Carragher, B.; et al. Unnatural Amino Acid Incorporation into Virus-Like Particles. Bioconjug. Chem. **2008**, 19 (4), 866–875. https://doi.org/10.1021/bc700390r.

(56) Ngo, J.; Champion, J.; Mahdavi, A.; Tanrikulu, I.; Beatty, K.; Connor, R.; Yoo, T.; Dieterich, D.; Schuman, E.; Tirrell, D. Cell-Selective Metabolic Labeling of Proteins. Nat. Chem. Biol. **2009**, 5 (10), 715–717. https://doi.org/10.1038/nchembio.200.

(57) Link, A. J.; Vink, M. K. S.; Agard, N. J.; Prescher, J. A.; Bertozzi, C. R.; Tirrell, D. A. Discovery of Aminoacyl-TRNA Synthetase Activity through Cell-Surface Display of Noncanonical Amino Acids. Proc. Natl. Acad. Sci. U. S. A. **2006**. https://doi.org/10.1073/pnas.0601167103.

(58) Yoo, T. H.; Tirrell, D. A. High-Throughput Screening for Methionyl-TRNA Synthetases That Enable Residue-Specific Incorporation of Noncanonical Amino Acids into Recombinant Proteins in Bacterial Cells. Angew. Chemie - Int. Ed. **2007**. https://doi.org/10.1002/anie.200700779.

(59) Datta, D.; Wang, P.; Carrico, I. S.; Mayo, S. L.; Tirrell, D. A. A Designed Phenylalanyl-TRNA Synthetase Variant Allows Efficient in Vivo Incorporation of Aryl Ketone Functionality into Proteins. J. Am. Chem. Soc. **2002**. https://doi.org/10.1021/ja0177096.

(60) Darwin, C. On the Origin of the Species; 1859.

(61) Blount, Z. D.; Borland, C. Z.; Lenski, R. E. Historical Contingency and the Evolution of a Key Innovation in an Experimental Population of Escherichia Coli. Proc. Natl. Acad. Sci. U. S. A. **2008**. https://doi.org/10.1073/pnas.0803151105.

(62) Arnold, F. H. Design by Directed Evolution. Acc. Chem. Res. **1998**. https://doi.org/10.1021/ar960017f.

(63) Cobb, R. E.; Chao, R.; Zhao, H. Directed Evolution: Past, Present, and Future.

AIChE J. **2013**. https://doi.org/10.1002/aic.13995.

(64) Savile, C. K.; Janey, J. M.; Mundorff, E. C.; Moore, J. C.; Tam, S.; Jarvis, W. R.; Colbeck, J. C.; Krebber, A.; Fleitz, F. J.; Brands, J.; et al. Biocatalytic Asymmetric Synthesis of Sitagliptin Manufacture. Science (80-.). **2010**. https://doi.org/10.1126/science.1188934.

(65) Pande, J.; Szewczyk, M. M.; Grover, A. K. Phage Display: Concept, Innovations, Applications and Future. Biotechnology Advances. 2010. https://doi.org/10.1016/j.biotechadv.2010.07.004.

(66) Benhar, I. Biotechnological Applications of Phage and Cell Display. Biotechnol. Adv. **2001**, 19, 1–33.

(67) Ploss, M.; Facey, S. J.; Bruhn, C.; Zemel, L.; Hofmann, K.; Stark, R. W.; Albert, B.; Hauer, B. Selection of Peptides Binding to Metallic Borides by Screening M13 Phage Display Libraries. BMC Biotechnol. **2014**. https://doi.org/10.1186/1472-6750-14-12.

(68) Villequey, C.; Kong, X. D.; Heinis, C. Bypassing Bacterial Infection in Phage Display by Sequencing DNA Released from Phage Particles. Protein Eng. Des. Sel. **2017**. https://doi.org/10.1093/protein/gzx057.

(69) Boder, E.; Wittrup, K. Yeast Surface Display for Screening Combinatorial Polypeptide Libraries. Nat. Biotechnol. **1997**, 15 (6), 553–557. https://doi.org/10.1038/nbt0697-553.

(70) Daugherty, P. S.; Chen, G.; Olsen, M. J.; Iverson, B. L.; Georgiou, G. Antibody Affinity Maturation Using Bacterial Surface Display. Protein Eng. **1998**, 11 (9), 825–832. https://doi.org/10.1093/protein/11.9.825.

(71) Daugherty, P. S. Protein Engineering with Bacterial Display. Curr. Opin. Struct. Biol. **2007**, 17 (4), 474–480. https://doi.org/10.1016/j.sbi.2007.07.004.

(72) Pepper, L. R.; Cho, Y. K.; Boder, E. T.; Shusta, E. V. A Decade of Yeast Surface Display Technology: Where Are We Now? Comb Chem High Throughput Screen **2009**, 11 (2), 127–134.

(73) Lipovsek, D.; Lippow, S.; Hackel, B.; Gregson, M.; Cheng, P.; Kapila, A.; Wittrup, K. Evolution of an Interloop Disulfide Bond in High-Affinity Antibody Mimics Based on Fibronectin Type {III} Domain and Selected by Yeast Surface Display: Molecular Convergence with Single-Domain Camelid and Shark Antibodies. J. Mol. Biol. **2007**, 368 (4), 1024–1041. https://doi.org/10.1016/j.jmb.2007.02.029.

(74) Rice, J.; Daugherty, P. Directed Evolution of a Biterminal Bacterial Display Scaffold Enhances the Display of Diverse Peptides. Protein Eng. Des. Sel. **2008**, 21 (7),

435–442. https://doi.org/10.1093/protein/gzn020.

(75) Sankaran, S.; Zhao, S.; Muth, C.; Paez, J.; del Campo, A. Toward Light-Regulated Living Biomaterials. Adv. Sci. **2018**. https://doi.org/10.1002/advs.201800383.

(76) Getz, J. A.; Rice, J. J.; Daugherty, P. S. Protease-Resistant Peptide Ligands from a Knottin Scaffold Library. ACS Chem. Biol. **2011**. https://doi.org/10.1021/cb200039s.

(77) Pantazes, R. J.; Reifert, J.; Bozekowski, J.; Ibsen, K. N.; Murray, J. A.; Daugherty, P. S. Identification of Disease-Specific Motifs in the Antibody Specificity Repertoire via next-Generation Sequencing. Sci. Rep. **2016**. https://doi.org/10.1038/srep30312.

(78) Burgess, A.; Chia, K. M.; Haupt, S.; Thomas, D.; Haupt, Y.; Lim, E. Clinical Overview of MDM2/X-Targeted Therapies. Frontiers in Oncology. 2016. https://doi.org/10.3389/fonc.2016.00007.

(79) Chène, P. Inhibiting the P53-MDM2 Interaction: An Important Target for Cancer Therapy. Nature Reviews Cancer. 2003, pp 102–109. https://doi.org/10.1038/nrc991.

(80) Kussie, P. H.; Gorina, S.; Marechal, V.; Elenbaas, B.; Moreau, J.; Levine, A. J.; Pavletich, N. P. Structure of the MDM2 Oncoprotein Bound to the P53 Tumor Suppressor Transactivation Domain. Science (80-.). **1996**. https://doi.org/10.1126/science.274.5289.948.

(81) Böttger, A.; Böttger, V.; Garcia-Echeverria, C.; Chène, P.; Hochkeppel, H. K.; Sampson, W.; Ang, K.; Howard, S. F.; Picksley, S. M.; Lane, D. P. Molecular Characterization of the Hdm2-P53 Interaction. J. Mol. Biol. **1997**, 269 (5), 744–756. https://doi.org/10.1006/jmbi.1997.1078.

(82) Li, C.; Pazgier, M.; Li, C.; Yuan, W.; Liu, M.; Wei, G.; Lu, W. Y.; Lu, W. Systematic Mutational Analysis of Peptide Inhibition of the P53-MDM2/MDMX Interactions. J. Mol. Biol. **2010**, 398 (2), 200–213. https://doi.org/10.1016/j.jmb.2010.03.005.

(83) Vassilev, L. T.; Vu, B. T.; Graves, B.; Carvajal, D.; Podlaski, F.; Filipovic, Z.; Kong, N.; Kammlott, U.; Lukacs, C.; Klein, C.; et al. In Vivo Activation of the P53 Pathway by Small-Molecule Antagonists of MDM2. Science (80-.). **2004**. https://doi.org/10.1126/science.1092472.

(84) Hu, B.; Gilkes, D. M.; Farooqi, B.; Sebti, S. M.; Chen, J. MDMX Overexpression Prevents P53 Activation by the MDM2 Inhibitor Nutlin. J. Biol. Chem. **2006**. https://doi.org/10.1074/jbc.C600147200.

(85) Wade, M.; Li, Y. C.; Wahl, G. M. MDM2, MDMX and P53 in Oncogenesis and

Cancer Therapy. Nature Reviews Cancer. 2013. https://doi.org/10.1038/nrc3430.

(86) Walensky, L. D.; Bird, G. H. Hydrocarbon-Stapled Peptides: Principles, Practice, and Progress. J. Med. Chem. **2014**, 57 (15), 6275–6288. https://doi.org/10.1021/jm4011675.

(87) Okamoto, T.; Zobel, K.; Fedorova, A.; Yang, H.; Fairbrother, W. J.; Huang, D. C. S.; Smith, B. J.; Deshayes, K.; Czabotar, P. E. Stabilizing the Pro-Apoptotic BimBH3 Helix (BimSAHB) Does Not Necessarily Enhance A Ffi Nity or Biological Activity. ACS Chem. Biol. **2013**, 14–19.

(88) Lam, K. S.; Lebl, M.; Krchňák, V. The "One-Bead-One-Compound" Combinatorial Library Method. Chem. Rev. **1997**. https://doi.org/10.1021/cr9600114.

(89) Rezaei Araghi, R.; Ryan, J. A.; Letai, A.; Keating, A. E. Rapid Optimization of Mcl-1 Inhibitors Using Stapled Peptide Libraries Including Non-Natural Side Chains. ACS Chem. Biol. **2016**, 11 (5), 1238–1244. https://doi.org/10.1021/acschembio.5b01002.

(90) Park, S. H.; Wang, X.; Liu, R.; Lam, K. S.; Weiss, R. H. High Throughput Screening of a Small Molecule One-Bead-One-Compound Combinatorial Library to Identify Attenuators of P21 as Chemotherapy Sensitizers. Cancer Biol. Ther. **2008**, 7 (12), 2015–2022. https://doi.org/10.4161/cbt.7.12.7069.

Chapter II: Directed Evolution Using Stabilized Bacterial Peptide Display

Adapted with permission from Navaratna et al. J. Am. Chem. Soc. 2020, 142, 4, 1882-1894.

Tejas Navaratna, Lydia Atangcho, Mukesh Mahajan, Vivekanandan Subramanian, Marshall Case, Andrew Min, Daniel Tresnak, and Greg M. Thurber

Abstract

Chemically stabilized peptides have attracted intense interest by academics and pharmaceutical companies due to their potential to hit currently 'undruggable' targets. However, engineering an optimal sequence, stabilizing linker location, and physicochemical properties is a slow and arduous process. By pairing non-natural amino acid incorporation and cell surface click chemistry in bacteria with high-throughput sorting, we developed a method to quantitatively select high affinity ligands and applied the SPEED (Stabilized Peptide Evolution by E. coli Display) technique to develop disrupters of the therapeutically relevant MDM2-p53 interface. Through in situ stabilization on the bacterial surface, we demonstrate rapid isolation of stabilized peptides with improved

affinity and novel structures. Several peptides evolved a second loop including one sequence (Kd = 1.8 nM) containing an i, i+4 disulfide bond. NMR structural determination indicated a bent helix in solution and bound to MDM2. The bicyclic peptide had improved protease stability, and we demonstrated that protease resistance could be measured both on the bacterial surface and in solution, enabling the method to test and/or screen for additional drug-like properties critical for biologically active compounds. We show that surface stabilization improves the correlation between binding measured on bacterial surfaces and in solution, demonstrating the broad potential of this technique.

Introduction

Estimates based on the human genome indicate that approximately two-thirds of all disease-associated genes are 'undruggable' by current therapeutics[1]. They reside inside cells, out of the reach of biologics, but lack a small hydrophobic binding pocket necessary for small molecule therapeutics[2,3]. This has led researchers to push the limits of intracellular therapeutics to larger sizes, capable of binding and disrupting intracellular protein function. Peptides, by mimicking protein binding epitopes, are an attractive option for target binding, but small linear peptides typically suffer from several liabilities including rapid proteolysis and low binding affinity. Covalent modification of peptides, however, can endow these agents with drug-like properties, such as oral delivery, high affinity, and increased stability[4–6].

One approach to improving drug properties involves introducing a covalent linker between two amino acids spanning 1 or 2 turns of the helix, which can improve affinity, in

vivo stability, and cellular uptake[7–10]. A vast and diverse literature exists on chemical methods to modify peptides and peptide libraries to connect these residues, including disulfide and amide bond formation, olefin metathesis, azide-alkyne cycloaddition, aryl-cysteine bond formation, and cysteine Michael addition, among others[11–18]. These approaches are nicely reviewed in Derda and Jafari 2018[19]. Some of the pioneering work was done by Roberts and colleagues using mRNA display[20] and demonstrated the power of stabilized libraries, and these technologies have been advanced to screen for peptides with multiple modifications[21], bicyclic peptides[17], and specific secondary structures such as alpha helices[22]. These stabilized alpha helices in particular have multiple applications including molecular imaging and intracellular therapeutics to disrupt protein-protein interactions[23]. For example, the p53-MDM2 complex involves a helix on p53 interacting with a groove on MDM2. This therapeutically important interaction causes downregulation of the central tumor suppressor protein p53. Due to the high frequency of dysregulation in many cancer types[24], there is a strong and multi-decade effort underway to develop better therapeutic inhibitors of this interaction. By disrupting the complex, p53 can no longer be downregulated by MDM2, increasing its tumor suppressor activity. Challenges remain for these and other stabilized peptides in this nascent field, with improvements to affinity, for instance, being sensitive to the positioning of the two modified amino acids and the linker identity. Improper peptide design can result in abrogation of binding[25]. Manual optimization of the staple position and flanking residues requires time-consuming solid phase peptide synthesis and affinity measurements, which results in low sampling

of the available design space (typically > 10^{12} peptide sequences) and a detrimental impact on peptide development.

The inherently vast chemical and sequence spaces have led to the development of multiple high-throughput techniques for stabilized peptide discovery. For example, DNA barcoded chemical-peptide libraries with reactive cysteine bridging have been developed to identify molecules that bind in the sub- and low nanomolar dissociation constant (K_d) range. However, relatively small library sizes are typically achieved with DNA barcoded and one-bead-one-compound libraries. In contrast, phage display allows for much larger library sizes[26]. Phage display can suffer from difficulties in achieving the highly efficient non-natural amino acid incorporation that is required for certain chemistries[27]. The phage display selection process of panning also does not yield precise values of affinity or stability, measurements that are accessible via cell surface display techniques. Phage therefore requires separate solid phase peptide synthesis and affinity quantification for validation, similar to the staple optimization challenges described above. However, due to concerns over undesirable reactivity with existing ubiquitous amino acid residues (e.g. cysteine and lysine) involved in alkylation or amide bond forming stabilization techniques, these chemistries are not suitable for selective reaction on the surface of cells. Therefore, a bio-orthogonal stabilization chemistry (i.e. one which doesn't react with common biological functional groups) was chosen for on-cell peptide stabilization and directed evolution.

The demand for next-generation peptide screening approaches led us to develop bio-orthogonal Stabilized Peptide Evolution by E. coli Display (SPEED), an approach

involving display of stabilized peptides on the surface of methionine auxotrophic E. coli. E. coli can display a large number of peptides on the cell surface, enabling quantitative on-cell screening (e.g. by fluorescence activated cell sorting). Using bio-orthogonal chemistry, directed evolution can be performed with the stabilizing linker in place, which often makes important target contacts in addition to stabilizing the structure[9,28]. Tirrell and coworkers demonstrated robust and highly efficient substitution of methionine by azidohomoalanine (AHA) in metE knockout E. coli[29], and several groups, including our own, have demonstrated the utility of incorporating multiple azides for cross-linking and helix stabilization[12,13,15]. By modifying the bacterial display eCPX scaffold[30], we conducted directed evolution of a cell-surface stabilized MDM2-binding peptide library of > 10^8 mutants. Using a randomization scheme that fixed the position of the cross-linking side chains but permitted the incorporation of natural amino acids including cysteine residues, we selected a novel bicyclic sequence with high affinity (1-2 orders of magnitude higher binding affinity than Nutlin 3a, a potent small molecular inhibitor of the intracellular p53-MDM2 interaction) with increased protease stability.

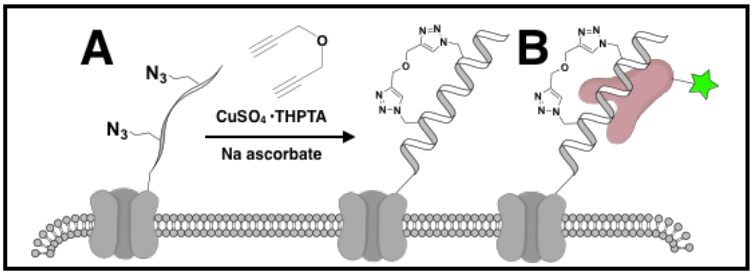

Scheme 1. Stabilized peptide engineering with E. coli display (SPEED). A: On the bacteria surface, the displayed peptides are reacted with a stabilizing, bis-alkyne

molecule (shown here as propargyl ether). B: Displaying bacteria are then incubated with a ligand of interest. After display, stabilization, labeling, and selection, the plasmids of desired cells are purified and re-transformed into fresh cells, completing the directed evolution cycle.

Results

In Situ Stabilization and Directed Evolution Using Chemical Biology

Due to the complex milieu of biomolecules on the surface of bacteria compared to phage, we selected a bio-orthogonal chemistry for in situ conjugation and peptide stabilization with a linker. The use of two identical non-natural amino acids in the peptide sequence requires an efficient and robust system for incorporation in large libraries (due to the dependence on the square of the incorporation efficiency). The residue replacement strategy of azidohomoalanine for methionine in bacterial auxotrophs satisfies all these criteria as >95% incorporation[31,32] is achievable. Once displayed, the peptide was stabilized with a bis-alkyne linker using copper(I)-catalyzed azide-alkyne cycloaddition (Scheme 1A). After surface reaction, the bacteria were incubated with the target protein (scheme 1B) to enable selection of binders in the presence of the stabilizing cross-linker on a library of > 10^8 compounds. The cell-surface screen also allowed rapid monitoring of affinity maturation without the need for sequencing, peptide synthesis, and solution phase binding measurements[33]. The use of a strong promoter (T5) and removal of methionine residues in the eCPX protein resulted in surface expression of ~10^4 azide-containing peptides per cell as quantified by fluorescent beads (Figure II - 1A) that could be specifically reacted (Figure II - 1B), highlighting the utility of a bio-orthogonal reaction. By titrating the linker concentration to balance the surface reaction yield versus doubly

reacted (bis-adduct) peptide (Figure II - 1C), we were able to achieve an estimated 75% stabilization on the surface (Figure II - 1D). The extent of stabilization was calculated based on measurements detailed in the methods and supporting information section since there is no mass change upon the 2nd cycloaddition reaction (precluding mass spectrometry analysis).

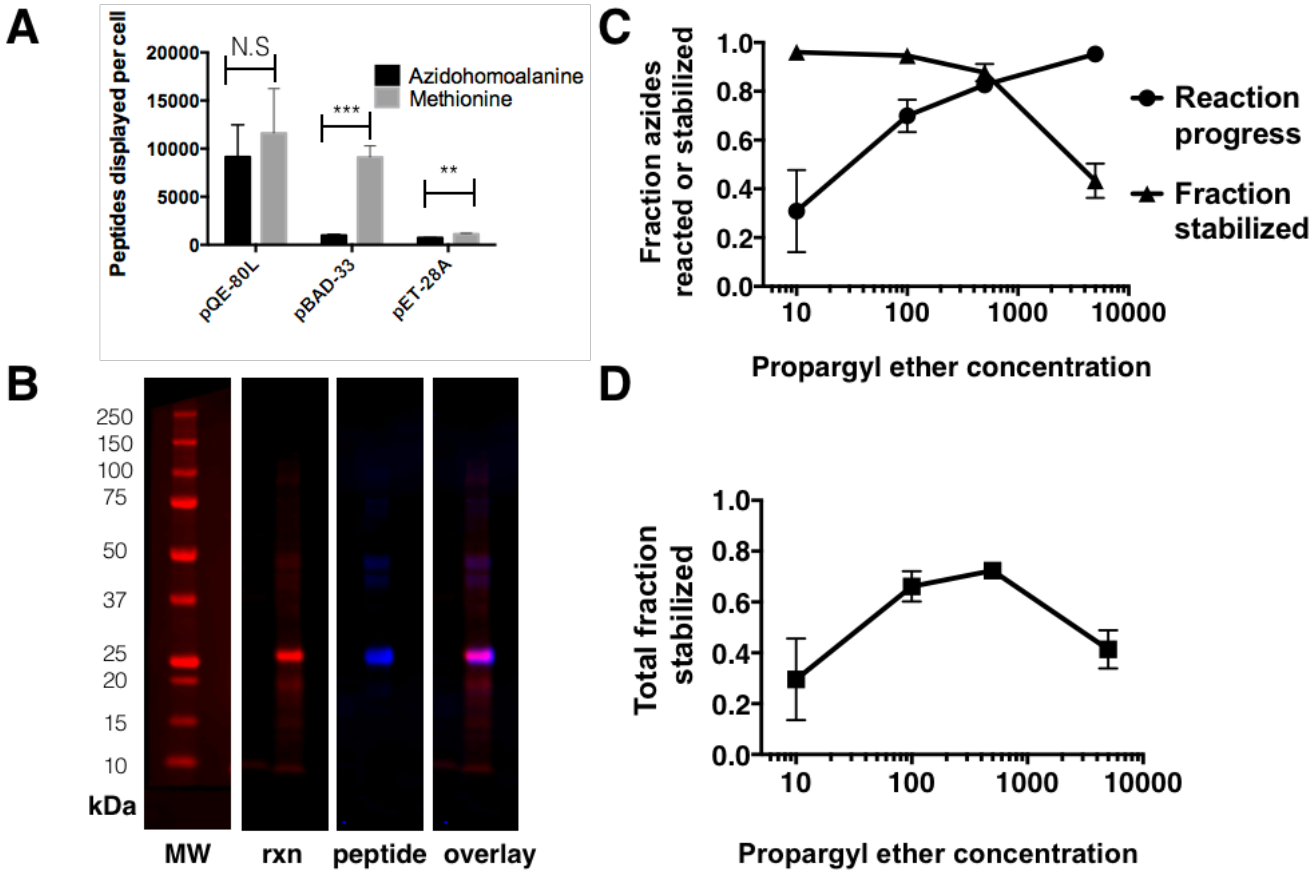

Figure II - 1. Chemical Biology Enabled Stabilization.
A: Comparison of display levels conferred by different vectors with and without azidohomoalanine incorporation. In this example, the 39 amino acid exendin peptide is displayed, labeled with an anti-exendin and fluorescent secondary antibody, and quantified by flow cytometry using quantitative beads (n = 3 independent bacteria cultures, unpaired t test two-tailed df = 4; t = 0.75, p = 0.50; t = 11.7, p = 0.0003; t = 6.61, p = 0.00270 respectively). B: SPD-M0-E(-2) with an HA tag generated using primers 9 and 10 displayed and reacted with SCy5-alkyne (red) and blotted with anti-HA (blue). C:

Reaction progress and fraction of reacted peptides that are also stabilized as a function of propargyl ether concentration (n = 3 independent blots per data point). D: Fraction of surface displayed peptides that are stabilized as a function of propargyl ether concentration (n = 3 independent blots per data point).

Library Design and Selection

P53-derived peptides provided an excellent model system and medically relevant target to develop a cell surface display screening method for stabilized alpha helices. In the native p53 – MDM2 interaction, residues F19, W23, and L26 are involved in key hydrophobic contacts[34] and mutagenesis studies have shown the importance of these for binding[35]. In fact, mutating either the phenylalanine or tryptophan to alanine (F19A or W23A) resulted in no detectable binding on the bacterial cell surface (Figure II - S1B). The individual contributions and interactions of and between other residues is less understood, and the formation of helix-stabilizing salt bridges and hydrogen bonding can influence binding[10,36]. In the context of chemical stabilization, we sought to investigate the roles of the less critical residues in native-like p53 interacting sequence (ETFXDLWRLLXEN) [12,37] by creating a library with NNC codons in the place of these amino acids while keeping the highly conserved F19, W23, L26, and azidohomoalanine positions 20 and 27 fixed (Figure II - 2A). The library generated had a size of $3x10^8$ transformants.

One round of magnetic-activated cell sorting (MACS) and serial rounds of fluorescence-activated cell sorting (FACS, up to seven) on the stabilized peptide library were conducted to select for improved affinity to MDM2 as assessed with the bacterial surface-displayed stabilized peptides (Figure II - 2B,C). After each round of selection, we

isolated the plasmids and directly transformed these into fresh cells (due to low viability after surface reaction) for sequencing or additional rounds of selection. Several positions had a high degree of residue conservation during selection, especially Y22 and D25 (Figure II - 2B, II - S2). After round 3, the apparent binding affinity for MDM2 by stabilized peptides displayed on the bacteria surface was measured for several clones to verify the method was selecting higher affinity sequences. We measured the affinity of two clones, SPD-M3-G1 and SPD-M3-V1 and found apparent K_d values of 2.0 and 9.8 nM respectively on the bacterial cell surface, which appeared promising (Table II - I, Figure II - 2C). Bulk-library labeling by MDM2 showed consistent improvement in signal over sorts (Figures 2A, S3). We also characterized several clones from very early in the sorting campaign (post-MACS and post-two rounds of FACS) to demonstrate significant affinity improvements (Figure II - S4). After seven rounds of sorting, we found that all clones measured show significantly improved apparent affinity over SPD-M0-E(-2) on the bacterial cell surface (Figure II - S5).

Table II - I – Measured dissociation constants of peptides
K_d values were determined on the bacterial surface (BSD, soluble MDM2) and in solution (BLI, surface-bound MDM2). Also included are CD-measured helicity values.

Name	Sequence	BSD K_d (nM)			BLI K_d (nM)			Helicity (%)		
		Stabilized (S)	Non-stabilized (NS)	Ratio (NS/S)	Stabilized (S)	Non-stabilized (NS)	Ratio (NS/S)	Stabilized (S)	Non-stabilized (NS)	Ratio (S/NS)
SPD-M0-E(-2)	ETFXDLWRLLXEN	9.6 ± 1.6	8.7 ± 0.2	0.9	15 ± 5.3	113 ± 16	7.5	53	30	1.8
SPD-M0-E(-1)	**Q**TFXDLWRLLXEN	11 ± 6.2	13 ± 6.8	1.2	17 ± 3.4	157 ± 29	9.2	40	29	1.4
SPD-M0-E(0)	**Q**TFXDLWRLLX**Q**N	12 ± 4.8	17 ± 5.5	1.5	74 ± 28	454 ± 106	6.1	41	37	1.1
SPD-M3-G1	GGTFXGYWADLXAF	2.0 ± 0.31	2.9 ± 1.0	1.4	5.1 ± 3.9	21 ± 3.7	4.1	18	17	1.1
SPD-M3-V1	**VLS**FXD**Y**W**N**LLX**GS**	9.8 ± 3.4	64 ± 33	6.6	14 ± 4.3	131 ± 40	9.4	NM	NM	-
SPD-M6-V1	VCDFXCYWNDLXGY	1.4 ± 0.10	15 ± 4.8	11	1.7 ± 0.16	6.8 ± 2.8	4	28	3	9.3
SPD-M0-E(-2)-F19A	ET**A**XDLWRLLX**EN**	ND	ND	ND	604 ± 177	>10,000	-	50	14	3.7

To confirm these affinities corresponded to higher binding when the peptide is in solution and validate the technique, we synthesized several sequences by solid-phase peptide synthesis (>95% purity, Table II - S2) and measured solution phase peptide binding by bio-layer interferometry (BLI) with immobilized MDM2. Selected clones were identified for solution phase characterization and comparison with bacterial surface

displayed apparent binding affinity values (Table II - I). Sequences were named according to the convention SPD (stabilized peptide display)-M (sort round)-first amino acid and unique number. These included the original p53-like peptide sequence (-2 formal charge, SPD-M0-E(-2)) and two site-directed charge mutants (E17Q mutant with a -1 formal charge, SPD-M0-E(-1), and E17Q and E28Q double mutant SPD-M0-E(0)) to evaluate the ability to characterize charge mutants given the importance for intracellular access[8,9]. SPD-M3-G1 was chosen as a higher affinity mutant from early in the screening process and SPD-M3-V1 due to the large increase in apparent binding affinity upon stabilization on the bacterial surface. Sequencing of 40 clones from round 7 of FACS showed enrichment of the SPD-M6-V1 sequence (13 of 40 clones, Figure II - S5), which contained a pair of i, i+4 cysteine residues. Mutagenesis of either cysteine residue to serine resulted in a greater than two-fold loss in binding (Figure II - 2D), indicating a direct role for the pair and likely disulfide bond formation. While this was within our design space, the evolution of an i,i+4 cysteine-containing sequence was unexpected from a topological perspective. Mass spectrometry and NMR confirmed disulfide bond formation for the synthesized peptide (Tables S2 and S3). The F19A mutant of the original starting sequence (SPD-M0-E(-2)) was included as a negative control (SPD-M0-E(-2)-F19A).

Development of peptide binders using bacterial surface display methods has sometimes led to a disconnect between the affinity of loop-insertional fusions versus solution phase binding[38]. To test the relationship between cell surface affinity measurements and solution phase binding, the affinity (dissociation constant) of stabilized and non-stabilized alpha helices was measured both on-cell (by bacterial surface display,

BSD) and in solution using BLI (Table II - I and Figure II - S6). We found that all 7 peptides for which we determined affinities exhibited improvements in binding in solution upon stabilization with propargyl ether, ranging from 4-fold for SPD-M6-V1 to 9.4-fold for SPD-M3-V1 (Table II - I and Figure II - S6). The differences in apparent affinity upon stabilization for the bacterial surface displayed peptides were more modest. The stabilized peptide affinity on the bacteria surface was similar to the stabilized peptide affinity in solution as expected, but the non-stabilized form on-surface also had similar affinity as the stabilized forms for most peptides (Table II - I). Binding affinity measurements and selection on the bacterial cell surface were performed using fluorescently tagged MDM2-GST because of the spurious loss of binding for some clones when incubated with smaller (truncated) MDM2-fluorescent dye conjugates. These same clones bound biotinylated MDM2 truncate (Figure II - S4A) and fluorescent MDM2-GST fusion protein (Table II - I) with high affinity, indicating the dye size/charge on the smaller truncate was likely mediating the effect. All BLI measurements used biotinylated MDM2 truncate. Avidity is a concern for accurate measurement of affinities on a crowded surface like the E. coli outer membrane. To verify the GST tag did not induce confounding effects from dimerization and impact affinity measurements, we measured K_d values with biotinylated MDM2 truncate (e.g. SPD-M6-V1 had an apparent K_d of 0.4 nM, figure S4A). As it did not appear that avidity effects were playing a strong role in explaining the closer measured affinities of stabilized and non-stabilized peptides on the bacterial cell surface, we hypothesize that the secondary structure of the non-stabilized peptides may be more helical on the surface, potentially from molecular crowding effects from the membrane or

lipopolysaccharide coating[39]. Molecular crowding can increase peptide helicity, but even weak intermolecular interactions with the crowding agents can dramatically reduce the effect[40,41], which could explain the sequence dependence of the phenomenon (Table II - I). Negative control peptides SPD-M0-E(-2)-F19A and SPD-M0-E(-2)-W23A did not exhibit measurable binding as displayed on the bacterial cell surface (Figure II - S1). Secondary structure (helicity) as examined by circular dichroism (CD) did not seem to correlate strongly with binding (Table II - I, Figure II - S7), indicating a more complex relationship of entropic and enthalpic effects than simply high helix pre-organization resulting in higher binding affinity[42,43].

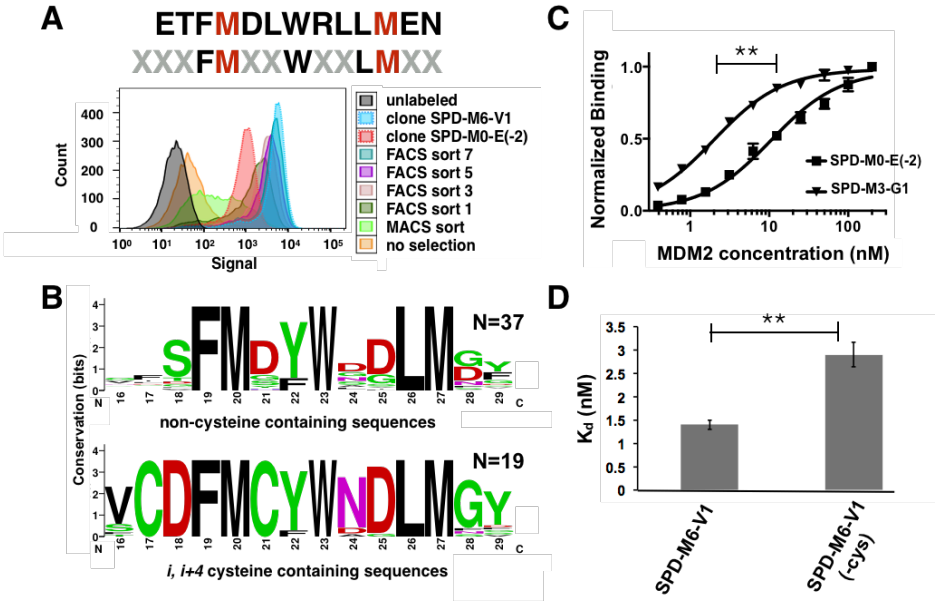

Figure II - 2. Stabilized Peptide Library Design and Selection.
A: top: randomization scheme for library generation showing the residues randomized (gray), kept constant (black), and stabilization sites (red). Bottom: population level and individual clone analysis by flow cytometry. Histograms are shown for approximately 12,000 events for samples labeled with 2.5 nM MDM2-GST. “No selection” is the original library containing 3 x 10^8 transformants. “MACS” refers to the population obtained from one round of positive selection with magnetic beads. FACS 1, 3, 5, 7 refer to the populations sorted after 1, 3, 5, and 7 rounds of fluorescence-based sorting. The even-numbered sorted populations are not shown here for clarity. B: Logo plot results of

selection showing relative frequencies of amino acids in non-cysteine containing sequences and i,i+4 containing sequences. C: SPD-M3-G1 exhibits a nearly 5-fold improvement in affinity over the starting sequence SPD-M0-E(-2) after only 3 rounds of sorting indicating the selection following surface reaction is effective (n = 3 independent trials of duplicates per data point, unpaired t test two-tailed, df = 4. t = 8.036, p = 0.0013). D: Disulfide bond formation is important for binding of SPD-M6-V1 and mutation of one of the cysteine residues results in reduced affinity on the bacteria surface (n = 3 independent trials, unpaired t test two-tailed, df = 4. t = 4.97, p = 0.0076).

Protease stability

For efficacy in vivo, peptides must survive protease exposure in a variety of biological milieus such as in the bloodstream and at the site of administration (i.e. for subcutaneously administered drugs[7] or for oral delivery[44]). We assessed the stability of several peptides on the bacterial surface and in solution using chymotrypsin to determine if cell surface display would enable measurement or screening for protease stability. The three stabilized peptide sequences tested, SPD-M3-G1, SPD-M0-E(-2), and SPD-M6-V1 showed the same trends on the bacterial surface (Figure II - 3A) as in solution (Figure II – 3B). Likewise, the non-stabilized peptides were much less protease-resistant on the surface (Figure II - 3C) and in solution (Figure II - 3D) as expected. Note that the time, temperature, and enzyme concentrations were optimized separately (surface versus solution) to ensure a good dynamic range for each. The disulfide loop in the SPD-M6-V1 likely contributes to its overall higher stability properties.

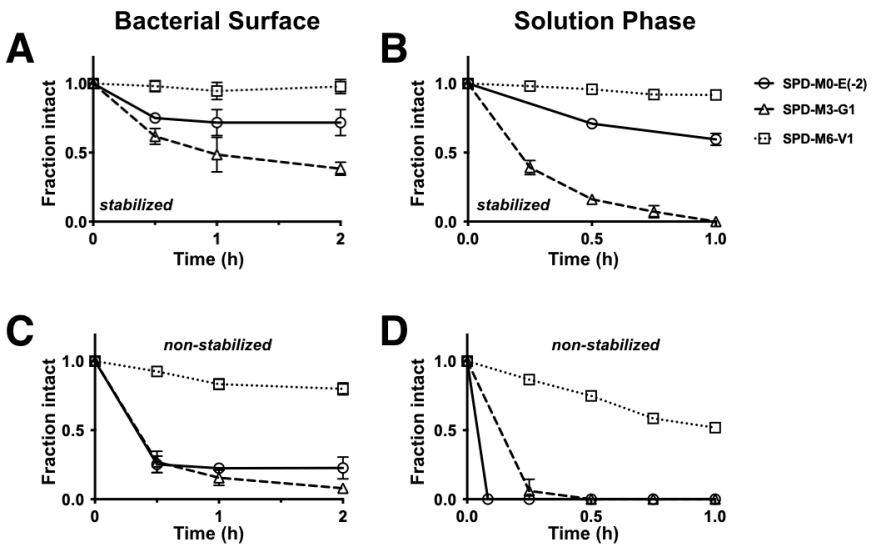

Figure II - 3. Chymotrypsin digest trajectories.
A: Bacteria displaying stabilized peptides were treated with chymotrypsin (1 μg/mL on ice) and labeled with MDM2-GST-AF647 for peptide detection. B: Stabilized peptides synthesized by SPPS were treated with chymotrypsin (5 μg/mL at 37 C) and quantified by HPLC for validation. C: As in A, except with non-stabilized peptides. D: As in B, except with non-stabilized peptides.

Structure determination

The directed evolution of a disulfide bond was surprising, since disulfide bonds generally destabilize alpha helices as seen by the low helicity signature (4%) from CD spectroscopy for SPD-M6-V1, non-stabilized (Table II - I and Figure II - S7). Therefore, we calculated the structure by solution NMR to investigate the mechanism(s) that gave this sequence a selective advantage. Homonuclear (^{1}H-^{1}H) NOESY (nuclear Overhauser effect spectroscopy) and TOCSY (total correlation spectroscopy) experiments were conducted to determine the free solution structure of the SPD-M6-V1 peptide (Figure II - 4, II - S8). The observed peaks implied a predominantly alpha-helical conformation for the stabilized structure with an interesting bend conferred by the bis-triazole linker (Figure II - 4A, Figure II - S7C). ^{1}H NMR spectrum indicated no significant structural changes in the peptide

upon binding to MDM2, implying that the molecule is highly ordered in solution, owing to the stabilization conferred by both the overlapping i, i+4 disulfide bond and the i, i+7 bis-triazole linker (Figure II - 4B,C).

To understand the interaction of SPD-M6-V1 with MDM2, one-dimensional saturation transfer difference (STD) NMR experiments were performed to identify peptide atoms interacting with the MDM2 binding interface. These data indicate close interactions between the target and Val16, Cys17, and several aromatic residues. There is also an interaction between the bis-triazole linker and MDM2 (Figure II - 4D). This interaction highlights a potential enthalpic contribution from the linker in addition to the entropic benefit of pre-organization, another advantage of screening in the context of the linker. The linker-target interaction is consistent with crystallographic structures reported for other stabilized peptide binders of MDM2[28] and other proteins[9].

Computational docking using Autodock Vina software was consistent with the STD data. In the calculated docking poses (Figure II - 4B), the three key hydrophobic residues F19, W23, and L26 are oriented towards the binding pocket as expected from the canonical p53-MDM2 interaction. The highly conserved Y22 residue appears to lie in a shallow notch defined by residues 93-96 of MDM2 and may be involved in pi-CH interactions with K94. D17, which was observed in 100% of i,i+4 binders (Figure II - 2B) may play a key role in enforcing binding conformation, together with the disulfide bond.

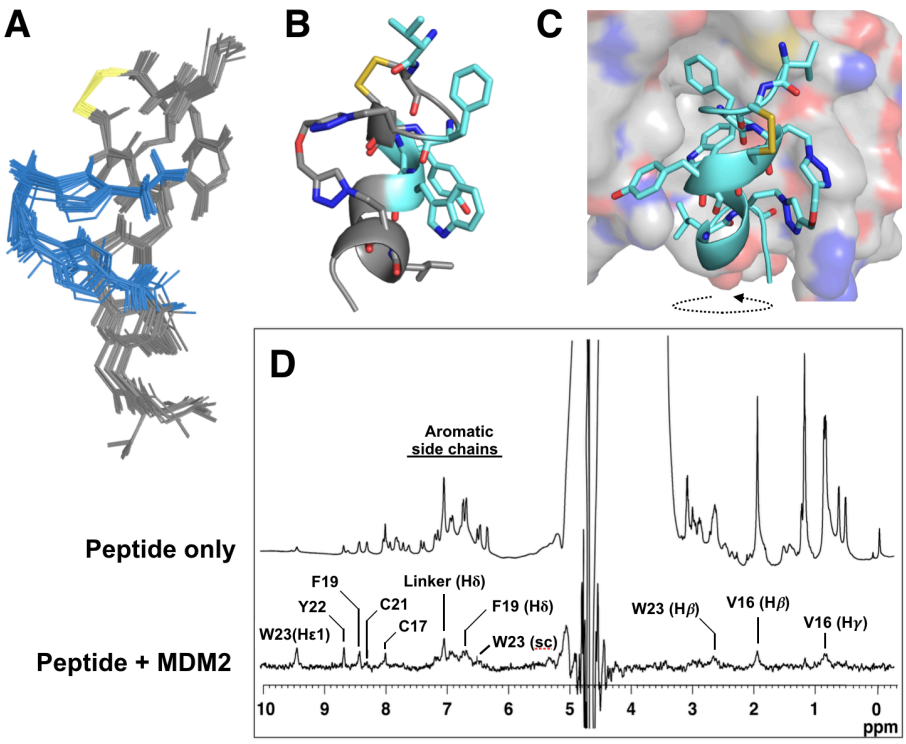

Figure II - 4. Structural characterization using solution NMR.
A: Ensemble of 20 lowest energy structures and B: representative single structure. C: Docked model showing likely bound conformation. D: Saturation transfer difference (STD) spectrum of SPD-M6-V1 bound to MDM2.

Discussion

Small, helical peptides are under intense investigation for applications in molecular imaging[15] and therapeutics[4,10,26] due to their unique physicochemical properties and the possibility of hitting currently 'undruggable' targets. Specifically, their potential to overcome limitations of large biologics by entering cells and ability to target intracellular proteins lacking small molecule binding pockets would dramatically increase the number of available drug targets in the human genome. Antibody-based biologics excel at targeting proteins and have achieved major clinical success in oncology, immune system disorders, and other diseases but are limited to extracellular targets owing to their large

size. Small molecule drugs can readily access cytosolic targets. However, intracellular protein-protein interactions involve large surface areas and typically lack small hydrophobic binding pockets, making a small molecule approach intractable for many cases[1,3]. These physical factors can also result in low potency and off target effects by small molecules, as they lack the physicochemical properties to maintain high affinity and high selectivity. Helical peptides lie at the intersection of these two fields, where their size is small enough for potential cytosolic access but large enough to specifically disrupt protein-protein interactions prevalent in cell signaling to enable targeting of new pathways in disease. Intracellular delivery is still a major hurdle, and high affinity is critical to efficacious targeting since intracellular peptide concentrations are likely to be low.

The complexity of protein-protein and protein-solvent interactions, particularly with dynamic binding interfaces, makes computational and rational design of high affinity binders challenging. Indeed, the design of stabilized helical peptides has largely been limited to targeting interactions with a solved X-ray crystal structure where an inhibitor can be rationally obtained[45–48], prompting us to develop a directed evolution platform for stabilized peptide engineering of novel drug leads on the cell surface, with several advantages over current techniques.

As ‘guardian of the genome,’ the critical p53 tumor suppressor protein is often disrupted in cancer, including through downregulation by the ubiquitin ligase MDM2[24]. Recent peptide efforts toward targeting the p53-MDM2 interaction have centered around hydrocarbon stapling, a promising approach with one candidate ALRN-6924 currently in phase II clinical trials[5]. Stapling is thought to confer improvements in binding from locking

one or more turns of a peptide, resulting in helical preorganization. However, current technologies for engineering these structures have several drawbacks including limited library size, multi-step characterization, or sequential sequence/linker optimization that can miss synergistic interactions. Given the importance of the therapeutic target and knowledge base around this protein interface[10,34,35], we used the p53-like peptide as a model system for engineering high affinity alpha helices using in situ stabilization.

In this approach, we applied non-natural amino acid incorporation and bio-orthogonal chemistry for in situ stabilization of surface displayed peptides followed by directed evolution using E. coli to engineer high affinity molecules (Scheme 1). Bacterial display allows rapid identification and decoding of high affinity binders through surface-enabled affinity measurements (in contrast to phage display, mRNA display, and bead-based libraries) and high throughput screening, enabled by larger libraries than typically generated with peptide arrays, one-bead-one-compound, yeast surface and mammalian surface display. Furthermore, we could characterize binding of several thousand clones by flow cytometry after every round of sorting (Figure II - 2A), allowing us to monitor selection progress in a straightforward manner. Engineering the display and stabilization reaction on the surface of bacteria using chemical biology techniques (Figure I -) resulted in the selection of high affinity sequences (low single-digit nanomolar dissociation constants) with improved binding affinity in the stabilized form (Figure II - 2).

Binding of multivalent ligands to the cell surface can result in avidity effects where, for example, rebinding of the second domain in a bivalent interaction slows apparent dissociation. Because GST fusion can cause dimerization of the binding domain[49](MDM2

in this example), we designed the selection scheme to mitigate potential impacts of avidity and expression levels on the cell surface. For several sorting rounds, we ran a competition sort where we first labeled with AF647-MDM2-GST followed by a wash and AF488-MDM2-GST. The addition of the competitor AF488-tagged molecule in excess would be able to effectively compete off AF647-MDM2-GST with high avidity/low affinity by preventing rebinding but not impact high affinity interactions that lack fast dissociation and rebinding. Because these rounds selected for high AF647 relative to AF488, only those clones with high monovalent affinity that were resistant to competition by AF488-MDM2-GST would be selected. This is seen with the lead clone selected from the sort (SPD-M6-V1) having a high monovalent affinity with similar measurements by BLI and on the bacterial surface. However, avidity could be leveraged with this technique to improve the selection of very weak binders early in the directed evolution process, such as by preloading magnetic beads with biotinylated target to increase multivalent interactions.

One of the original goals of screening peptides containing a cross-linking 'staple', as opposed to post-screening stapling, was to avoid steric clashes that would result in 'false positives' during the selection process (i.e. sequences selected from the library that lose affinity after the addition of the linker). This is indeed the case, where placing the linker in a different location lowers the affinity on the bacterial surface (data not shown). We were also able to generate a series of affinity mutants with varying charge and lipophilicity for future investigation, given the importance of physicochemical properties on cytosolic access[8,9] and the potential to detect favorable interactions with the staple itself[9,28]. Interestingly, there were some sequences (e.g. SPD-M3-V1) that had a low

apparent binding affinity when not stabilized on the bacterial surface (K_d = 64 nM) but demonstrated high apparent affinity when stabilized on the bacterial surface (K_d = 9.8 nM) or in solution (K_d = 14 nM). This indicates that stabilization can also help avoid 'false negatives' where a sequence that exhibits high affinity when stabilized in solution (a desired sequence) might be missed when using a selection scheme without surface stabilization due to low apparent affinity (when non-stabilized) on the bacterial surface.

From a structural perspective, our work here suggests that stabilization of a single helix improves selection of high affinity ligands, but using directed evolution, we found an additional conformational constraint that further enhanced binding to the target: disulfide loops (Figures 3B and 3D). We did not anticipate the selection of disulfide bonds since they typically destabilize alpha helices and the peptides bind MDM2 in a helical conformation. However, we did allow for selection of peptides containing cysteines through the NNC degenerate codon, so disulfide bonds were within the possible evolution space. In fact, over two-thirds of the clones sequenced after round 7 of FACS had cysteines at i,i+4 or i,i+5 positions, strongly suggesting selection pressure for disulfide bonds (Figure II - S5A). While increased constraint within a binding partner does not necessarily result in improved affinity due to enthalpy/entropy compensation[43], disulfide bonds often evolve under selection to improve the binding energy of proteins/peptides[50]. We obtained 3D NMR structures to get a more detailed picture of the impact of pre-organization on binding. NMR data and docking analysis showed interactions between the cysteine residues and MDM2, one interaction between the linker structure and MDM2, and a rigid structure induced by both constraints (Figure II - 4C and 4D). Therefore, the

affinity improvements observed upon linker stabilization appear to result from both entropic contributions (conformational constraint) and direct enthalpic interactions. This is similar to the interactions observed between other stapled peptides and their targets, including an MCL-1 binding molecule[9] and a p53-based hydrocarbon stapled peptide and MDM2[6], and it supports the strategy of directed evolution in the presence of the linker as demonstrated here. We hypothesize that the disulfide bond further constrains the structure in parallel with the bis-triazole staple. Together, we posit that this structural rigidity confers binding improvements through a decrease in entropic penalty of binding and direct interactions further contribute to the free energy of binding.

Notably, the highest affinity sequence from the selection, the disulfide-containing peptide SPD-M6-V1, would likely not have been discovered using non-orthogonal cysteine-directed strategies such as alkylation[28] or arylation[17]. SPD-M6-V1 without stabilization exhibits poor helicity (Table II - I), which is partially remedied by reaction with the bis-alkyne linker, and this results in high affinity. Its relatively poor bacterial surface affinity without click stabilization (15 nM, worse than the original template sequence) also implies that stabilization prior to sorting was necessary for discovery. The original linear starting sequence (K_d = 113 nM, table II - 1) had an affinity similar to the MDM2 inhibitor Nutlin 3a[11]. Click-stabilization increased the affinity ~7-fold followed by directed evolution to improve the affinity ~8-fold yielding a 1.8 nM binder. This value is similar to the reported K_d of pDI (8 nM for sequence LTFEHYWAQLTS[51]). However, pDI is a linear peptide with negligible activity in cells[52], likely due to proteolytic instability and reduced intramolecular hydrogen bonding for crossing membranes. Therefore, it required extensive stapling and

amino acid optimization to develop ATSP-7041[51], the preclinical precursor to ALRN-6924. The current platform yielded a high affinity stabilized peptide binder directly from the library and work is ongoing to investigate sequence- and linker- dependence on cellular and in vivo efficacy.

We were surprised to find that the correlation between the binding affinity on the bacterial surface and in solution was stronger for the stabilized peptides than the linear versions (Table II - I and Figure II - S11). In particular, the higher apparent affinity of unstabilized peptides on the bacterial cell surface relative to affinities in solution was unexpected. These peptides are fused only by their C-termini, so they are not within a constrained loop. The outer leaflet in gram negative bacteria such as E. coli is primarily composed of lipopolysaccharide (LPS) that forms a coat that is several nanometers in thickness[39]. We speculate that the observed enhancement of surface affinity without chemical stabilization could be due to increased helicity/pre-organization from molecular crowding on the bacterial surface. Molecular crowding can increase peptide helicity, but even weak intermolecular interactions with the crowding agents can dramatically reduce the effect[40,41], which could explain the sequence dependence of the phenomenon (Table II - I). We speculate that the bacterial surface environment itself may have imparted some helicity resulting in affinities closer to the stabilized alpha helices but in a less robust manner than stabilization by the linker.

Despite the advantages of this approach, there are several limitations and areas for improvement. Even with library sizes of ~10^9 in bacteria, the diversity of 11 positions is still much larger at ~$2x10^{14}$. Computational methods (eg. by Bullock 2011[6]) could be

used as a starting point followed by maturation of affinity, linker location, and stability using the present approach. For three key properties of intracellular biologics – membrane permeability, binding affinity, and stability – only the latter two can be engineered with the presented approach. As knowledge around membrane permeability improves, deep sequencing of libraries[53] sorted for affinity and stability could be used to identify peptides with properties associated with improved membrane permeability, such as high amphiphilic moments. Finally, the proximity of helices to the bacterial surface could impact quantitative measurements. As non-natural amino acid incorporation improves in other organisms such as yeast[54], where the Aga2 mating protein involved in extracellular protein-protein interactions (flocculation) has been adapted for surface display and panning[33], additional cell-surface methods may improve the molecular engineering of stabilized alpha helices.

This work represents a unique application of helix stabilization and cell surface display to engineer new affinity ligands. The directed evolution of stabilized helices yielded the novel bicyclic peptide SPD-M6-V1 containing a disulfide bond and double-click staple for the two macrocycles, a motif that due to its high binding affinity and customizability has translational potential upon chemical optimization (such as replacing the disulfide with an intracellularly stable linker). The stability and intra-molecular hydrogen bonding from these stabilized alpha helices increase the efficiency of intracellular delivery[55] and are the subject of current investigation in our lab and others. The surface display and binding of other peptides (Figure II - S9) highlights the potential for using this technique against additional targets. In summary, the combination of non-

natural amino acid incorporation and bio-orthogonal chemistry can be used with directed evolution for the molecular engineering of high affinity stabilized alpha helices through in situ stabilization and screening for novel drug leads.

Methods

Plasmid construction and library design

All primers were purchased from Integrated DNA Technologies (Coralville, IA), and all restriction enzymes were purchased from New England Biolabs (Ipswich, MA). The eCPX gene from pB33eCPX (a gift from P.S Daugherty, Addgene plasmid # 23336) was modified to avoid extraneous AHA incorporation and reaction. All non-start codon methionine sites (M99, M153, M156) were mutated[56] to leucine with primers 1 and 2 to generate pB33-eCPX(-met) without a significant difference in surface display levels. eCPX(-met) was inserted into pqe80L using EcoRI and HindIII sites with primers 3 and 4 (see Table II - S1).

For surface display comparisons of vector systems, exendin-4 was cloned into pB33eCPX using primers 5 and 2 with SfiI as described in ref. 57. Exendin-4 was cloned into pet28A using primers 6 and 2 with pB33eCPX(-met)-exendin as the template, and restriction enzymes NcoI and HindIII.

The p53-like-peptide sequence ETFMDLWRLLMEN (SPD-M0-E(-2)) was cloned into pqe80L-eCPX(-met) using primers 7 and 8 to generate pQE80L-eCPX(-met)-SPD-M0-E(-2). For surface chemistry optimization, the HA tag was cloned adjacent and downstream of the peptide using SOE PCR with primers 9, 10, 8, and 11.

A library containing NNC degenerate codons to mutate all positions in the SPD-M0-E(-2) sequence except F19, M20, W23, L26, and M27 was generated using PCR as detailed in ref. 57 using primers 12 and 8 using pQE80L-eCPX(-met) as the template. Charge mutants involving the mutations E17Q and E28Q were made using primers 13 and 14 using pQE80L-eCPX(-met)-SPD-M0-E(-2) as the template to generate SPD-M0-E(-1) and SPD-M0-E(0).

SfiI cut and gel extracted insert was ligated into SfiI cut pQE80L-eCPX(-met) and transformed into electrocompetent methionine auxotrophic E. coli, a generous gift from J. van Deventer with cloning procedures adapted from ref. 57.

Surface display of individual clones

Individual clones were grown overnight at 37°C in M9 medium containing 20 amino acids as described in ref. 58 and diluted 1:25 in M9 + 20 AAs. Cells were grown to OD_{600} 0.6-1 (about 3 hours) at 37°C, centrifuged at 4000xg for 5 minutes, and then grown for 30 minutes in M9 medium containing 19 amino acids (no methionine) for metabolic depletion. Cells were centrifuged and then induced with 0.5 mM IPTG in M9 medium with 19 amino acids and 40 µg/mL azidohomoalanine at room temperature for 3 hours. Azidohomoalanine was synthesized in-house according to ref. 59. Cells were then reacted as below.

For flow cytometric quantification of exendin display in various vector systems, cells with the respective plasmid were induced as above and labeled with 10 µg/mL mouse anti-exendin (Abcam ab23407) in PBS/0.2% BSA. Cells were pelleted and

resuspended in PBS/BSA containing 10 μg/mL chicken anti-mouse AF647 (Thermo Fisher) and analyzed by flow cytometry. Median fluorescent values were compared with a standard curve made from Quantum Simply Cellular anti-Mouse beads (Bangs Laboratories) labelled with the same stock of chicken anti-mouse AF647.

Display and reaction conditions

The pBAD33 arabinose promoter system (originally utilized for bacterial surface display for tightly controllable expression and low induction-driven toxicity[60]) resulted in poor expression of peptide displayed in AHA incorporation conditions (Figure I - A). Likewise, low levels of display were obtained with the pET28A T7 system commonly used for over-induction of recombinant proteins, as was similarly observed by Ayyadurai and coworkers with homopropargylglycine (HPG)[61]. Cloning of the gene into the pQE80L/T5 vector (Figure II - S10C) resulted in robust expression under both methionine and AHA incorporation conditions, and reaction and gel analysis showed promising specificity of AHA incorporation (Figure II - 1B). Mutation of all non-start codon methionine sites (M99, M153, M156) resulted in decreased extraneous reaction (Figure II - S10A).

We optimized reaction conditions to maximize stabilized peptide yield on-surface. Propargyl ether was chosen as the bis-alkyne linker to connect the i, i+7 azides in the peptide sequences due to its helix-inducing propensity[15], flexibility, and solubility. With directed evolution using cell surface display, typically selected cells are immediately cultured after sorting, but the copper catalyst needed for the azide-alkyne stabilization reaction is toxic to bacteria[62]. We therefore tested several copper chelators (based on previously reported improvements in toxicity and reactivity[63]) and temperature/time

conditions but found that in order to achieve high reaction efficiency, the viability of the bacteria was too low for continual outgrowth after sorting (data not shown). The plasmids could be 'rescued' from the sorted bacteria by polymerase chain reaction (PCR), but PCR can introduce errors and biases into the sorted libraries (especially when the diversity is high)[64]. To avoid this bias, we directly transformed the plasmids into new bacteria following whole plasmid extraction with good yield[65]. The transformation efficiency of this step was approximately 1/3 of the number of sorted cells, in line with ref. 65, so we oversampled our desired stringency typically by 20x to account for sequence coverage and loss of clones from transformation. For example, with a library of diversity $1x10^6$ clones where the brightest 1% of cells were desired, $2x10^7$ cells were sampled and $2x10^5$ cells were collected, which typically yielded $6x10^4$ transformants.

We performed quantitative fluorescence analysis on western blots of cells reacted with either SulfoCy5-alkyne or SulfoCy5.5-azide dyes after reaction with the linker and normalized the signal to an anti-hemagglutinin tag (Figure II - 1C). From these experiments, we deduced the fraction of displayed peptide-specific azides that were reacted and the fraction of reacted peptides that were also stabilized to calculate the overall stabilization efficiency (Figure II - 1D) by fitting to a series of reaction equations (supporting information) since mass spectrometry cannot track the 2nd intramolecular stabilizing reaction. The concentration of propargyl ether that gave the best stabilization was 500 μM; this was used for all selection and characterization experiments.

Library expression

The libraries encoding p53 peptide variants were grown from frozen stock in M9 medium containing all 20 amino acids at 5-10x sequence coverage at starting OD_{600} of approximately 0.1. At OD_{600} 0.6-1, cells were centrifuged at 4000xg and methionine depleted for 30 minutes in M9 medium containing 19 amino acids (without methionine). Cells were centrifuged and then induced with 0.5 mM IPTG at room temperature in M9 medium containing 19 amino acids and 40 µg/mL azidohomoalanine for 4 hours at room temperature. Cells were then reacted as below.

On surface reaction of displayed peptide

For reaction characterization and binding measurements of unique sequences, typically 1 mL induced cells displaying AHA-incorporated peptide were centrifuged at 4000xg for 2 min and washed twice with ice-cold PBS (155 mM NaCl, 1 mM potassium phosphate, 3 mM sodium phosphate pH 7.4). The pellet was then reacted in 1.8 mL ice-cold PBS containing 100 µM $CuSO_4$, 500 µM Tris(3-hydroxypropyltriazolylmethyl)amine (THPTA), 5 mM sodium ascorbate, and 500 µM propargyl ether for 4 h at 4°C. After the reaction, the cells were pelleted and resuspended in 1 mL PBS containing 0.2% w/v bovine serum albumin (PBS/BSA). For library selections, these volumes were scaled up accordingly.

For surface reaction optimization, cells displaying AHA-incorporated SPD-M0-E(-2)-HA were washed once in PBS following propargyl ether reaction and then reacted further with 50 µM SCy5-alkyne or SCy5.5-azide with 100 µM CuSO4, 500 µM THPTA, and 5 mM sodium ascorbate overnight. Cells were then pelleted, washed 1X with cold

PBS, and then resuspended in 1 mL PBS. For each well, 5 µL cells were lysed in a total volume of 20 µL containing 50 mM Tris-HCl pH 6.8, 2% SDS, 10% glycerol, 1% beta-mercaptoethanol and 12.5 mM EDTA, and loaded onto a Bolt 4-12% Bis-Tris Plus gel (Invitrogen). Bands were transferred to a PVDF membrane using the iBlot system (Thermo Fisher), blocked overnight at 4°C with gentle shaking with 2% BSA in Tris-buffered saline with 0.1% Tween 20 (TBST), and probed with 2 µg/mL anti-HA in TBST (Thermo Fisher, clone 2-2.2.14) with 0.2% BSA for 4 hours at room temperature. After 3 washes in TBST, the membrane was probed with 1 µg/mL goat anti-mouse-IRDye800CW (Licor) for 1 hour at room temperature. The blot was scanned on a Licor Odyssey CLx scanning fluorescence imager following 3 washes in TBST and bands quantitated. The ratio of 700 nm channel fluorescence (for SCy5 and SCy5.5 dyes) to 800 nm channel (for anti-HA, loading normalization) was reported.

Protein expression and purification

pGEX-4T MDM2 WT was a gift from Mien-Chie Hung (Addgene plasmid # 16237) and was transformed into BL21DE3 cells and induced by 0.5 mM IPTG at 30°C for 5 hours after reaching OD_{600} = 1.0. Expressed GST-tagged MDM2 was purified as described by ref 66.

Magnetic selection with MDM2

MDM2-GST was biotinylated by reaction with NHS-PEG4-Biotin (Thermo Fisher). Library-expressing and reacted cells were labelled with 2 nM biotin-MDM2 at 4°C for 1 hour in 15 mL PBS/BSA and cells were washed once with PBS/BSA to remove weakly-bound and

residual biotin-MDM2. Labelled cells were incubated with Dynabeads MyOne Streptavidin T1 (Thermo Fisher) in a 1:1 ratio with end-over-end rotation at 30 rpm using MACSmix (Miltenyi Biotec). Following incubation, magnetic beads were isolated by application of a magnetic field and beads washed twice with 15 mL PBS/BSA. DNA from bound cells was isolated as follows: beads were resuspended in 250 µL buffer P1 from the Qiaprep spin miniprep kit (Qiagen), bound cells lysed with 250 µL buffer P2, and neutralized with 350 µL buffer. After centrifugation, the supernatant was applied to a Qiaprep column and after washing with buffer PE, DNA was eluted with 30 µL H_2O (yielding approximately 100 ng DNA) and re-transformed into electrocompetent methionine auxotrophic E. coli.

Fluorescence activated selection with MDM2

Following library expression and surface stabilization, the MACS sorted library underwent selection by increasingly stringent rounds of FACS on a MoFlo Astrios instrument as follows: FACS round 1: labeled with 1.5 nM MDM2-AF647, brightest 1.2% of events collected, $3x10^5$ transformants obtained; round 2: labeled with 0.2 nM MDM2-AF647, brightest 1.2% of events collected, $1.1x10^5$ transformants obtained; round 3: labeled with 20 nM MDM2-AF647 for 30 min, washed 2x, labeled with MDM2-AF488 at 200 nM. Top 2.5% of events positive for AF647 and low for AF488 collected, $1.1x10^5$ transformants obtained; round 4: similar scheme as round 3, brightest 15% of cells collected, $2.3x10^5$ transformants obtained; round 5: similar scheme as round 3, brightest 2% of events collected, $1.8x10^5$ transformants obtained; round 6: labeled with 0.5 nM MDM2-AF647, brightest 1% of events collected, $3.0 x10^4$ transformants obtained; round 7: labeled with 0.5 nM MDM2-AF647, brightest 0.05% of events collected, $3.2x10^3$ transformants

obtained. All cell labeling steps with primary MDM2-AF647 were done for a minimum of four hours prior to sorting, and all labeling steps with secondary MDM2-AF488 were done for a minimum of one hour.

The plasmid contents of selected cells were extracted as detailed in ref. 65 and re-transformed into electrocompetent methionine auxotrophic E. coli for further selection and/or binding characterization.

Characterization of selected clones

From each round of selection, typically 8 clones were sequenced by Sanger sequencing (32 clones were sequenced after FACS round 7) using primer 11. For characterization of individual clones, each clone was grown up and reacted as detailed previously. For binding titrations, appropriate concentrations and volumes (10-fold excess) of AlexaFluor647 tagged MDM2-GST diluted with PBS with 0.2% BSA was added to approximately $1x10^6$ cells and incubated on ice for 3 hours. Labeled cells were centrifuged at 4000xg for 2 minutes, washed once with 300 µL PBS with 0.2% BSA, and resuspended in 200 µL PBS for analysis by flow cytometry (Attune Focusing Cytometer). Median fluorescence intensities were normalized to the highest concentration and fit to a one-site binding model in GraphPad Prism v. 6.

Peptide Synthesis and Stabilization

Solid phase peptide synthesis of i,i+7 diazido peptides was carried out using a CEM Liberty Blue Microwave Peptide Synthesizer with 0.3 mmol/g loading Rink amide resin and Fmoc amino acids in dimethylformamide (DMF). The peptides were synthesized at

0.05 mmol scale and cleaved by addition of a cocktail composed of 93% (v/v) trifluoroacetic acid (TFA), 5% (v/v) H2O, 5% (w/v) phenol, and 2% (v/v) triisopropylsilane (TIPS). The resulting solution was evaporated under nitrogen to a small volume and precipitated via dropwise addition to tert-butyl methyl ether. The precipitate was then collected, lyophilized, and purified by preparative reverse phase gradient HPLC with water and acetonitrile mobile phases buffered with 0.1% TFA for all peptides except for SPD-M6-V1, which was purified with 25 mM triethylammonium acetate (TEAA) in H_2O/MeCN. The resin and Fmoc amino acids were purchased from ChemPep Inc. Fmoc-Azidohomoalanine was synthesized as in the method outlined by Lau[67] or purchased from ChemPep, Inc. All other reagents were purchased from Sigma Aldrich.

Diazido peptides were stabilized in solution via copper catalyzed azide alkyne cycloaddition. Peptides were stabilized in 1:1 water:tert-butanol at 1 mM concentration (1 equiv) with propargyl ether (1 equiv) by addition of copper (II) sulfate (10 equiv), tris(3-hydroxypropyltriazolylmethyl)amine (10 equiv) and sodium ascorbate (50 equiv) at room temperature overnight. The reaction mixtures were purified by HPLC in water and acetonitrile mobile phases buffered with 0.1% TFA (except for SPD-M6-V1 which was purified in triethylammonium acetate (25 mM) in H_2O/MeCN) and the product fractions were lyophilized and characterized via electrospray ionization mass spectrometry (ESI-MS) and reported in Table II - S2.

Solution phase binding kinetics

Binding affinities with the peptide in solution were measured via biolayer interferometry (BLI) using an Octet RED96 system (Pall ForteBio). MDM2 truncate (residues 10-118,

provided by Prof. Jeanne Stuckey) was biotinylated with NHS-PEG4-Biotin (Thermo Fisher). The resulting protein was diluted to 500 nM in the assay buffer (0.3% (w/v) bovine serum albumin (BSA) in phosphate buffered saline (PBS)) and loaded onto Super Streptavidin Biosensors. Peptide samples were prepared in the same assay buffer and each measurement was done in a 96 well plate using 10 concentrations per peptide. Resulting binding curves were fitted using Graphpad Prism v. 6. For each peptide, dissociation data was globally fit for all concentrations using a one-phase exponential decay model to yield k_{off}. The association data were fit for each concentration to yield values for k_{on}, and K_d is reported as k_{off} / k_{on}. The reported standard deviations of K_d are between values from all data sets (~8 association/dissociation curves per peptide each day measured on 3 separate days).

Circular Dichroism

Solution phase peptide helicity values were estimated by circular dichroism on a JASCO J-815 spectropolarimeter. Samples were diluted in 1:1 water:acetonitrile to 10 μM and transferred to a 1 mm path length quartz cell. Measurements were recorded in three accumulations from 250 nm to 190 nm. Percent helicity values were determined from molar ellipticity at 222 nm divided by the calculated maximum molar ellipticity for 13 and 14-mer peptides.

NMR Spectroscopy, Data Processing, and Structure Calculations

High-resolution NMR spectra of free SPD-M6-V1 peptide were obtained in sodium phosphate buffer, pH 6.8. Lyophilized peptide (SPD-M6-V1) was dissolved in 10 mM

aqueous sodium phosphate buffer (pH 6.8) with 10% D_2O to a final concentration of 300 µM. All NMR spectral measurements were acquired at room temperature (298K) in a Bruker AVANCE II 600 MHz spectrometer equipped with a cryoprobe and water signal was suppressed using WATERGATE. For resonance assignment and NOE contacts, 2-D homonuclear TOCSY (mixing time 80 ms with 32 scans) & NOESY (mixing time 200 ms with 88 scans) experiments were acquired using spectral width of 13 ppm with 2 K × 512 complex points and the States-TPPI for quadrature detection at the t1 dimension. To probe the interactions of SPD-M6-V1 with MDM2, a saturation transfer difference (STD) experiment was conducted by addition of MDM2(10-118) to a final concentration of 9 µM, pH 6.8. MDM2(10-118) was saturated at 0.15 ppm with a cascade of 40 selective Gaussian-shaped pulses (49 ms each) in an interval of 1 ms resulting in total saturation time of 2 s. An identical experiment one-dimensional STD experiment (as a control) was conducted with only SPD-M6-V1 peptide at same concentration. All NMR data were processed using TopSpin 2.6 (Bruker), and the chemical shifts were referenced directly to the frequency of water (4.7 ppm). After zero filling along the t1 dimension, 2 K (t2) × 1 K (t1) data matrices were obtained. All the spin system assignment and spectral analysis were done using SPARKY 3.113[68].

Sequence-specific resonance assignments of peptide was achieved by analyses of two-dimensional ^1H–^1H TOCSY and NOESY spectra[69]. Most of the resonances of SPD-M6-V1 are unambiguously identified (Figure II - S8). Analyses of ^1H–^1H NOESY spectra reveal backbone/backbone, backbone/sidechain, and sidechain/sidechain NOE contacts for the peptide. SVD-M6-V1 peptide contains 4 aromatic amino acids and a number of

NOEs could be identified involving aromatic ring protons with the backbone and side chain protons of aliphatic residues (Figure II - S8C). NOE contacts detected for peptide folding are summarized in Figure II - S8B and characterized by sequential and medium range interactions.

Assigned NOESY peaks were classified as weak, medium or strong and translated to an upper bound distance restraints: 5.0, 3.5 and 2.8 Å, respectively. Backbone dihedral angles ϕ and ψ were predicted using TALOS using ^{1}Hα chemical shifts. The structure of SPD-M6-V1 was calculated using CYANA 2.1. The CYANA library for the unnatural amino acid was created using the algorithm cylib developed by the Güntert group[70] (Table II - S5). During the CYANA runs, both amino acids (X20 and X27) were combined through an oxo group (Figure II - 4A) in side chains of the unnatural amino acids. The structure calculation was done in a stepwise manner to get the final ensemble with low RMSD and low violation of distance and dihedral angle constraints.

Protease digests

On-surface peptides were expressed as mentioned above and approximately 10^5 displaying bacteria were incubated with 1 μg/mL chymotrypsin in 80 μL PBS on ice. At each time point, samples were quenched by addition to 2% BSA in PBS, centrifuged and resuspended in 0.2% BSA in PBS. Resulting cells were labelled with 50 nM MDM2-GST-AF647 on ice for 2 h in 0.2% PBS/BSA, washed, and analyzed by flow cytometry (Biorad ZE5). Median fluorescent intensities were analyzed to obtain the curves in Figures II - 3A and II - 3C. For in solution measurements of protease degradation, stabilized and non-stabilized peptides were incubated with chymotrypsin at 5 μg/mL in PBS. Peptides were

first diluted to 50 μM in PBS before adding the enzyme and incubating at 37 C. After each time point, samples were flash-frozen in liquid nitrogen to stop digestion and stored at -80 C until analysis. Samples were analyzed via reverse-phase HPLC at 214 nm and 280 nm wavelengths. The fraction of intact peptide remaining at each time point was quantified by the AUC of the intact peptide peak on the chromatograph at 214 nm. Exponential decay curves and half-lives were fit in GraphPad Prism v.8.

Structure-guided docking

AutoDock Vina[71] was used to dock the calculated solution structure of SPD-M6-V1 to the MDM2 crystal structures in 3EQS[51]. Alignment of several crystal structures (2GV2, 1T4F, 1YRC, 3V3B, 4HFZ, 3G03, 3EQS) MDM2 showed similar binding groove composition and amino acid side chain conformation, so 3EQS was selected for structure-based docking. MDM2 and peptide were pH-adjusted to physiological pH (7.4) using the PDB2PQR server[72]. AutoDockTools (ADT) was used to prepare the protein and peptide PDB files and determine the search space for conformational flexibility. MDM2 residue side chains on the periphery of the binding pocket (L54, F55, Y100) were allowed to flex using ADT. Polar hydrogen atoms were added, non-polar ones were removed, and Gasteiger partial atom charges were calculated. Structures were visualized using PyMOL (Schrödinger, Delano Scientific, LLC, New York, NY, USA). The selected structure (Figure II - 4B) was chosen based on agreement with experimental data (Figure II - 4C) showing interactions between MDM2 and V16, C18, F19, Y22, and W23.

Statistics

Statistical analyses for Figs. 1A, 2C, and 2D were performed in GraphPad Prism v. 6.

Acknowledgements

We thank A.-M. Deslauriers-Cox, M. Savary, and D. Adams of the University of Michigan Flow Cytometry Core for assistance with FACS. We acknowledge the help of H. Remmer of the University of Michigan Proteomics and Peptide Synthesis Core for productive discussions regarding solid phase peptide synthesis as well as J. DelProposto from the University of Michigan Life Sciences Institute for assistance with biolayer interferometry (BLI) measurements. We thank members of the T. Scott laboratory for use and assistance with their solid phase peptide synthesizer. We thank J. van Deventer and H. Gao for helpful discussions and J. Bardwell for conversations and assistance in editing the manuscript. We also thank Peter Güntert and Sina Kazemi for helping with CYANA library generation.

This work was supported by an NSF CAREER Award CBET 1553860 (to G.M.T) and NSF Graduate Fellowships (to T.N. and L.A.). Additional support was provided by NIH Grant R35 GM128819 (to G.M.T).

Supporting information

Table II - S1 – Primers used

No.	Description	Sequence
1	Met removal 1	CAACCCGCTGGAAAACGTTGCTCTGGACTTCTCTTACG
2	Met removal 2	ACGCTCAGGGCCAACTGAACAAACTGGGCGGTTTCAACCTGAAATACCGCT
3	EcoRI eCPX for pQE80L insertion	CACAGAATTCATTAAAGAGGAGAAATTAACTATGAAAAAAATTGCATGTCTTTCAGCACT
4	pB33 rev	GGCTGAAAATCTTCTCTC
5	eCPX-exendin fwd	ACTTCCGTAGCTGGCCAGTCTGGCCAGCATGGCGAAGGCACCTTTACCAGCGATCTGAGCAAACAGATGGAAGAAGAAGCGGTGCGTATGTTTATTGAATGGCTGAAAAACGGTGGTCCAAGCAGCGGTGCACCACCACCAAGCGGAGGGCAGTCTGGGCAGTCTG
6	NcoI-eCPX	GAATTCGAGCTCGCCATGGGTACCTTTGAGGTGGTTATG
7	PLP-eCPX	ACTTCCGTAGCTGGCCAGTCTGGCCAGGAAACCTTTATGGATCTGTGGCGCCTGCTGATGGAAAACGGCGGTGGCAGCGGAGGGCAGTCTGGGCAGTCTG
8	pQE80L rev	GAGGTCATTACTGGATCTATCAACAGGAGTCCAAGCTCAGC
9	PLP-HA fwd	TATCCGTACGATGTGCCGGATTATGCGGGAGGGCAGTCTGGGCAGTCT
10	PLP-HA rev	CGCATAATCCGGCACATCGTACGGATAGCTGCCACCGCCGTTTTCCAT
11	pQE80L fwd	CCCGAAAAGTGCCACCTGACG
12	NNC PLP	ACTTCCGTAGCTGGCCAGTCTGGCCAGNNCNNCNNCTTTATGNNCNNCTGGNNCNNCCTGATGNNCNNCGGCGGTGGCAGCGGAGGGCAGTCTGGGCAGTCTG
13	E17Q for PLP(-1)	TCCGTAGCTGGCCAGTCTGGCCAGCAAACCTTTATGGATCTGTGGCGCCTGC
14	E28Q for PLP(0)	ACCTTTATGGATCTGTGGCGCCTGCTGATGCAAAACGGCGGTGGCAGCGGAGGGCAGT

Table II - S2 – Peptide mass spectrometry and purity

Name	Sequence	Stabilized		% Purity	Non-stabilized		% Purity
		Predicted Mass	Observed Mass	HPLC at 214 nm	Predicted Mass	Observed Mass	HPLC at 214 nm
SPD-M0-E(-2)	ETFXDLWRLLXEN	1823.0	1823.0	97.7%	1728.9	1728.9	>98%
SPD-M0-E(-1)	QTFXDLWRLLXEN	1822.0	1822.0	95.8%	1727.9	1727.9	95.4%
SPD-M0-E(0)	QTFXDLWRLLXQN	1821.0	1821.0	95.1%	1726.9	1726.9	97.7%
SPD-M3-G1	GGTFXGYWADLXAF	1690.3	1690.8	96.2%	1596.7	1596.7	>98%
SPD-M3-V1	VLSFXDYWNLLXGS	1800.9	1800.9	>98%	1705.8	1706.8	>98%
SPD-M6-V1	VCDFXCYWNDLXGY	1881.7	1881.0	>98%	1787.7	1787.7	97.5%
SPD-M0-E(-2)-F19A	ETAXDLWRLLXEN	1746.9	1746.9	>95%	1652.8	1652.8	>95%

Table II - S3 – SPD-M6-V1 proton NMR chemical shifts in ppm

Residue	H	Hα	Hβ	Hγ	Hδ	Hε
Val-16	8.062	3.934	1.953	0.845		
Cys-17	7.993	4.649	2.363/2.442			
Asp-18	8.459	4.162	2.493/2.617			
Phe-19	8.447	4.103	2.895/3.011		6.705	6.483
UAA-20	7.952	4.199	3.540/3.646			
Cys-21	8.340	4.743	2.931			
Tyr-22	8.710	4.304	2.630/2.979		7.401	6.709
Trp-23	7.739	4.315	2.643		7.813	6.522 (ε3) 9.495 (ε1)
Asn-24	7.848	4.582	2.65			
Asp-25						
Leu-26	7.839	3.893	1.405	1.516		
UAA-27	7.683	4.216	4.003/4.081			
Gly-28	7.644	3.777	3.894			
Tyr-29	7.817	4.565	2.666			

Table II - S4 – Structural statistics of twenty lowest energy structures of SPD-M6-V1

Distance constraints	
Intra residue (i = j)	40
Sequential (i–j = 1)	32
Medium range [1 < li–jl ≤ 4]	29
Total	101
Angle constraints	
ϕ, ψ constraints	24
Deviation from mean structure (RMSD)	
All backbone atoms	0.20 Å
All heavy atoms	0.87 Å
Ramachandran plot for the mean structure	
% residues in the most favored region	33.3
% residues in the additionally allowed region	66.7
% residues in the generously allowed region	0.0
% residues in the disallowed region	0.0

Table II - S5 – CYANA library file for the linker

```
RESIDUE   XUN     8   28    3   27
1 OMEGA    0    0    0.0000 -O   -C    N    H
2 PHI      0    0    0.0000 -C    N    CA   C
3 CHI1     0    0    0.0000  N    CA   CB   HB2  O5
4 CHI2     0    0    0.0000  CA   CB   CG   N1   O5
5 CHI3     0    0    0.0000  CB   CG   N1   N2 O5
6 CHI4     0    0    0.0000  CD   CE   CZ   O5 O5
7 CHI5     0    0    0.0000  CE   CZ   O5   O5 O5
8 PSI      0    0    0.0000  N    CA   C   +N
1 C     C_BYL    0    0.0000    0.0000    0.0000    0.0000 -O    N
2 O     O_BYL    0    0.0000   -0.6700    0.0000   -1.0322 -C
3 N     N_AMI    0    0.0000    1.3290    0.0000    0.0000 -C    H    CA
4 H     H_AMI    0    0.0000    1.8069   -0.0007    0.8553  N
5 CA    C_ALI    0    0.0000    2.0929   -0.0011   -1.2414  N    HA   CB   C
6 HA    H_ALI    0    0.0000    2.7479   -0.8605   -1.2295  CA
7 CB    C_ALI    0    0.0000    1.1392   -0.1380   -2.4612  CA   HB2  HB3  CG
8 HB2   H_ALI    0    0.0000    0.1585    0.2327   -2.1632  CB   -    -    -    QB
9 HB3   H_ALI    0    0.0000    1.1625   -1.1929   -2.7339  CB   -    -    -    QB
10 QB   PSEUD    0    0.0000    0.6605   -0.4800   -2.44860
11 CG   C_ALI    0    0.0000    1.5735    0.6318   -3.7403  CB   HG2  HG3  N1
12 HG2  H_ALI    0    0.0000    1.6155    1.6991   -3.5217  CG   -    -    -    QG
13 HG3  H_ALI    0    0.0000    2.5045    0.1736   -4.0734  CG   -    -    -    QG
14 QG   PSEUD    0    0.0000    2.0598    0.9366   -3.79707
15 N1   N_AMI    0    0.0000    0.4964    0.3682   -4.9496  CG   CD   N2
16 CD   C_ARO    0    0.0000    0.1424    0.6380   -6.3514  N1   HD   CE
17 HD   H_ARO    0    0.0000    0.7249    1.1857   -7.0924  CD
18 CE   C_ARO    0    0.0000   -1.2008   -0.0088   -6.5356  CD   N3   CZ
19 N3   N_AMO    0    0.0000   -1.5724   -0.5758   -5.4308  CE   N2
20 N2   N_AMO    0    0.0000   -0.6727   -0.3850   -4.5762  N1   N3
21 CZ   C_ALI    0    0.0000   -2.0142   -0.0017   -7.8431  CE   HZ2  HZ3  O5
22 HZ2  H_ALI    0    0.0000   -2.0363    1.0090   -8.2516  CZ   -    -    -    QZ
23 HZ3  H_ALI    0    0.0000   -1.5522   -0.7495   -8.4875  CZ   -    -    -    QZ
24 QZ   PSEUD    0    0.0000   -1.7946    0.1301   -8.36898
25 O5   O_HYD    0    0.0000   -3.3496   -0.4375   -7.5771  CZ
26 C    C_BYL    0    0.0000    2.9378    1.2621   -1.3672  CA   O    +N
27 O    O_BYL    0    0.0000    2.4397    2.3166   -1.7634  C
28 N    N_AMI    0    0.0000    4.2169    1.1488   -1.0273  C
```

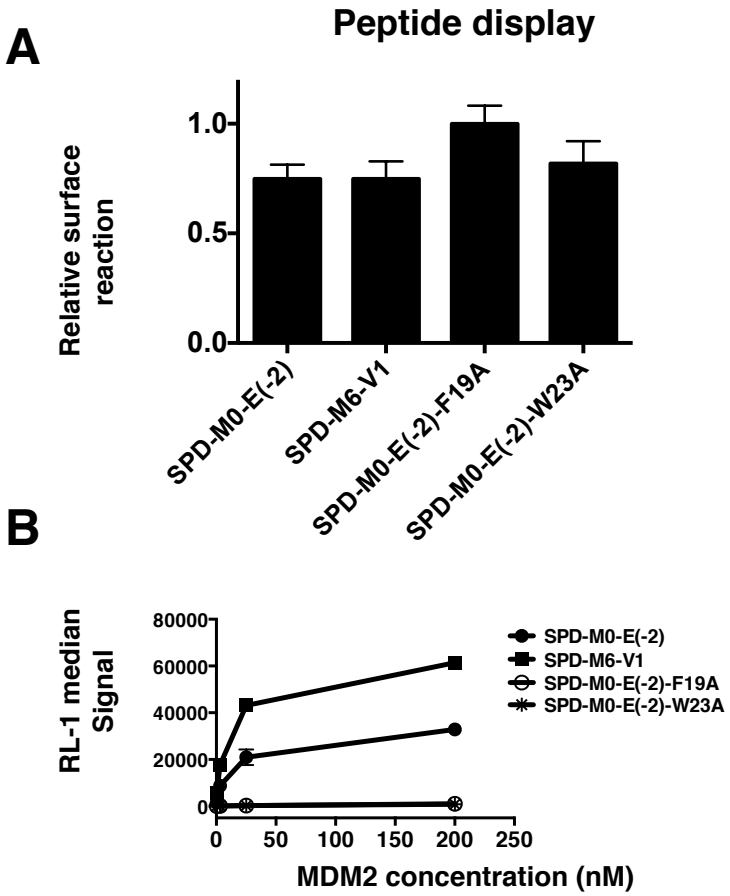

Figure II - S1. Specific Surface Binding
A: Displayed peptides were reacted with SCy5-alkyne and run on a polyacrylamide gel after normalization by BCA assay. Fluorescence was quantified using the Odyssey CLx imager in the 700 nm channel. B: W23A and F19A do not exhibit appreciable binding to MDM2 as quantified by flow cytometry, despite similar levels of surface display (A).

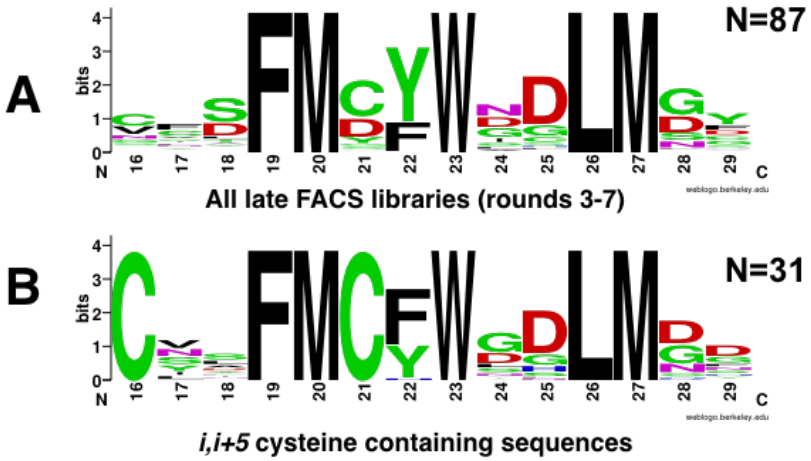

Figure II - S2. Logo plots for pooled sequences (A) and i, i+5 containing sequences (B).

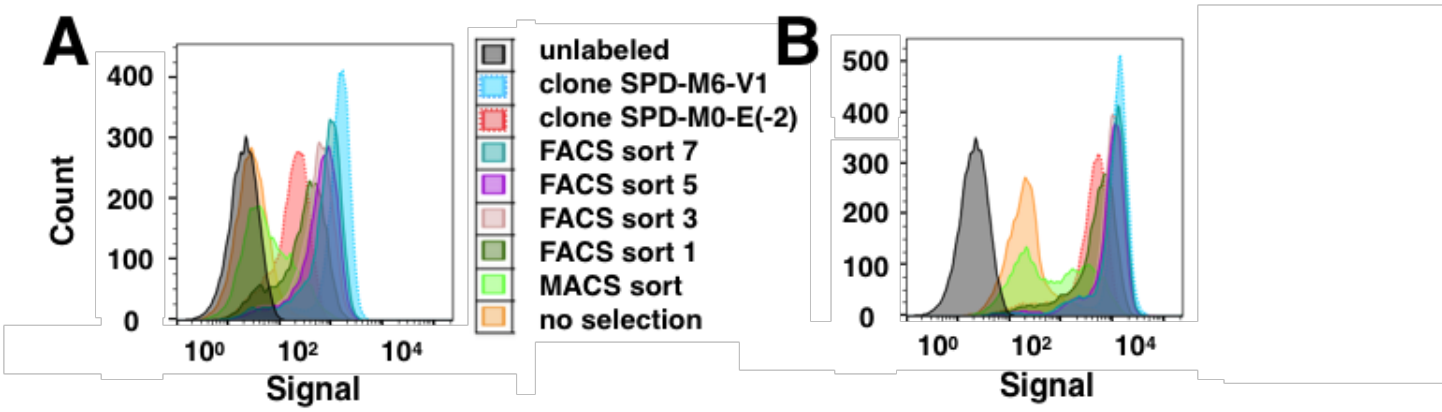

Figure II - S3. Population level and individual clone analysis by flow cytometry. Histograms are shown for approx. 12,000 events for samples labeled with 0.25 nM MDM2-GST (A) and 25 nM MDM2-GST (B). No selection is the original library containing 3×10^8 transformants. MACS refers to the population obtained from one round of positive selection with magnetic beads. FACS 1, 3, 5, 7 refer to the populations sorted after 1, 3, 5, and 7 rounds of fluorescence-based sorting. The even-numbered sorted populations are not shown here for clarity.

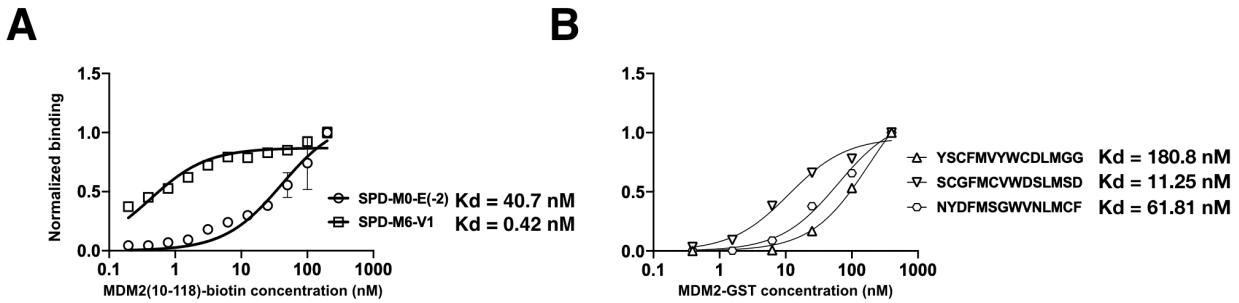

Figure II - S4. MDM2 truncate and MDM2-GST cell-surface binding.
(A) MDM2(10-118)-biotin was titrated against surface displayed peptide (SPD-M0-E(-2) or SPD-M6-V1) and labelled with Streptavidin-Alexafluor-647 prior to flow cytometric analysis. (B) Clones from earlier sorting rounds were also characterized for binding affinity with MDM2-GST to validate sorting for improvements. Sequences YSC… and SCG… were obtained from the resultant library of MACS, and sequence NYD… was obtained from 2 subsequent rounds of FACS.

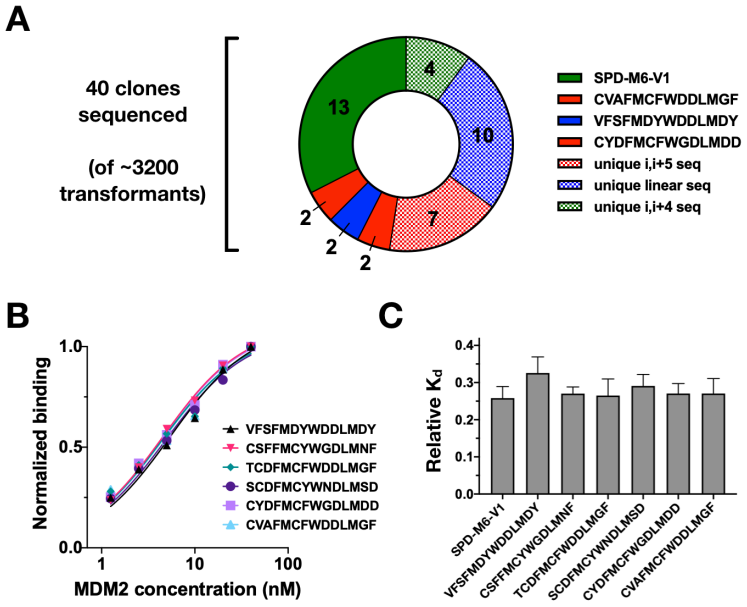

Figure II - S5. Analysis of clones after round 7 of FACS.
After 1 round of MACS and 7 rounds of FACS, 3200 transformants were obtained, and 40 individual colonies were sequenced. A. The distribution of sequences shows that 13 of these colonies are SPD-M6-V1, motivating the selection of this sequence for further study. A large fraction of clones showed cysteines at i,i+4 (green) and i,i+5 (red) positions. B. The apparent binding affinity on the cell surface of 6 clones from the last sort. C. The measured K_d values of these 6 clones and SPD-M6-V1 all show similar improvement over SPD-M0-E(-2).

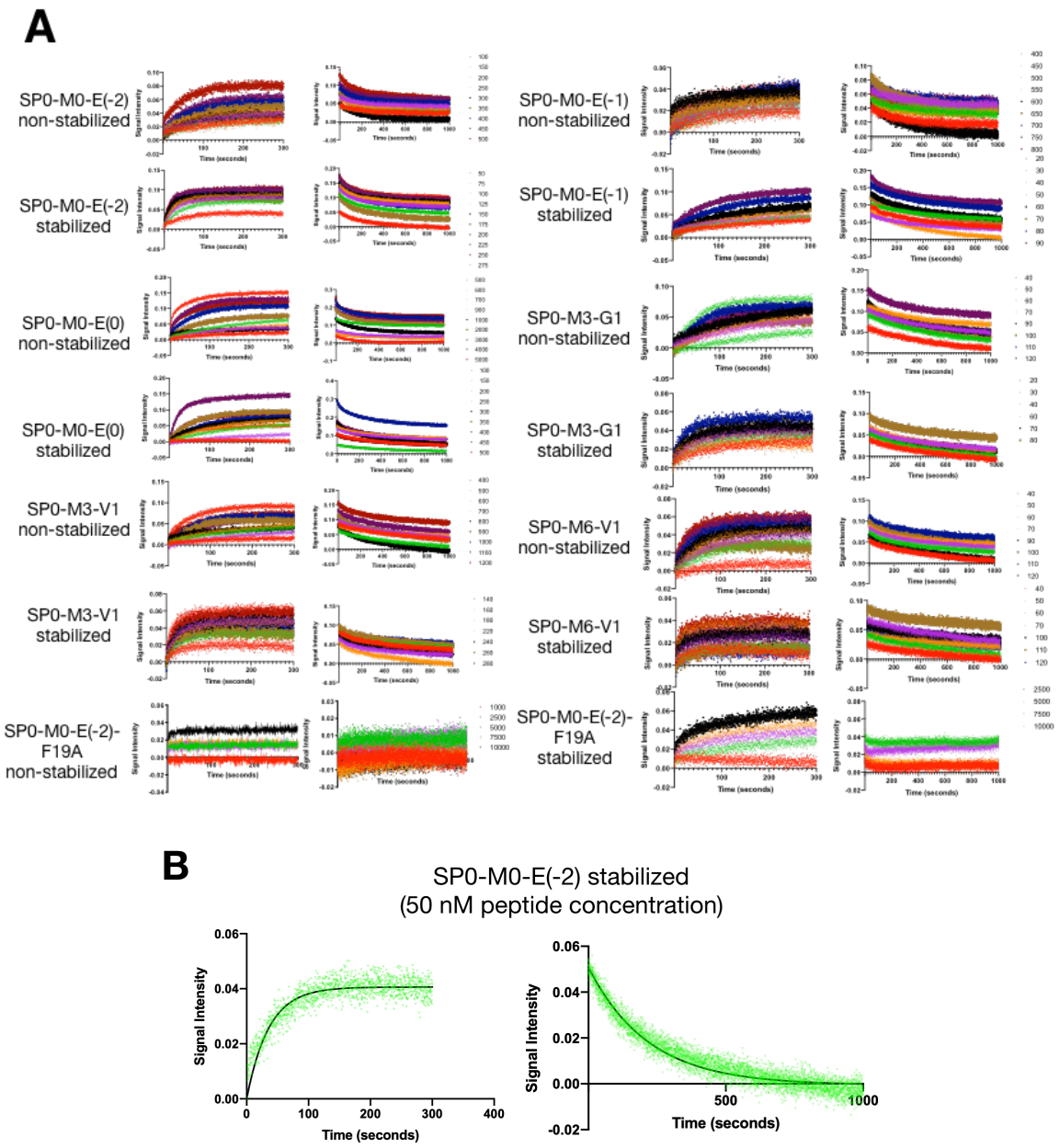

Figure II - S6. Solution Phase Peptide Binding Affinity.
(A**)** BLI sensograms for the on-phase (left) and off-phase (right) of peptides binding to immobilized MDM2(10-118). (B) Representative peptide analysis showing on-phase and off-phase data points fitted to an association equation (left) and dissociation equation (right) respectively in Graphpad Prism v. 6. Curves with significant instrument drift were eliminated from analyses.

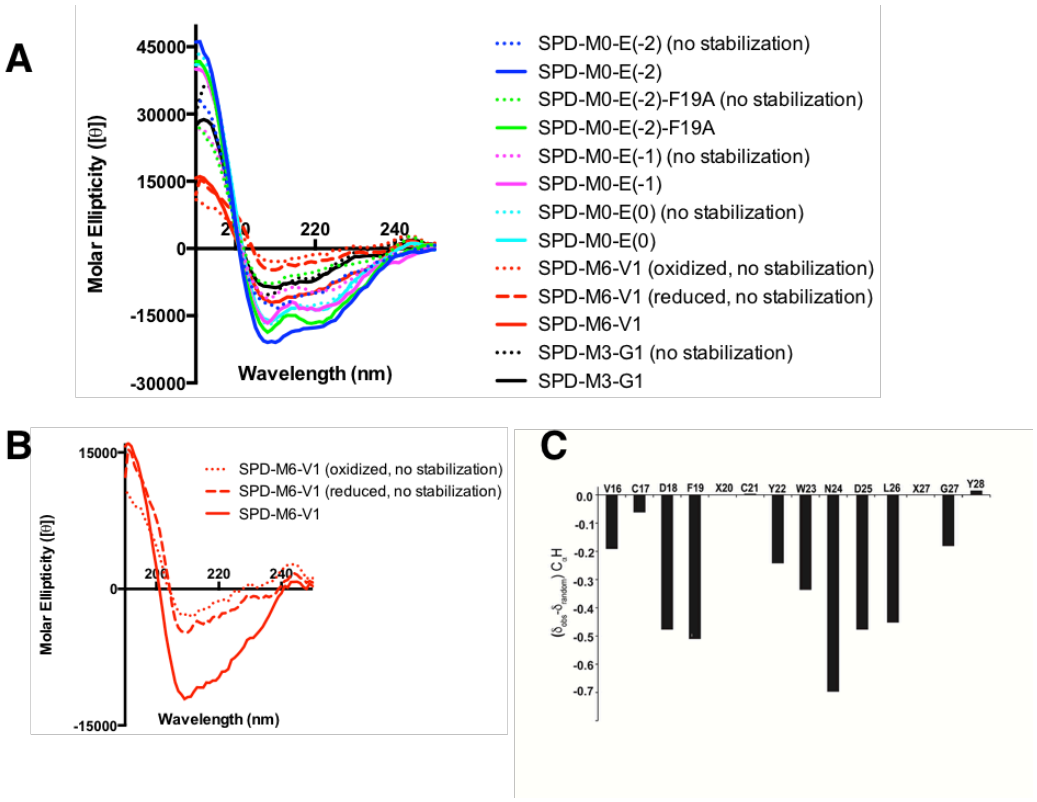

Figure II - S7. Secondary structure measurements
(A) Grouped circular dichroism (CD) spectra for peptides presented with (solid line) and without (dotted line) stabilization. (B) CD spectra for SPD-M6-V1 and reaction variants. (C) αH chemical shift deviation from random coil values of SPD-M6-V1. The negative deviation of residues indicates α-helix structure.

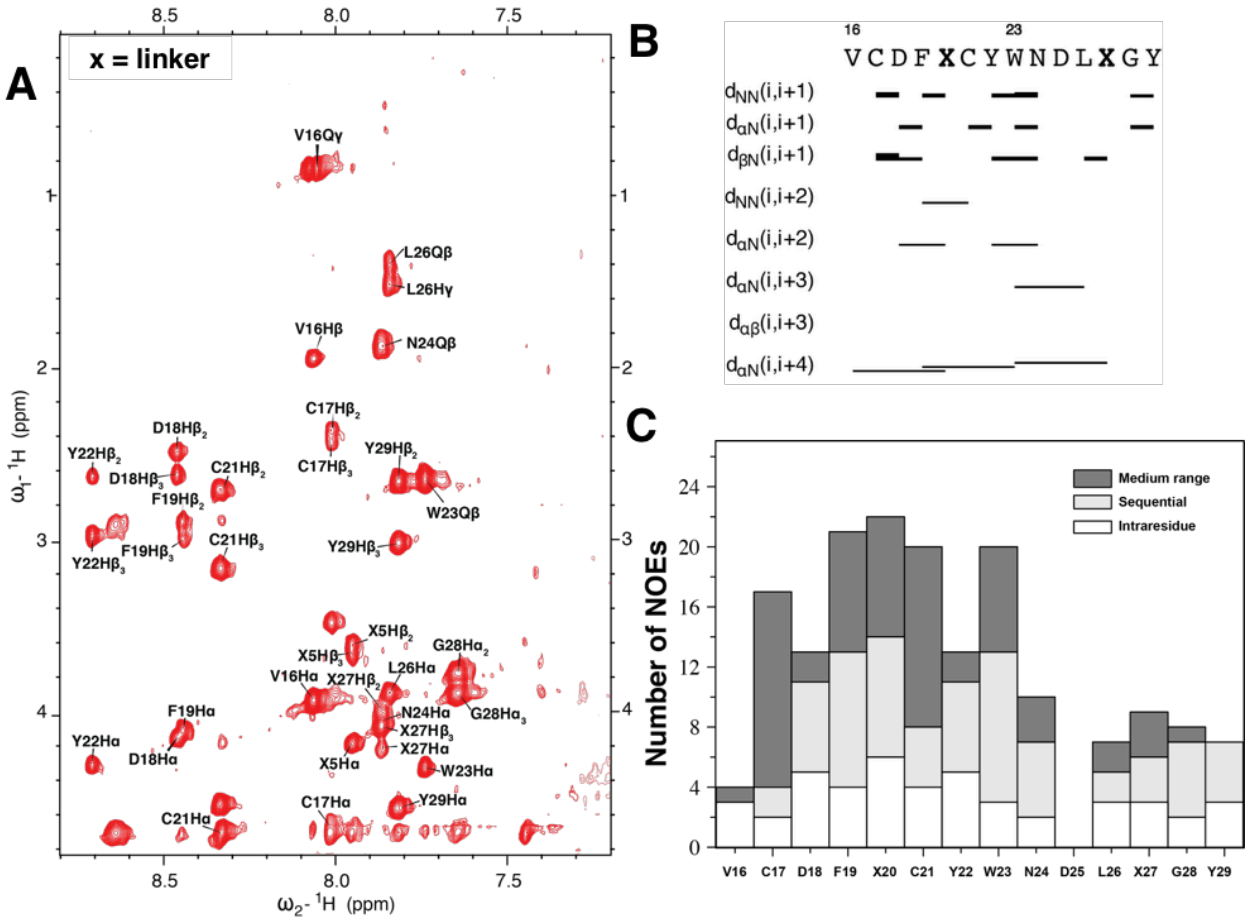

Figure II - S8. NMR Characterization.
(A) ^{1}H-^{1}H homonuclear 2D TOCSY spectrum showing amide fingerprint region of **SPD-M6-V1**. (B) Depiction of amino acid connectivity as inferred from NOESY spectra. (C) Histogram of interactions at each amino acid position of **SPD-M6-V1** as estimated from NOESY and TOCSY experiments.

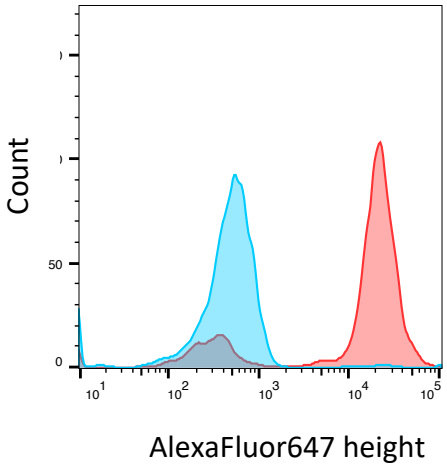

Figure II - S9. Surface Exendin-4 display and binding.
20 nM anti-exendin antibody was incubated with bacterial surface displayed exendin-4 peptide and labelled with anti-mouse-Alexafluor-647 secondary antibody prior to flow cytometric analysis (red). Negative cells were stained with isotype control antibody and anti-mouse Alexafluor-647 secondary antibody (cyan).

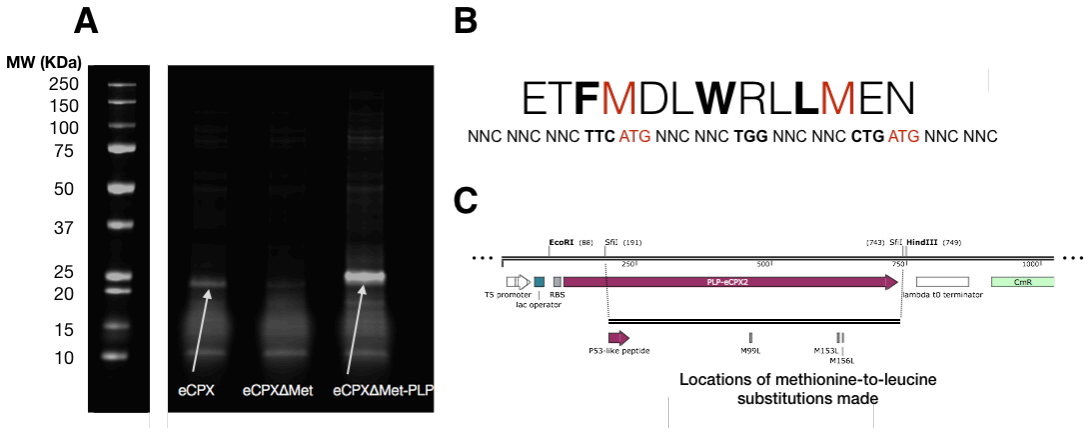

Figure II - S10. eCPX Modifications.
Reducing, denaturing protein gel of eCPX constructs post-SCy5-alkyne reaction. The starting eCPX protein exhibits low, but specific signal despite not displaying a peptide. (A) Mutation of the 3 non-start methionine residues results in abrogation of this signal. Genetic incorporation of the SPD-M0-E(-2) peptide restores high levels of signal. (B) DNA sequence of the peptide region of the primer used to encode the randomized library. (C) plasmid map of the eCPX gene cloned into pQE80L showing restriction sites EcoRI/HindIII for gene insertion, SfiI sites (used to introduce the peptide sequences), and the M to L mutation sites. The sequence located N-terminally of P53-like peptide is cleaved prior to translocation into the outer membrane, resulting in display of the peptide as an N-terminal fusion to eCPX.

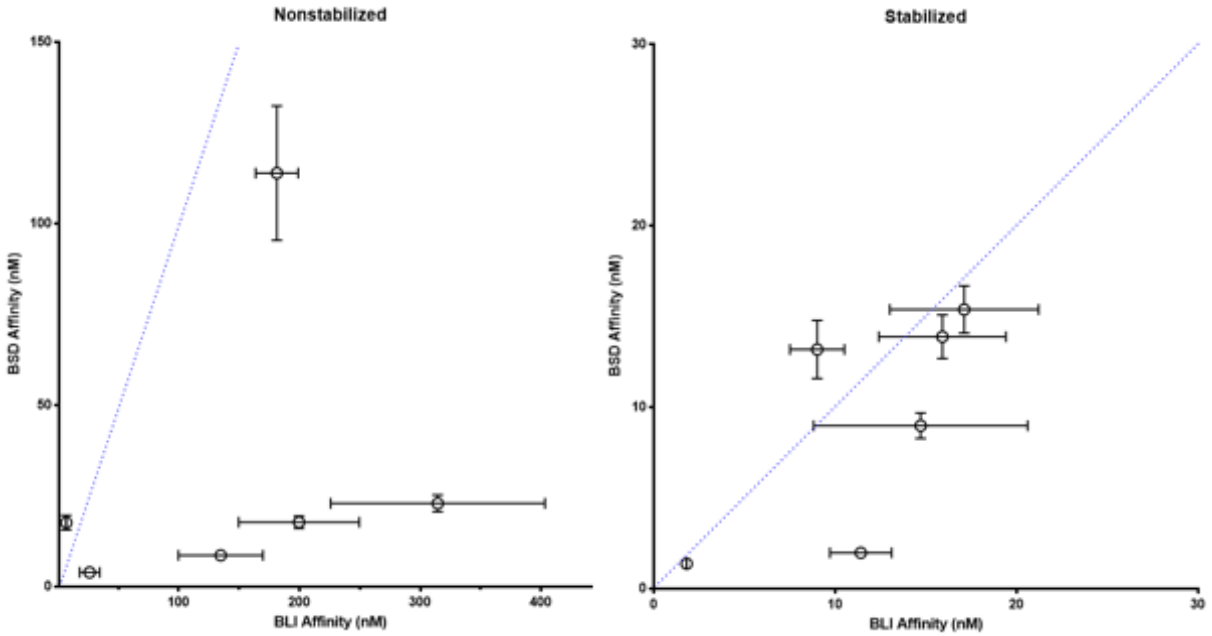

Figure II - S11. Surface-solution correlations.
Stabilization improves the correlation between affinity measured in solution (BLI affinity) and on the bacterial surface (BSD affinity). For non-stabilized peptides, the slope of the best-fit line is not significantly different from 0 ($p = 0.16$, $t = 1.63$, $df = 5$) whereas a positive slope is obtained for stabilized peptides ($p = 0.018$, $t = 3.47$, $df = 5$) ($n = 3$ independent trials per data point).

Supplementary modeling discussion

To calculate the extent of surface reaction, we modelled the system using the equations implemented below in MATLAB v. 2018a. Because mass spectrometry cannot be used to independently identify species B and C, the stabilized bacteria underwent a 2nd reaction with azide- or alkyne-dyes. Species A and B react with alkyne dyes, while species B and D react with azide-dyes. By analyzing the peptide band by SDS-PAGE and normalizing to the total peptide in the eCPX-peptide band (because 'C' does not react with either dye), the fraction of C could be calculated from the data set.

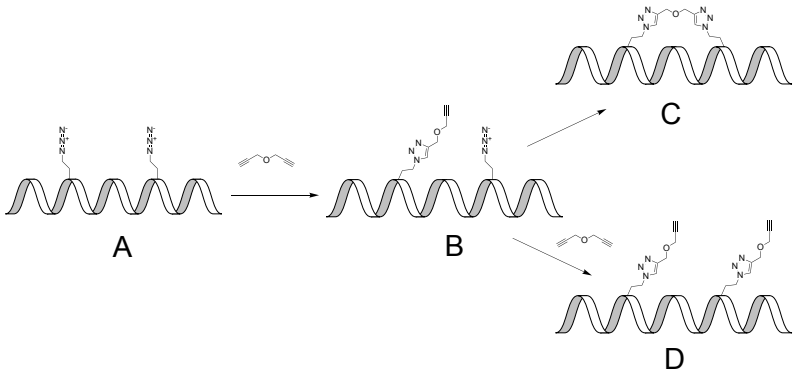

A, surface-displayed peptide; B, singly-reacted; C, stabilized peptide; D, two linker-reacted peptide; L, linker

k_1 is rate of reaction of one site with L. k_2, rate of stabilization

$$\frac{d[A]}{dt} = -k_1[L] \cdot [A]$$

$$\frac{d[B]}{dt} = k_1[L] \cdot [A] - k_2[B] - k_1[L] \cdot [B]$$

$$\frac{d[C]}{dt} = k_2[B]$$

$$\frac{d[D]}{dt} = k_1[L] \cdot [B]$$

Modelled rates: $k_1 = 1.8$; $k_2 = 9$

Initial conditions: $A(0) = 42.6$; $B(0) = 0$; $C(0) = 0$; $D(0) = 0$

The parameters were varied to test the robustness of the predictions. The ratios of the modelled azide signal from species B and D at each concentration (e.g. the azide signal at 100 μM alkyne species to the azide signal at 5 μM alkyne species) is relatively insensitive to the values of the modelled rates and accurately maps to the experimental found signal, as long as the ratio of k_2 to k_1 is between 3 and 6 (currently 5) and that the modelled end-point corresponds to the experimentally found fraction of displayed azides reacted.

References

(1) Hopkins, A. L.; Groom, C. R. The Druggable Genome. Nat. Rev. Drug Discov. **2002**, 1 (9), 727–730. https://doi.org/10.1038/nrd892.

(2) Sawyer, T. K.; Partridge, A. W.; Kaan, H. Y. K.; Juang, Y.-C.; Lim, S.; Johannes, C.; Yuen, T. Y.; Verma, C.; Kannan, S.; Aronica, P.; et al. Macrocyclic α Helical Peptide Therapeutic Modality: A Perspective of Learnings and Challenges. Bioorg. Med. Chem. **2018**, 26 (10), 2807–2815. https://doi.org/10.1016/J.BMC.2018.03.008.

(3) Arkin, M.; Wells, J. Small-Molecule Inhibitors of Protein-Protein Interactions: Progressing towards the Dream. Nat. Rev. Drug Discov. **2004**, 3 (4), 301–317. https://doi.org/10.1038/nrd1343.

(4) Lau, J.; Bloch, P.; Schäffer, L.; Pettersson, I.; Spetzler, J.; Kofoed, J.; Madsen, K.; Knudsen, L. B.; McGuire, J.; Steensgaard, D. B.; et al. Discovery of the Once-Weekly Glucagon-Like Peptide-1 (GLP-1) Analogue Semaglutide. J. Med. Chem. **2015**, 58 (18), 7370–7380. https://doi.org/10.1021/acs.jmedchem.5b00726.

(5) Shustov, A. R.; Horwitz, S. M.; Zain, J.; Patel, M. R.; Goel, S.; Sokol, L.; Meric-Bernstam, F.; Shapiro, G.; Nasta, S. D.; Janakiram, M.; et al. Preliminary Results of the Stapled Peptide ALRN-6924, a Dual Inhibitor of MDMX and MDM2, in Two

Phase IIa Dose Expansion Cohorts in Relapsed/Refractory TP53 Wild-Type Peripheral T-Cell Lymphoma. Blood **2018**, 132 (Suppl 1), 1623–1623. https://doi.org/10.1182/BLOOD-2018-99-116780.

(6) Chang, Y. S.; Graves, B.; Guerlavais, V.; Tovar, C.; Packman, K.; To, K.-H.; Olson, K. A.; Kesavan, K.; Gangurde, P.; Mukherjee, A.; et al. Stapled A–helical Peptide Drug Development: A Potent Dual Inhibitor of MDM2 and MDMX for P53-Dependent Cancer Therapy. Proc. Natl. Acad. Sci. **2013**, 110 (36), E3445–E3454. https://doi.org/10.1073/pnas.1303002110.

(7) Zhang, L.; Navaratna, T.; Thurber, G. M. A Helix-Stabilizing Linker Improves Subcutaneous Bioavailability of a Helical Peptide Independent of Linker Lipophilicity. Bioconjug. Chem. **2016**, 27 (7), 1663–1672. https://doi.org/10.1021/acs.bioconjchem.6b00209.

(8) Bird, G. H.; Mazzola, E.; Opoku-Nsiah, K.; Lammert, M. A.; Godes, M.; Neuberg, D. S.; Walensky, L. D. Biophysical Determinants for Cellular Uptake of Hydrocarbon-Stapled Peptide Helices. Nat. Chem. Biol. **2016**, 12 (10), 845–852. https://doi.org/10.1038/nchembio.2153.

(9) Rezaei Araghi, R.; Bird, G. H.; Ryan, J. A.; Jenson, J. M.; Godes, M.; Pritz, J. R.; Grant, R. A.; Letai, A.; Walensky, L. D.; Keating, A. E. Iterative Optimization Yields Mcl-1–Targeting Stapled Peptides with Selective Cytotoxicity to Mcl-1–Dependent Cancer Cells. Proc. Natl. Acad. Sci. **2018**, 115 (5), 201712952. https://doi.org/10.1073/pnas.1712952115.

(10) Bernal, F.; Tyler, A. F.; Korsmeyer, S. J.; Walensky, L. D.; Verdine, G. L. Reactivation of the P53 Tumor Suppressor Pathway by a Stapled P53 Peptide. J. Am. Chem. Soc. **2007**, 129 (9), 2456–2457. https://doi.org/10.1021/ja0693587.

(11) Spokoyny, A. M.; Zou, Y.; Ling, J. J.; Yu, H.; Lin, Y. S.; Pentelute, B. L. A Perfluoroaryl-Cysteine SNAr Chemistry Approach to Unprotected Peptide Stapling. J. Am. Chem. Soc. **2013**, 135 (16), 5946–5949. https://doi.org/10.1021/ja400119t.

(12) Lau, Y. H.; de Andrade, P.; Quah, S.-T.; Rossmann, M.; Laraia, L.; Skold, N.; Sum, T. J.; Rowling, P. J. E.; Joseph, T. L.; Verma, C.; et al. Functionalised Staple Linkages for Modulating the Cellular Activity of Stapled Peptides. Chem. Sci. **2014**, 5 (5), 1804–1809. https://doi.org/10.1039/C4SC00045E.

(13) Torres, O.; Yüksel, D.; Bernardina, M.; Kumar, K.; Bong, D. Peptide Tertiary Structure Nucleation by Side-Chain Crosslinking with Metal Complexation and Double “Click” Cycloaddition. ChemBioChem **2008**, 9 (11), 1701–1705. https://doi.org/10.1002/cbic.200800040.

(14) Walensky, L. D.; Bird, G. H. Hydrocarbon-Stapled Peptides: Principles, Practice, and Progress. J. Med. Chem. **2014**, 57 (15), 6275–6288.

https://doi.org/10.1021/jm4011675.

(15) Zhang, L.; Navaratna, T.; Liao, J.; Thurber, G. M. Dual-Purpose Linker for Alpha Helix Stabilization and Imaging Agent Conjugation to Glucagon-like Peptide-1 Receptor Ligands. Bioconjug. Chem. **2015**, 26 (2), 329–337. https://doi.org/10.1021/bc500584t.

(16) Patgiri, A.; Jochim, A. L.; Arora, P. S. A Hydrogen Bond Surrogate Approach for Stabilization of Short Peptide Sequences in α-Helical Conformation. Acc. Chem. Res. **2008**, 41 (10), 1289–1300. https://doi.org/10.1021/ar700264k.

(17) Heinis, C.; Rutherford, T.; Freund, S.; Winter, G. Phage-Encoded Combinatorial Chemical Libraries Based on Bicyclic Peptides. Nat. Chem. Biol. **2009**, 5 (7), 502–507. https://doi.org/10.1038/nchembio.184.

(18) Peraro, L.; Siegert, T. R.; Kritzer, J. A. Conformational Restriction of Peptides Using Dithiol Bis-Alkylation. In Methods in Enzymology; 2016; Vol. 580, pp 303–332. https://doi.org/10.1016/bs.mie.2016.05.035.

(19) Derda, R.; Jafari, M. R. Synthetic Cross-Linking of Peptides: Molecular Linchpins for Peptide Cyclization. Protein Pept. Lett. **2018**, 25 (12), 1–25. https://doi.org/10.2174/0929866525666181120090650.

(20) Millward, S. W.; Takahashi, T. T.; Roberts, R. W. A General Route for Post-Translational Cyclization of MRNA Display Libraries. J. Am. Chem. Soc. **2005**, 127 (41), 14142–14143. https://doi.org/10.1021/JA054373H.

(21) Kale, S. S.; Villequey, C.; Kong, X.-D.; Zorzi, A.; Deyle, K.; Heinis, C. Cyclization of Peptides with Two Chemical Bridges Affords Large Scaffold Diversities. Nat. Chem. **2018**, 10 (7), 715–723. https://doi.org/10.1038/s41557-018-0042-7.

(22) Diderich, P.; Bertoldo, D.; Dessen, P.; Khan, M. M.; Pizzitola, I.; Held, W.; Huelsken, J.; Heinis, C. Phage Selection of Chemically Stabilized α - Helical Peptide Ligands. ACS Chem. Biol. **2016**, 1–6. https://doi.org/10.1021/acschembio.5b00963.

(23) Robertson, N. S.; Spring, D. R. Using Peptidomimetics and Constrained Peptides as Valuable Tools for Inhibiting Protein−Protein Interactions. Molecules **2018**, 23 (4). https://doi.org/10.3390/molecules23040959.

(24) Chène, P. Inhibiting the P53-MDM2 Interaction: An Important Target for Cancer Therapy. Nature Reviews Cancer. 2003, pp 102–109. https://doi.org/10.1038/nrc991.

(25) Bird, G. H.; Gavathiotis, E.; Labelle, J. L.; Katz, S. G.; Walensky, L. D. Distinct BimBH3 (BimSAHB) Stapled Peptides for Structural and Cellular Studies. ACS Chem. Biol. **2014**, 9 (3), 831–837. https://doi.org/10.1021/cb4003305.

(26) Gray, B. P.; Brown, K. C. Combinatorial Peptide Libraries: Mining for Cell-Binding Peptides. Chemical Reviews. 2014, pp 1020–1081. https://doi.org/10.1021/cr400166n.

(27) Urquhart, T.; Daub, E.; Honek, J. F. Bioorthogonal Modification of the Major Sheath Protein of Bacteriophage M13: Extending the Versatility of Bionanomaterial Scaffolds. Bioconjug. Chem. **2016**, 27 (10), 2276–2280. https://doi.org/10.1021/acs.bioconjchem.6b00460.

(28) Baek, S.; Kutchukian, P. S.; Verdine, G. L.; Huber, R.; Holak, T. a.; Lee, K. W.; Popowicz, G. M. Structure of the Stapled P53 Peptide Bound to Mdm2. J. Am. Chem. Soc. **2012**, 134 (1), 103–106. https://doi.org/10.1021/ja2090367.

(29) Link, a J.; Vink, M. K. S.; Tirrell, D. a. Presentation and Detection of Azide Functionality in Bacterial Cell Surface Proteins Presentation and Detection of Azide Functionality in Bacterial. **2004**, 2 (25 mL), 10598–10602. https://doi.org/10.1021/ja047629c.

(30) Rice, J.; Daugherty, P. Directed Evolution of a Biterminal Bacterial Display Scaffold Enhances the Display of Diverse Peptides. Protein Eng. Des. Sel. **2008**, 21 (7), 435–442. https://doi.org/10.1093/protein/gzn020.

(31) Kiick, K.; Saxon, E.; Tirrell, D.; Bertozzi, C. Incorporation of Azides into Recombinant Proteins for Chemoselective Modification by the Staudinger Ligation. Proc. Natl. Acad. Sci. U. S. A. **2002**, 99 (1), 19–24. https://doi.org/10.1073/pnas.012583299.

(32) Strable, E.; Prasuhn, D. E.; Udit, A. K.; Brown, S.; Link, A. J.; Ngo, J. T.; Lander, G.; Quispe, J.; Potter, C. S.; Carragher, B.; et al. Unnatural Amino Acid Incorporation into Virus-Like Particles. Bioconjug. Chem. **2008**, 19 (4), 866–875.

(33) Boder, E.; Wittrup, K. Yeast Surface Display for Screening Combinatorial Polypeptide Libraries. Nat. Biotechnol. **1997**, 15 (6), 553–557. https://doi.org/10.1038/nbt0697-553.

(34) Böttger, A.; Böttger, V.; Garcia-Echeverria, C.; Chène, P.; Hochkeppel, H. K.; Sampson, W.; Ang, K.; Howard, S. F.; Picksley, S. M.; Lane, D. P. Molecular Characterization of the Hdm2-P53 Interaction. J. Mol. Biol. **1997**, 269 (5), 744–756. https://doi.org/10.1006/jmbi.1997.1078.

(35) Li, C.; Pazgier, M.; Li, C.; Yuan, W.; Liu, M.; Wei, G.; Lu, W. Y.; Lu, W. Systematic Mutational Analysis of Peptide Inhibition of the P53-MDM2/MDMX Interactions. J. Mol. Biol. **2010**, 398 (2), 200–213. https://doi.org/10.1016/j.jmb.2010.03.005.

(36) Marqusee, S.; Baldwin, R. L. Helix Stabilization by Glu-...Lys+ Salt Bridges in Short Peptides of de Novo Design. Proc. Natl. Acad. Sci. U. S. A. **1987**, 84 (24), 8898–

8902.

(37) Schon, O.; Friedler, A.; Bycroft, M.; Freund, S. M. V; Fersht, A. R. Molecular Mechanism of the Interaction between MDM2 and P53. J. Mol. Biol. **2002**, 323 (3), 491–501. https://doi.org/10.1016/s0022-2836(02)00852-5.

(38) Rice, J.; Schohn, A.; Bessette, P.; Boulware, K.; Daugherty, P. Bacterial Display Using Circularly Permuted Outer Membrane Protein OmpX Yields High Affinity Peptide Ligands. Protein Sci. **2006**, 15 (4), 825–836. https://doi.org/10.1110/ps.051897806.

(39) Patel, D. S.; Qi, Y.; Im, W. Modeling and Simulation of Bacterial Outer Membranes and Interactions with Membrane Proteins. Curr. Opin. Struct. Biol. **2017**, 43, 131–140. https://doi.org/10.1016/J.SBI.2017.01.003.

(40) Gallardo, I. F.; Webb, L. J. Demonstration of ??-Helical Structure of Peptides Tethered to Gold Surfaces Using Surface Infrared and Circular Dichroic Spectroscopies. Langmuir **2012**, 28 (7), 3510–3515. https://doi.org/10.1021/la204927q.

(41) Knotts IV, T. A.; Rathore, N.; De Pablo, J. J. An Entropic Perspective of Protein Stability on Surfaces. Biophys. J. **2008**, 94 (11), 4473–4483. https://doi.org/10.1529/biophysj.107.123158.

(42) Sia, S. K.; Carr, P. a; Cochran, A. G.; Malashkevich, V. N.; Kim, P. S. Short Constrained Peptides That Inhibit HIV-1 Entry. Proc. Natl. Acad. Sci. **2002**, 99 (23), 14664–14669. https://doi.org/10.1073/pnas.232566599.

(43) Fox, J. M.; Zhao, M.; Fink, M. J.; Kang, K.; Whitesides, G. M. The Molecular Origin of Enthalpy/Entropy Compensation in Biomolecular Recognition. Annu. Rev. Biophys. **2018**, 47 (1), 223–250. https://doi.org/10.1146/annurev-biophys-070816-033743.

(44) Bird, G.; Madani, N.; Perry, A.; Princiotto, A.; Supko, J.; He, X.; Gavathiotis, E.; Sodroski, J.; Walensky, L. Hydrocarbon Double-Stapling Remedies the Proteolytic Instability of a Lengthy Peptide Therapeutic. Proc. Natl. Acad. Sci. U. S. A. **2010**, 107 (32), 14093–14098. https://doi.org/10.1073/pnas.1002713107.

(45) Bullock, B. N.; Jochim, A. L.; Arora, P. S. Assessing Helical Protein Interfaces for Inhibitor Design. J. Am. Chem. Soc. **2011**, 133 (36), 14220–14223. https://doi.org/10.1021/ja206074j.

(46) Leshchiner, E. S.; Parkhitko, A.; Bird, G. H.; Luccarelli, J.; Bellairs, J. A.; Escudero, S.; Opoku-Nsiah, K.; Godes, M.; Perrimon, N.; Walensky, L. D. Direct Inhibition of Oncogenic KRAS by Hydrocarbon-Stapled SOS1 Helices. Proc. Natl. Acad. Sci. **2015**, 112 (6), 1761–1766. https://doi.org/10.1073/pnas.1413185112.

(47) Walensky, L. D.; Kung, A. L.; Escher, I.; Malia, T. J.; Barbuto, S.; Wright, R. D.; Wagner, G.; Verdine, G. L.; Korsmeyer, S. J. Activation of Apoptosis in Vivo by a Hydrocarbon-Stapled BH3 Helix. Science **2004**, 305 (5689), 1466–1470. https://doi.org/10.1126/science.1099191.

(48) Moellering, R. E.; Cornejo, M.; Davis, T. N.; Bianco, C. Del; Aster, J. C.; Blacklow, S. C.; Kung, A. L.; Gilliland, D. G.; Verdine, G. L.; Bradner, J. E. Direct Inhibition of the NOTCH Transcription Factor Complex. Nature **2009**, 462 (7270), 182–188. https://doi.org/10.1038/nature08543.

(49) Maru, Y.; Afar, D. E.; Witte, O. N.; Shibuya, M. The Dimerization Property of Glutathione S-Transferase Partially Reactivates Bcr-Abl Lacking the Oligomerization Domain. J. Biol. Chem. **1996**, 271 (26), 15353–15357. https://doi.org/10.1074/jbc.271.26.15353.

(50) Kruziki, M. A.; Sarma, V.; Hackel, B. J. Constrained Combinatorial Libraries of Gp2 Proteins Enhance Discovery of PD-L1 Binders. ACS Comb. Sci. **2018**, 20 (7), 423–435. https://doi.org/10.1021/acscombsci.8b00010.

(51) Pazgier, M.; Liu, M.; Zou, G.; Yuan, W.; Li, C.; Li, C.; Li, J.; Monbo, J.; Zella, D.; Tarasov, S.; et al. Structural Basis for High-Affinity Peptide Inhibition of P53 Interactions with MDM2 and MDMX. Proc. Natl. Acad. Sci. U. S. A. **2009**, 106 (12), 4665–4670. https://doi.org/10.1073/pnas.0900947106.

(52) Phan, J.; Li, Z.; Kasprzak, A.; Li, B.; Sebti, S.; Guida, W.; Schönbrunn, E.; Chen, J. Structure-Based Design of High Affinity Peptides Inhibiting the Interaction of P53 with MDM2 and MDMX. J. Biol. Chem. **2010**, 285 (3), 2174–2183. https://doi.org/10.1074/jbc.M109.073056.

(53) Case, B. A.; Kruziki, M. A.; Johnson, S. M.; Hackel, B. J. Engineered Charge Redistribution of Gp2 Proteins through Guided Diversity for Improved PET Imaging of Epidermal Growth Factor Receptor. Bioconjug. Chem. **2018**, 29 (5), 1646–1658. https://doi.org/10.1021/acs.bioconjchem.8b00144.

(54) Stieglitz, J. T.; Kehoe, H. P.; Lei, M.; Van Deventer, J. A. A Robust and Quantitative Reporter System To Evaluate Noncanonical Amino Acid Incorporation in Yeast. ACS Synth. Biol. **2018**, 7 (9), 2256–2269. https://doi.org/10.1021/acssynbio.8b00260.

(55) Atangcho, L.; Navaratna, T.; Thurber, G. M. Hitting Undruggable Targets: Viewing Stabilized Peptide Development through the Lens of Quantitative Systems Pharmacology. Trends Biochem. Sci. **2018**. https://doi.org/10.1016/j.tibs.2018.11.008.

(56) Liu, H.; Naismith, J. H. An Efficient One-Step Site-Directed Deletion, Insertion, Single and Multiple-Site Plasmid Mutagenesis Protocol. BMC Biotechnol. **2008**, 8

(1), 91. https://doi.org/10.1186/1472-6750-8-91.

(57) Getz, J. A.; Schoep, T. D.; Daugherty, P. S. Peptide Discovery Using Bacterial Display and Flow Cytometry. Methods Enzymol. **2012**, 503, 75–97. https://doi.org/10.1016/B978-0-12-396962-0.00004-5.

(58) Van Deventer, J. a.; Yuet, K. P.; Yoo, T. H.; Tirrell, D. a. Cell Surface Display Yields Evolvable, Clickable Antibody Fragments. ChemBioChem **2014**, 15 (12), 1777–1781. https://doi.org/10.1002/cbic.201402184.

(59) Link, A. J.; Vink, M. K. S.; Tirrell, D. A. Preparation of the Functionalizable Methionine Surrogate Azidohomoalanine via Copper-Catalyzed Diazo Transfer. Nat. Protoc. **2007**, 2 (8), 1879–1883. https://doi.org/10.1038/nprot.2007.268.

(60) Daugherty, P. S.; Olsen, M. J.; Iverson, B. L.; Georgiou, G. Development of an Optimized Expression System for the Screening of Antibody Libraries Displayed on the Escherichia Coli Surface. Protein Eng. **1999**, 12 (7), 613–621. https://doi.org/10.1093/protein/12.7.613.

(61) Ayyadurai, N.; Neelamegam, R.; Nagasundarapandian, S.; Edwardraja, S.; Park, H. S.; Lee, S. J.; Yoo, T. H.; Yoon, H.; Lee, S. G. Importance of Expression System in the Production of Unnatural Recombinant Proteins in Escherichia Coli. Biotechnol. Bioprocess Eng. **2009**, 14 (3), 257–265. https://doi.org/10.1007/s12257-009-0009-z.

(62) Dupont, C. L.; Grass, G.; Rensing, C. Copper Toxicity and the Origin of Bacterial Resistance—New Insights and Applications. Metallomics **2011**, 3 (11), 1109. https://doi.org/10.1039/c1mt00107h.

(63) Soriano Del Amo, D.; Wang, W.; Jiang, H.; Besanceney, C.; Yan, A. C.; Levy, M.; Liu, Y.; Marlow, F. L.; Wu, P. Biocompatible Copper(I) Catalysts for in Vivo Imaging of Glycans. J. Am. Chem. Soc. **2010**, 132 (47), 16893–16899. https://doi.org/10.1021/ja106553e.

(64) Kanagawa, T. Bias and Artifacts in Multitemplate Polymerase Chain Reactions (PCR). J. Biosci. Bioeng. **2003**, 96 (4), 317–323. https://doi.org/10.1016/S1389-1723(03)90130-7.

(65) Ramesh, B.; Frei, C. S.; Cirino, P. C.; Varadarajan, N. Functional Enrichment by Direct Plasmid Recovery after Fluorescence Activated Cell Sorting. Biotechniques **2015**, 59 (3), 157–161. https://doi.org/10.2144/000114329.

(66) Zhang, Q.; Lu, H. Identification of Small Molecules Affecting P53-MDM2/MDMX Interaction by Fluorescence Polarization. Methods Mol. Biol. **2013**, 962, 95–111. https://doi.org/10.1007/978-1-62703-236-0-8.

(67) Lau, Y. H.; Spring, D. R. Efficient Synthesis of Fmoc-Protected Azido Amino Acids. Synlett **2011**, No. 13, 1917–1919. https://doi.org/10.1055/s-0030-1260950.

(68) Goddard, T. D.; Kneller, D. G. SPARKY 3. University of California, San Francisco.

(69) Wüthrich, K. NMR of Proteins and Nucleic Acids. J. Magn. Reson. **1988**, 79 (3), 586. https://doi.org/10.1016/0022-2364(88)90098-4.

(70) Yilmaz, E. M.; Güntert, P. NMR Structure Calculation for All Small Molecule Ligands and Non-Standard Residues from the PDB Chemical Component Dictionary. J. Biomol. NMR **2015**, 63 (1), 21–37. https://doi.org/10.1007/s10858-015-9959-y.

(71) Trott, O.; Olson, A. J. AutoDock Vina: Improving the Speed and Accuracy of Docking with a New Scoring Function, Efficient Optimization, and Multithreading. J. Comput. Chem. **2010**, 31 (2), 455–461. https://doi.org/10.1002/jcc.21334.

(72) Dolinsky, T. J.; Nielsen, J. E.; McCammon, J. A.; Baker, N. A. PDB2PQR: An Automated Pipeline for the Setup of Poisson-Boltzmann Electrostatics Calculations. Nucleic Acids Res. **2004**, 32 (Web Server), W665–W667. https://doi.org/10.1093/nar/gkh381.

Chapter III: Evolving MDM2-Binding Peptides with Staple Diversity

Tejas A. Navaratna*, Marshall Case*, Sophie Gable, Greg M. Thurber

*Denotes equal contribution

This is an unsubmitted manuscript currently under preparation.

Abstract

Directed evolution has seen numerous impactful applications in enzyme technology, antibody engineering, other biomolecular recognition systems, and industrial microbe development. When paired when display techniques, such as with phage, bacteria, and yeast, it affords a high-throughput way of screening diverse libraries of biomolecules. We have previously developed a method to screen stapled peptide libraries on the surface of E. coli to discover propargyl ether click-stabilized inhibitors of the p53-MDM2 interaction. The modular nature of the double-click peptide stapling strategy invites introducing physicochemical diversity into the linker to improve or add properties like cell penetrance, fluorescence, protease stability, and binding affinity by increasing contact area. In this work, we introduce diversity into p53-like click-stabilized peptides by using an all-hydrocarbon aliphatic staple, a rigid benzene staple, and an extended linker containing a functionalizable amine group. We conducted one round of magnetic sorting and 4 rounds of fluorescence-activated cells sorting (FACS) to generate enriched libraries for each

unique linker. Flow cytometric analysis of sorted populations revealed affinity improvements in all linker libraries, including those with initially poor binding. Extensive deep sequencing of each library after each round elucidated sequence-linker dependencies and trends. This work represents the application of chemically diverse linker libraries for the high throughput screening of MDM2-binding stapled peptides.

Introduction

Targeting protein-protein interactions (PPIs) can result in therapeutic outcomes, but due to the large surface area over which PPIs occur, have largely failed to be effectively inhibited by small molecule drugs[1]. They are involved in all disease states and dysfunctional PPIs, due to mutation or epigenetic changes, are found in many cancers. A few prominent examples of PPIs include p53-MDM2[2], Bim-BCL2[3], and SOS1-KRAS[4], two of which have avoided clinical inhibition by small molecules, with venetoclax only recently receiving FDA approval for targeting BCL2[5]. Much larger proteins, like antibodies and molecules based off antibodies like scFvs, affibodies, nanobodies, and Fab fragments, while offering highly specific and potent target engagement, are largely restricted to extracellular binding, with engagement of cytoplasmic targets only reported in a few cases[6,7], with no clear understanding of the targeting mechanism. In contrast, stapled peptides have been developed against a range of cytoplasmic and extracellular targets[4,8–12]. It is well understood that the linker size and charge play a large role in determining intracellular access[13–16] and several assays have been developed to determine cytoplasmic peptide localization[17–19].

Directed evolution has been used to screen libraries of biomolecules, including peptides, for high affinity binding. Examples include phage display[20], bacterial[21] and yeast surface display[22], and mRNA display[23], and each approach has its relative merits and disadvantages. All of these methods couple genotype (encoding nucleic acid sequence) to phenotype (protein binding), making selection by cellular sorting or panning followed by sequencing possible. Post-sort stapling was used to develop ATSP-7041[24], the precursor to the ALRN-6924, an MDM2 inhibitor that is currently in clinical trials. However, it is also understood that inappropriate stapling location and flanking residue identity can result in binding losses[25], making post-selection stapling optimization time-consuming and expensive, as each option has to be synthesized by solid phase peptide synthesis (SPPS) and characterized for potency[11].

There is a nascent effort underway to select peptides that have been stapled while displayed, that is, prior to sorting, so that physicochemical changes conferred by stapling interact with amino acid residue identity in a synergistic manner. Heinis and coworkers displayed cysteine-bridged alpha helices with bis-bromo containing linkers using phage display to discover beta-catenin binders[9]. Araghi et al. used one-bead-one-compound technology to screen a small library of all-hydrocarbon olefin metathesis stapled peptides against Bcl-2[26] and used mass spectrometry to decode peptides. Our lab has developed SPEED, an approach using azidohomoalanine incorporation in E. coli to display bio-orthogonally double-clicked stabilized peptides and applied it to discover potent inhibitors of the p53-MDM2 interaction[27]. In this earlier work, we generated a library of propargyl ether **(1)** stabilized peptides and conducted several rounds of magnetic and fluorescence-

based sorting. We found a lead compound, SPD-M6-V1, that contained two cysteines involved in a disulfide bond, an affinity-enhancing motif that notably could not arise from a cysteine-modifying strategy.

Despite the high affinity of bacterially-displayed propargyl ether-stabilized p53-like sequence[28] and even higher affinity of SPD-M6-V1 (K_d values of 15 nM and 1.7 nM respectively), other staple linkers could increase or decrease binding through unpredictable and significant effects on helicity and contacts with MDM2. The role of staple length and rigidity has been previously investigated by Zhang et al. for double-click stabilization of GLP1R ligands, finding a modest loss in affinity for 1,3-diethynylbenzene-stabilized GLP1 and exendin-4 and no significant loss in affinity for AlexaFluor680-conjugated linker stabilized molecules compared to propargyl ether[29]. Lau and coworkers have conducted extensive comparison studies with linear and aromatic hydrocarbon bis-alkyne linkers of different lengths and found ~2-fold loss in affinity for a phage-evolved sequence when stapled with the rigid 1,3-diethynylbenzene staple vs. a linear molecule[30]. Conjugating a mono-arginine, bi-arginine, or tri-arginine motif to the staple led to decreases in measured affinity as well[31]. Furthermore, Kale et al. screened large phage libraries with a variety of cysteine-modifying linkers to study the importance of staple length and staple dependence on sequence[32]. As we have found disulfide bond formation important for potent MDM2 binding[27], we were motivated to study directed evolution with diverse staples in a bioorthogonal manner (i.e. preserving the role of cysteines and other residues) to understand how linker-sequence synergy results in affinity improvements.

Results

P53-like sequence and SPD-M6-V1 are poor MDM2 binders with diverse double-click linkers

Using the on-surface optimized click stabilization method from our previous work[27], we stabilized the p53-like sequence with propargyl ether **(1)**, 1,6-heptadiyne **(2)**, 1,3-diethynylbenzene **(3)**, and an amine-functionalizable extended linker **(4)** first developed for peptide imaging agent synthesis[29,33] (Figure III - 1A). After stabilization, bacteria were labeled with fluorescent MDM2-GST and analyzed by flow cytometry. This revealed significant loss in signal for the p53-like sequence reacted with **(2)** compared to unreacted, and even larger losses for **(3)** and **(4)** (Figure III - 1B, left). For the propargyl ether-evolved SPD-M6-V1 sequence, we observed no loss in signal for **(2)**, which is consistent with the similar but not identical structures, with a substitution of an oxygen for a carbon. We did however observe large losses in binding for **(4)** and especially **(3)** for SPD-M6-V1 (Figure III - 1B, right).

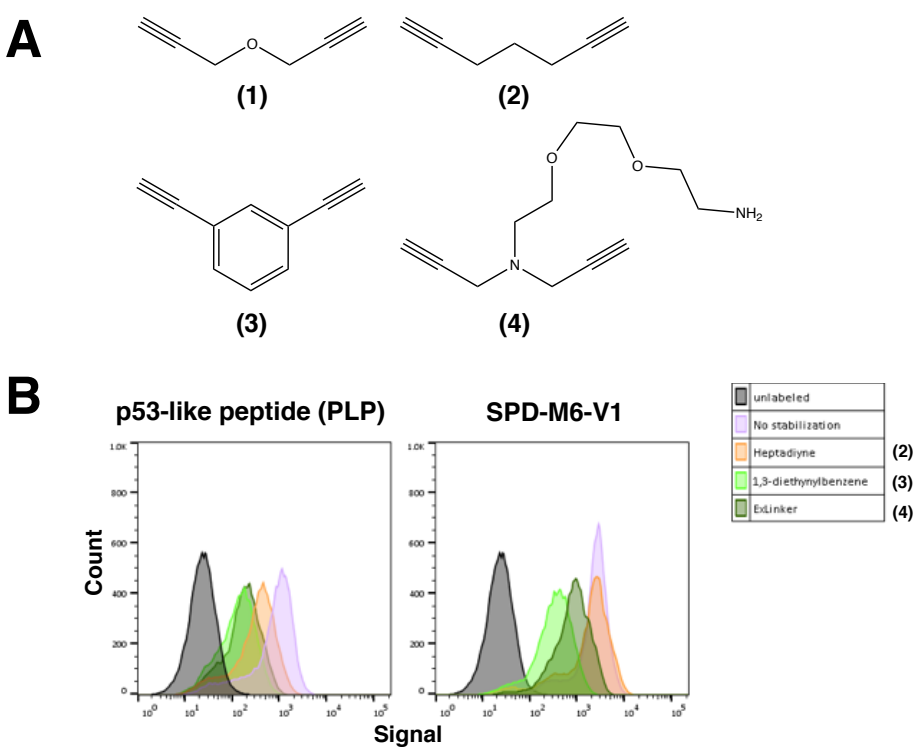

Figure III - 1. Structures and binding histograms of previously reported sequences (A) structures of stabilizing bis-alkyne linkers used in this paper, **(1)**, propargyl ether, **(2),** 1,6-heptadiyne, (**3)**, 1,3-diethynylbenzene, **(4)**, amine functionalizable extended linker. (B) Flow cytometry histograms of bacteria displaying bis-alkyne linker stabilized p53-like peptide (PLP, left) or SPD-M6-V1 (right).

Staple location strongly influences binding affinity for the p53-like sequence

The construction of our bacterial surface libraries allows the pooling and decoding of libraries containing many possible staple locations. To establish the importance of stapling location, we modified the starting p53-based sequence (PLP) with alternative stapling locations, 1-8 and 6-13. We selected these positions based on our docked structure of SPD-M6-V1 binding to MDM2[27] (Figure III – 2A), hypothesizing that the 1-8 location would be staple-permissive, while the stapling at the 6-13 location would abrogate binding. Indeed, affinity determination on the bacterial cell surface (Figure III –

2B) confirmed that stapling dramatically worsens affinity at the 6-13 position (Table III – 1). We have shown that for the PLP sequence in particular, bacterial surface measurements underestimate stapling affinity gains[27]. and thus, the "true" in-solution affinity loss upon stapling PLP(6-13) is likely greater the reported ~6 fold (Table III -1).

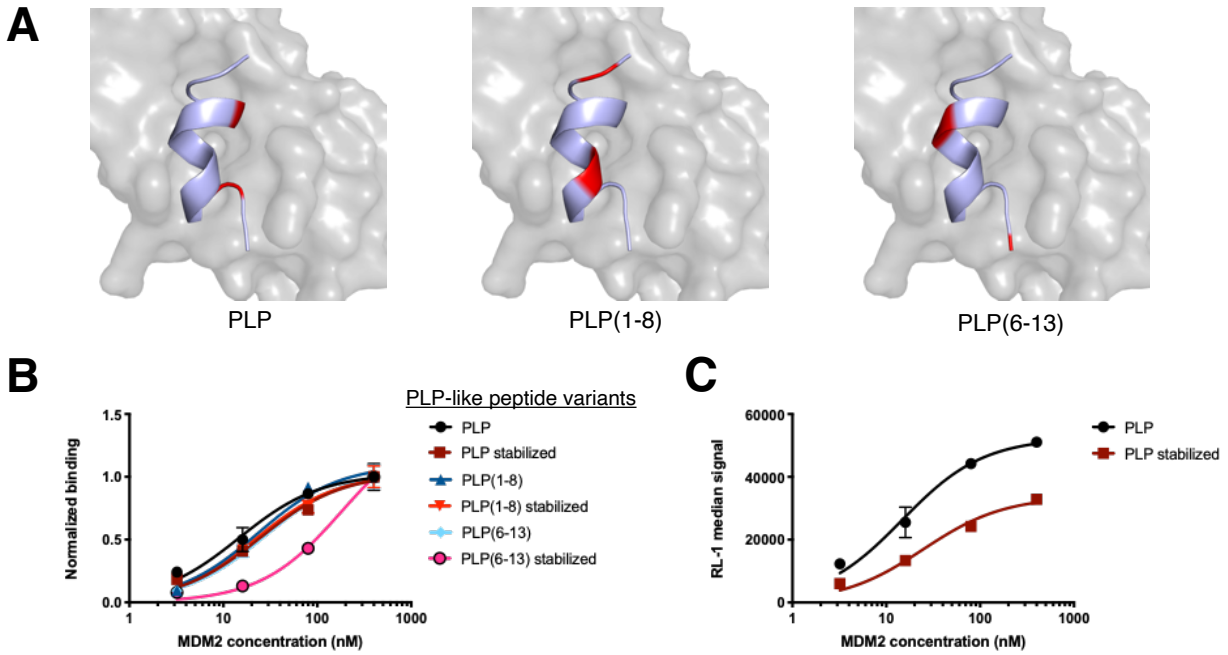

Figure III - 2. Staple scan locations and measured affinity.
A) Based on our calculated structure of SPD-M6-V1 bound to MDM2[27], two additional pairs of locations (1-8 and 6-13) were chosen for mutagenesis to methionine, AHA replacement, and stapling. Stapling residues are highlighted in red. In PLP (left), residues 4 and 11 were chosen as the stabilization sites, as well was in the library based on PLP[27]. Analysis of the structure suggests PLP and PLP(1-8) would exhibit minimal clashes upon stapling with propargyl ether, whereas stapled PLP(6-13) is expected to exhibit steric clashes with MDM2. (B) Measurement of binding affinity on the bacterial cell surface corroborates the stapling location clash hypothesis, with PLP and PLP(1-8) exhibiting minimal loss in affinity upon stapling with propargyl ether (see Table III – 1 for values), but PLP(6-13) exhibiting significant affinity loss. (C) Total signals from PLP and stabilized PLP, showing a marked decrease in signal upon stabilization despite similar affinity (Table III – 1).

Table III - 1. Affinity data for chosen alternate stapling locations.
Peptides with stapled with propargyl ether and X in the sequence represents azidohomoalanine.

Name	Sequence	Non-stabilized K_d	Stabilized K_d
PLP	ETFXDLWRLLXEN	15 ± 2.5 nM	27 ± 3.8 nM
PLP(1-8)	XTFSDLWXLLPEN	23 ± 3.5 nM	23± 4.3 nM
PLP(6-13)	ETFSDMWRLLPEM	28 ± 4.3 nM	180 ± 42 nM

Directed evolution of a randomized i,i+7 azidohomoalanine library yields affinity-improved binders with diverse linkers

Because of poor MDM2 binding after stabilization with linkers (2), (3), and (4) of p53-like and SPD-M6-V1 sequences, we evolved randomized peptides displayed with eCPX based on the p53 binding sequence to MDM2. Library construction was carried out as reported previously[27], and briefly, the three critical MDM2-binding residues (F19, W23, L26) as well as the two Met sites for stabilization (X20, X27) were kept fixed. All other sites were randomized by an NNC codon scheme permitting 15 possible amino acids and no stop codons at each position. Peptides were displayed as N-terminal fusions to the met-removed eCPX scaffold expressed in the pQE80L vector[27]. Libraries were stabilized and sorted first by MACS and then by 4 serial rounds of FACS. In between rounds, cells were lysed, DNA extracted, and fresh cells were transformed. Freshly transformed libraries were grown up, induced, and reacted with a given linker (see methods), or no linker at all **(0)** as a negative control.

Flow cytometric analysis of sorted populations revealed that binders were enriched in all three linker and no linker populations (Figure III - 3). However, the magnitude of

binding improvements depended strongly on linker identity. No linker **(0)** and 1,6-heptadiyne **(2)** showed most improvement, and this was apparent as early as the first round of sorting (by MACS, Figure III - 3A, 3B). 1,3-diethynylbenzene **(3)** showed the most minimal enrichment, though sorted populations after MACS and after 4 rounds of FACS could still be discerned from the unsorted population (Figure III - 3C). The extended linker molecule **(4)** showed an intermediate phenotype improvement with a less evident MACS shift (Figure III - 3D).

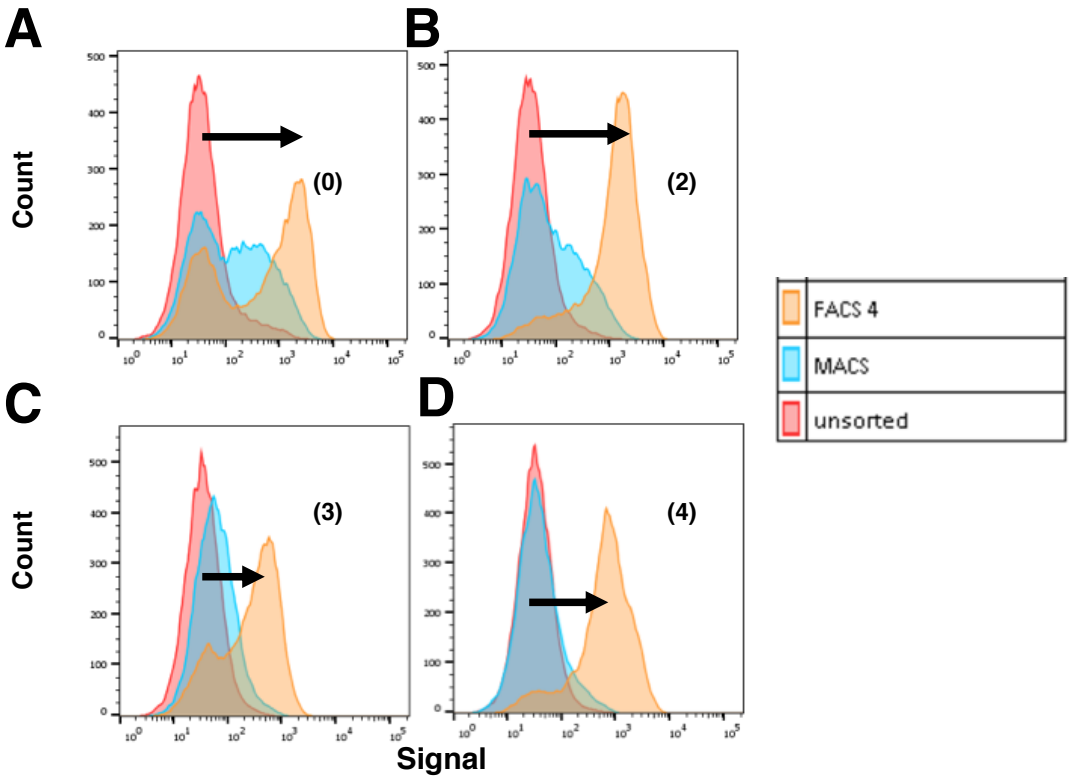

Figure III - 3. Flow cytometry histograms of populations differentially stabilized. Populations were stabilized with no linker (**0**; A) or different linkers (**2, 3, 4;** B-D)**.** In all four subplots, MACS and FACS enrichment are evident but the magnitude depends on the linker, with **0** and **2** showing the most improvement in both MACS and after 4 rounds of FACS. **3** shows the least FACS improvement, while **4** shows a modest shift. A population shift similar to the magnitudes in (A) and (B) is apparent for selections carried out with propargyl ether as reported in our previous work (Figure 2A)[27].

Mixed reaction analysis reveals linker identity dependencies

As the traditional approach in developing high affinity stapled peptides involves non-stabilized peptide display and post-screen stapling[34,35], we evaluated the impact of stapling on MDM2 binding of libraries evolved with and without stapling. We also tested the impact of neglecting to staple on a library screened with the least binding-improved staple, 1,3-diethynylbenzene **(3).** These results showed that for peptides evolved with 1,3-diethynylbenzene stapling, a lack of stapling actually conferred higher binding than with stapling (Figure III - 4A, 4C). Importantly though, the converse test, in which peptides evolved without stapling were evaluated, post-screening 1,3-diethynylbenzene stabilization conferred the poorest binding properties (Figure III - 4D). In other words, the 1,3-diethynnylbenzene staple reduces affinity of the peptide even with evolution, this 'penalty' in binding is reduced relative to peptides evolved without stapling. This is consistent with the idea that given a need for stabilization (for protease stability, cell penetration, in vivo circulation, etc.), it is preferable to staple pre-screen (Figure III - 4A) than post-screen (Figure III - 4D).

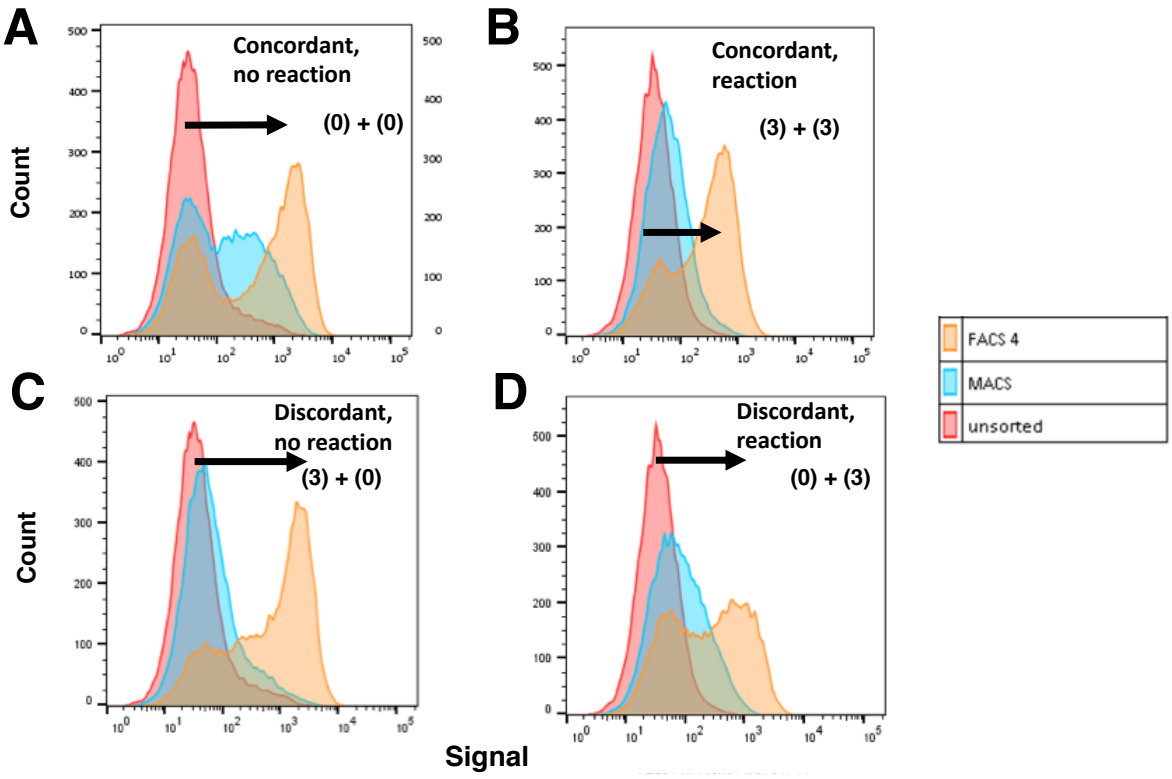

Figure III - 4. Analysis of binding for peptide libraries with or without 1,3-diethynylbenzene stapling.
(A) "concordant, no reaction", where displayed peptides evolved without reaction are also not reacted, showing high improvement. (B) "concordant with reaction," where displayed peptides evolved with **(3)** are reacted with **(3)**, showing modest improvement. (C) "discordant, no reaction", where peptides evolved with **(3)** are not reacted, showing similarly high improvement. (D) "discordant with reaction," where peptides evolved without **(3)** are reacted, showing the poorest binding and little separation between unsorted and most sorted population.

Affinity analysis of individual sequences shows linker-specific and linker-independent evolution

We sequenced several clones from each final library (following MACS and 4 rounds of FACS) and surface-expressed peptide stabilized with each linker (see methods) and titrated three concentrations of MDM2-GST to assess target affinity. 1,3-

diethynylbenzene **(3)** reacted peptides uniformly showed decreased signal relative to the other linkers, but in a sequence-dependent manner (Figure III - 5). In all cases except for the peptide evolved and stabilized with the functionalizable linker **(4)**, Figure III - 5D, peptides exhibited highest signal without reaction. We also observed significant decreases in signal for known binder PLP upon stapling even with saturating concentrations of MDM2 (Figure III – 2C) and are currently working on determining the cause. This may be a difficult-to-avoid consequence of a reaction with multiple side-products (see Figure III - 7 and modeling methods), and we hypothesize that the double-reacted peptide products may compromise binding and reduce signal.

Because of the mix of shared 'target-specific' mutations (e.g. i,i+5 cysteines) versus target specific contributions, it is difficult to generate concrete conclusions from isolated examples. Therefore, we sought to use next-generation sequencing (NGS) of the libraries to analyze the enrichment in a high-throughput manner.

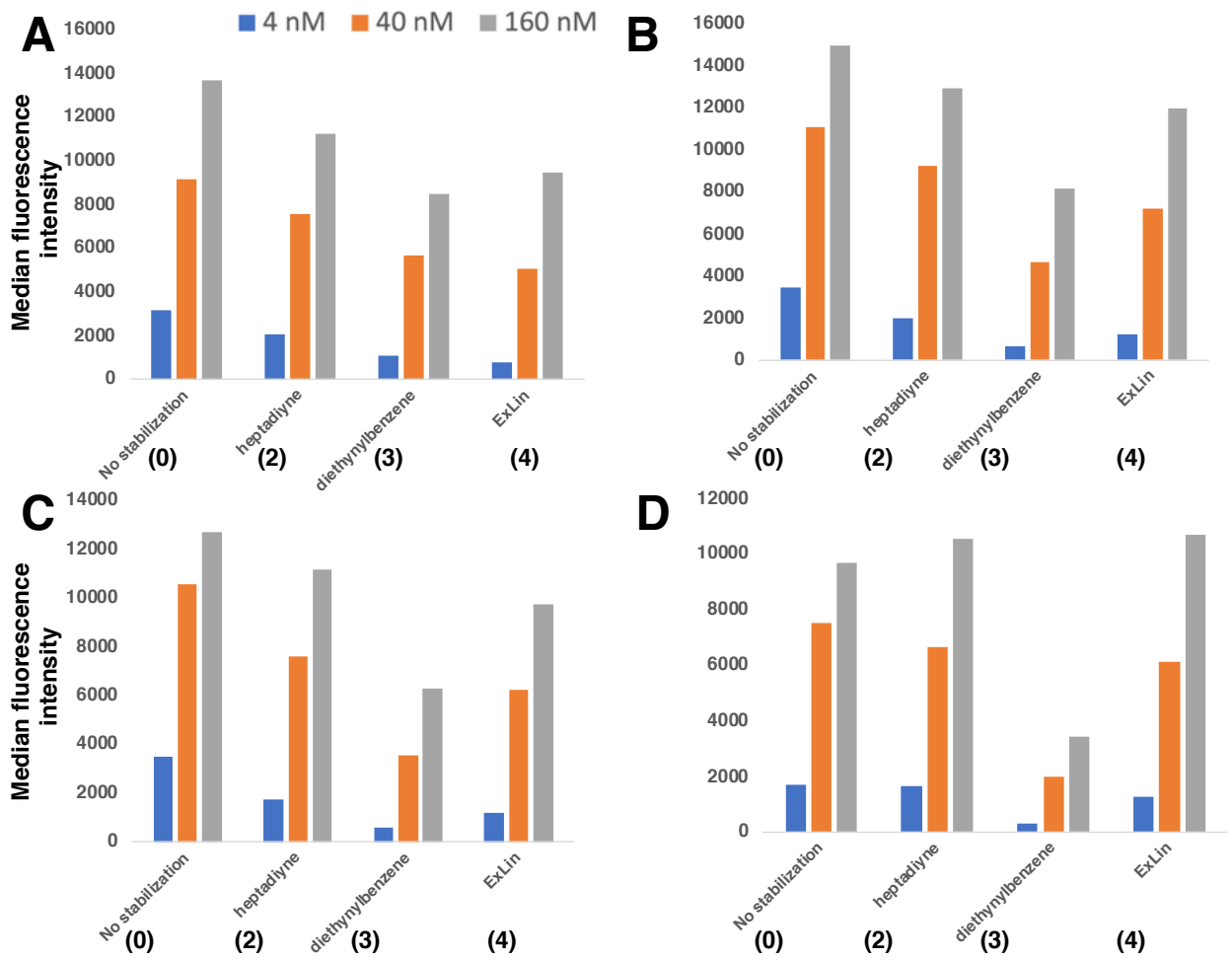

Figure III - 5. Binding analyses of 4 peptides isolated after 4 rounds of FACS from each library.
(A) CVTFMCYWGDLII**,** from evolution with no peptide stabilization, exhibits highest signal without stabilization and depressed signal when stabilized with either **(3)** or **(4)**. (B) CFTFMCYWSDLMGN from evolution with stabilization with **(2)**, shows slightly higher signal without stabilization but comparable signals for **(2)** and **(4)**, with the greatest decrease for **(3)**. (C) CITFMCFWGNLMAD, from evolution with stabilization with **(3),** was an unexpected poor binder with **(3)** and showed best signal without stabilization (D). CIFFMCFWNDLMGY, from evolution with **(4),** interestingly exhibits highest binding signal with **(4)**, but decreased affinity relative to **(0)**, comparing the 40 nM labeling to the 160 nM labeling signals. Reaction with **(3)** indicates that this sequence is a poor 1,3-diethynylbenzene binder, supporting the idea that evolution in the desired staple context is important to discover good binders.

Deep sequencing reveals linker-specific and broader conservation trends

We performed deep sequencing for each linker library for each round of selection to uncover sequence patterns using the Illumina NovaSeq platform and obtained between 2 million – 12 million reads per library. After quality control and barcode assignment, we generated amino acid logo plots[36] for the most abundant sequences from the 4th round of FACS for all linker libraries (Figure III - 6A) and computed frequencies of unique sequences (Figure III - 6B). All libraries except for those evolved with 1,3-diethynylbenzene **(3)** showed clear enrichment patterns, with the no reaction library being glycine-rich and consistently losing the second stabilization site. We speculate that sequences that undergo the M12I mutation may be better displayers, as AHA incorporation at two sites modestly reduces display level[27]. 1,6-heptadiyne (**2)** sequences show strong and clear enrichment of fan N-terminal i,i+5 cysteines motif, suggesting disulfide bond formation. The functionalizable linker **(4)**, in contrast, shows position-specific preference for serine and asparagine residues with a significant minority of peptides containing i,i+5 cysteines. Sequences evolved with 1,3-diethynylbenzene **(3)** reaction show very little evidence of residue conservation (Figure III - 6A), and analysis of the frequencies of 300 peptides reveals many more low abundance peptides than any of the other libraries, indicating weak selection pressure (Figure III - 6B). In addition to these linker-specific trends, a number of conserved residues were common to no reaction **(0)**, 1,6-heptadiyne **(2)**, and the functionalizable linker **(4)**, such as D10 and Y/F7, with a clear bias against Y7 for the functionalizable linker. Put together, the deep sequencing of

sorted libraries identified both linker-specific and linker-agnostic sequence patterns for MDM2 binding.

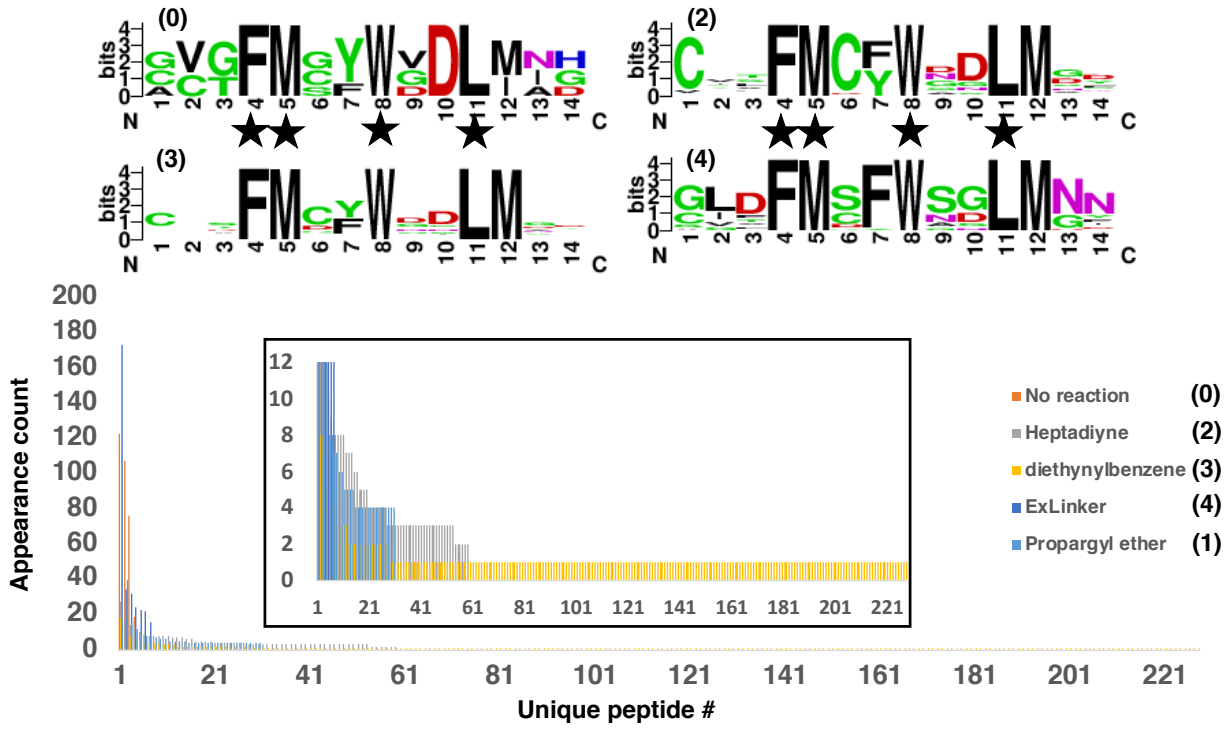

Figure III - 6. Deep sequencing analysis.
(A) Logo plots for the 300 most abundant clones after four rounds of FACS. Starred residues (F4, M5, W8, L11) were fixed in the generated library. Differential conservation patterns are observed for all three linkers and lack of linker, with loss of the methionine at position 12 without the linker **(0)**, consistent with not requiring AHA substitution at that site. An i,i+5 cysteine motif was very prominent for **(2)**, indicating a role for a disulfide bond in binding. **(3)** showed very little sequence conservation at any site, indicating low efficiency in sorting or lack of binding enhancement conferred by specific amino acids. This is consistent with the relatively poor binding for populations and individual clones observed. (B) Ranked frequency plot of 300 sequences present in each library with zoomed-in inset. This shows that for evolution done with **(0)**, **(1)**, **(2)**, and especially **(4)**, a few sequences dominate the population, but for **(3)**, there are many sequences that appear only once, indicating lack of conservation as also shown in Figure III - 6A.

Reaction analysis shows inefficient stabilization for 1,3-diethynylbenzene (3)

We had previously optimized reaction conditions, including Cu^{2+} concentration, chelator identity and concentration, and sodium ascorbate (reducing agent) concentration, bis-

alkyne concentration using propargyl ether as the linker[27]. Other bis-alkyne linkers have been reported to react with similar kinetics in solution, prompting the use of identical conditions for sorts[30,31]. However, the generally poor binding to MDM2 observed at the library and clonal level for 1,3-diethynylbenzene **(3)** stabilized peptides (Figure III – 3C, III - 3D) led us to investigate stabilization efficiency for surface displayed p53-like peptide. Cell lysates following click-stabilization were run on a gel after reaction with one of two reactive dyes to probe unreacted azide sites (SCy5-alkyne, Figure III - 7A, left) or unreacted alkynes from incomplete peptide stapling (SCy5.5-azide, Figure III - 7A, right). Analysis (using a computational approach, see methods) revealed the virtual lack of stabilized peptides when reaction was carried out with 1,3-diethynylbenzene **(3).** Differential equation modeling, fit to the azide- and alkyne- reactivity dataset (Figure III - 7A), showed that propargyl ether and 1,3-diethynylbenzene react very differently, with propargyl ether favoring the stabilized species but 1,3-diethynylbenzene favoring the two-reacted side product. In fact, due to incomplete reaction (Figure III - 7B), changing the concentration of 1,3-diethynylbenzene alone to favor more stabilization would not improve the fraction reacted. These results explain the lack of enrichment and sequence consensus in the 1,3-diethynylbenzene sorted libraries. Other experimental approaches, like decreasing or changing the catalyst, or decreasing reductant concentrations might reveal improved conditions for reaction with **(3).** For the other two linkers studied in this paper, inferred fraction reacted and fraction stabilized values are consistent with propargyl ether-like reactivity and are suitable for stabilizing peptides on the surface of bacteria.

A

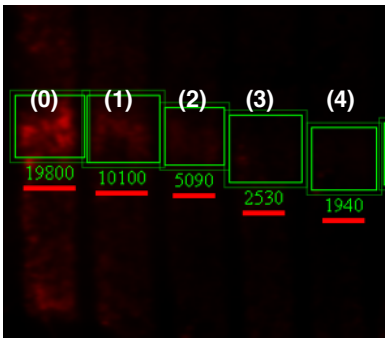

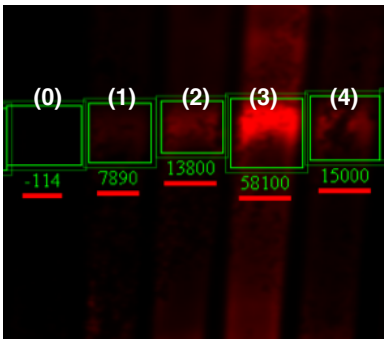

Cell surface double-click + SCy5-alkyne

Cell surface double-click + SCy5.5-azide

B

	fraction reacted	fraction stabilized
no reaction **(0)**	0.00	N/A
Propargyl ether **(1)**	0.57	0.45
Heptadiyne **(2)**	0.61	0.36
Diethynylbenzene **(3)**	0.77	0
ExLinker **(4)**	0.61	0.37

C

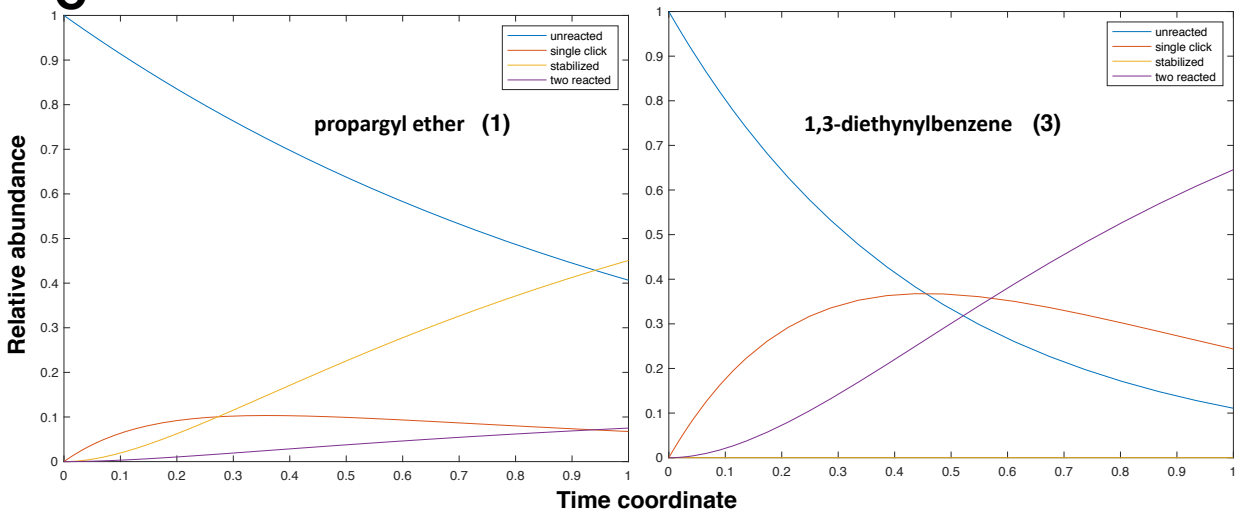

Figure III - 7. Reactivity and modeling of stabilization on the bacterial surface.
(A) Quantification of free azides (left) and free alkynes (right) on the bacterial surface following click-stabilization with different linkers. Free azides result from AHA incorporation into the peptide and the maximum signal is given by the result from **(0)**. Free alkynes result from incomplete stabilization, i.e. when only one of the alkyne moieties on the staple reacts with a surface displayed molecule. The highlighted band corresponds to eCPX-p53-like sequence. (B) Model fitting to the azide and alkyne quantification reveals fraction reacted AHA residues and fraction stabilized peptides. (C) Model trajectories for propargyl ether **(1)**, a successful click-stabilizer and for 1,3-diethynylbenzene **(3)**, which primarily results in two molecules of **(3)** reacting per peptide.

Discussion

Stapled peptides have been developed as powerful modulators of traditionally "undruggable" protein-protein interactions. Due to the slow kinetics of peptide cellular uptake relative to lipophilic small molecule drugs, only a small amount of an administered peptide typically accesses the cytoplasm, and thus the target affinity must be very high to observe efficacy. Linker identity has been widely reported to influence the affinity and target engagement of stapled peptides[29–31] as well as bioavailability in subcutaneously administered imaging agents[33]. This could be due to numerous factors, like target engagement[11,24,37] by the staple contributing to enthalpic gains, or protease resistance[33,38]. Of course, a stapled peptide's sequence and accompanying characteristics such as conformation, charge, and ability to form intermolecular bonds with the target strongly impact its drug-like behavior as well. Staple location matters as well; exhaustive staple location scanning is typically carried out to identify the best two sites[11] and we have shown the importance of avoiding the 6-13 site (Figure III – 2B). Despite the preponderance of directed evolution techniques to find high affinity binding sequences, there are no reports of simultaneously evolving sequence and linker. We hypothesized that sequence and linker synergize and that the optimum linker for a particular sequence is sequence-dependent. To test this, we conducted multiple rounds of sorting on a randomized MDM-binding library with different linkers to discover synergies. This was motivated by the fact that in the p53-MDM2 system, we tested a p53 mimic and a propargyl ether-evolved lead compound SPD-M6-V1 and found that they bound to MDM2 in a highly linker-dependent manner (Figure III - 1).

In this work, we characterized the reaction between various linkers and bacterially displayed peptide and found that 1,3-diethynylbenzene reacts poorly and does not result in stapling. Thus, all screens with libraries reacted with 1,3-diethynylbenzene likely contained peptides with predominantly double-reacted product (with two linkers per peptide). This potentially explains why less selection was observed when evolved with 1,3-diethynylbenzene (Figure III - 3) and all individual clones showed poor binding upon reaction with 1,3-diethynylbenzene (Figure III - 5). The linker must undergo efficient reaction and cross-linking to enable proper sorting.

The other two linkers for which libraries were evolved showed sufficient cross-linking efficiency. Deep sequencing has proved to be a powerful tool to understand sorting and evolution and we applied this technology to understand our libraries. Consistent with the lack of optimal reactivity, 1,3-diethynylbenzene showed poor enrichment and limited selection. Most interestingly, deep sequencing revealed unique residue conservation fingerprints in evolved peptides both non-stabilized and stabilized with 1,6-heptadiyne **(3)**, propargyl ether (**1**, data in chapter II of this dissertation), and the functionalizable linker **(4)** in Figure III - 6. Specifically, glycine residues at several sites (G1, G3, G6) and methionine loss at position 12 are favored in the no reaction evolution. Conservation of both I,i+4 and i, i+5 motifs is present in propargyl ether libraries[27] whereas the i, i+5 cysteine motif is strictly conserved for libraries stabilized with 1,6-heptadiyne. The specific sequence GLDFMSFWSGLMNN was highly conserved in evolution with the functionalizable linker, and work is ongoing in the lab to elucidate the biophysical properties of this molecule. At position 7, different linkers have preferences for either Y

or F only, with propargyl ether and no reaction favoring Y, heptadiyne and 1,3 diethynylbenzene having roughly equal abundance of Y or F, and functionalizable linker favoring F nearly exclusively. There are a few pan-linker conservation trends as well: D10 and N-terminal i, i+5 motifs are abundant in every final round sort library.

These analyses largely support the idea that the linker identity and sequence should not be developed independently of one other; rather, a linker should first be selected based on desired application. Some specific examples of linker choice are a fluorophore-containing linker for imaging applications[29,31,33], a polyarginine motif for cellular penetration[15], or others for protease stability. These linkers then would be reacted with a randomized library, and selections carried out with the presence of the particular linker. This approach would avoid the need to do expensive, post-screen optimization of sequence to tolerate the linker.

Co-crystal structures of stapled peptides with their targets have identified linker-protein contacts[37] and therefore it makes sense that linker identity can affect binding and moreover, synergy between linker and sequence can enforce the binding conformation with higher affinity. Additionally, machine learning approaches are amenable to the abundance of data from next generation sequencing ($>10^8$ sequences). Future work in our lab will involve use of deep learning methods to identify sequences with linker-specific and linker-agnostic binding followed by synthesis, biophysical characterization, and efficacy studies.

Methods

Materials

All chemicals were purchased from Sigma Aldrich unless noted below. PBS was obtained from Invitrogen (1X). The functionalizable bis-alkyne linker **(4)** was synthesized in-house according to the procedure in ref. 29 which is reproduced in the Appendix of this dissertation. All DNA oligos were purchased from Integrated DNA Technologies (Coralville, IA), and all restriction enzymes were purchased from New England Biolabs (Ipswich, MA). The eCPX gene in pB33eCPX (a gift from P.S Daugherty, Addgene plasmid # 23336) was modified as described in ref. 27 to avoid undesired methionine substitution at non-peptide sites. The Met auxotrophic E. coli strain TYJV2 was a generous gift from J. van Deventer. Electrocompetent cells for transformation and library generation were made according to the procedure described in ref. 39. MDM2-GST for sorting and analysis was recombinantly expressed and purified as described in ref. 40.

Staple mutants

Staple mutants PLP(1-8) and PLP(6-13) were generated using primers ACTTCCGTAGCTGGCCAGTCTGGCCAGATGACCTTTAGCGATCTGTGGATGCTGC TGCCGGAAAACGGCGGTGGCAGCGGAGGGCAGTCTGGGCAGTCTG and ACTTCCGTAGCTGGCCAGTCTGGCCAGGAAACCTTTAGCGATATGTGGCGCCTGC TGCCGGAAATGGGCGGTGGCAGCGGAGGGCAGTCTGGGCAGTCTG respectively, using the loop insertion procedure on the eCPX(-met) template[27] as described by Getz et al.[41]

Library generation

A methionine-free version of eCPX (except for the start codon) was used as a PCR template for generating the NNC library as described in ref. 27. After digestion and ligation, the library was transformed into electrocompetent Met auxotrophic TYJV2 E. coli achieving a library size of approximately 3 x 10^8 members.

Library expression and on-surface peptide reaction

As discussed in ref. 27, generated libraries or single clones for characterization were grown in M9 medium containing 20 amino acids (with 10x oversampling if a library). Upon reaching OD_{600} of 0.8, cells were methionine depleted in M9 medium containing 19 amino acids (no Met) for 15-45 minutes. Cells were then induced in M9 medium containing 19 amino acids plus 40 mg/L azidohomoalanine with 0.5 mM IPTG for 2 – 4 hours.

Following peptide expression with AHA incorporation, cells were washed twice with cold phosphate-buffered saline (PBS) and reacted in PBS containing premixed copper and chelator (final reaction concentration of 100 µM $CuSO_4$, 500 µM Tris(3-hydroxypropyltriazolylmethyl)amine), 5 mM sodium ascorbate, and 300 µM bis-alkyne linker for 4 h at 4°C. Cells were then resuspended in 0.2% bovine serum album/PBS (PBS/BSA).

Magnetic selections

MDM2-GST-biotin for MACS was prepared as in ref. 27. 50 mL of bis-alkyne reacted cells were first labelled with 18 nM MDM2-GST-biotin in 0.2% PBS/BSA. Cells were then washed once with PBS/BSA and incubated with 500 uL MyOne C1 beads (Thermo

Fisher) for 25 min at 4 °C with gentle rotation using MACSmix (Miltenyi Biotec). Magnetic beads were pulled down by a DynaMag-5 magnet (Thermo Fisher) and washed gently with 5 mL PBS/BSA. Isolated bead-bound cells were miniprepped using a Qiagen miniprep kit according to ref. 27. Resulting DNA, generally 100-500 ng total, was transformed into fresh TYJV2 cells for additional sorting and analysis.

Fluorescence selections

For each linker library, 5 mL of cells were grown out, induced, and reacted as described above. Serial rounds of FACS were carried out with increasing stringency. The first round of sorting, cells were incubated with 4 nM MDM2-GST-AF647 (collecting 2% brightest cells), second round 1 nM (collecting 0.5% brightest cells) , and the third and fourth rounds incubated with 1 nM of MDM2-GST-AF647 first and then 30 nM MDM2-GST-AF488 as described in ref. 27 to select for tight binders regardless of display level (roughly 1% of cells collected). Sorting was carried out in a MoFlo Astrios FACS instrument, and plasmids extracted and re-transformed into TYJV2 cells for further analysis and sorting if needed.

Deep sequencing

Plasmids were isolated from bacterial pellets by miniprep (Qiagen). Illumina Nextera XT sequencing primers were added to either side of the eCPX-peptide gene by PCR amplification using Q5 DNA polymerase (New England Biolabs). PCR products were cleaned by gel extraction and re-concentrated using a ZymoClean Clean & Concentrate kit. Another PCR amplification was performed also using Q5 to add the P5 and P7 Illumina

sequences for flow cell annealing as well as a unique 8 letter barcode on each end of the amplicon for demultiplexing. The second round of PCR was cleaned and re-concentrated identically. DNA concentrations were quantified using a QuBit fluorimeter, pooled, and submitted to the University of Michigan DNA Advanced Genomics core for analysis. Samples were demultiplexed by sorting samples with perfectly matched barcodes and ones that differed by up to one base pair. Samples were then analyzed with FastQC and samples with a PHRED score of less than 36 were discarded. Fastq files were then analyzed using Python scripts with Biopython and SeqIO packages. Forward and reverse reads were pairwise analyzed, discarding any sequences with differences in base pairs. The portion of the read that corresponds to the p53-based peptide was translated.

Reaction efficiency

To determine extent of reaction and stabilization, cells dually expressing p53-like sequence and HA tag were reacted as described above, washed, and further reacted in solution containing either 25 μM SCy5-alkyne or 25 uM Scy5.5-azide. Cell lysates, generated by boiling in SDS-PAGE loading buffer, were loaded onto a 4-12% Bis-Tris gel and run under denaturing conditions. The gel was transferred to a blot using the iBlot system (Invitrogen) and then probed for anti-HA signal to confirm even loading. Extent of reaction was quantified through normalization with the unreacted control and extent of stabilization determined through parameter fitting as described below:

The system of equations was adapted from Navaratna et al. 2020[27]:

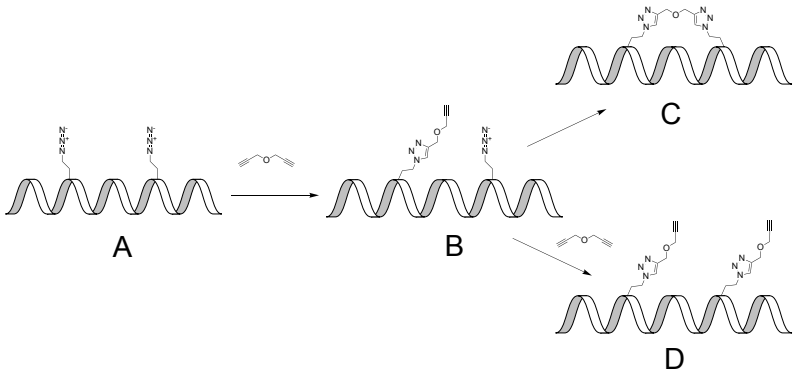

A, surface-displayed peptide; B, singly-reacted; C, stabilized peptide; D, two linker-reacted peptide; L, linker

k_1 is rate of reaction of one site with L. k_2, rate of stabilization

$$\frac{d[A]}{dt} = -k_1[L] \cdot [A]$$

$$\frac{d[B]}{dt} = k_1[L] \cdot [A] - k_2[B] - k_1[L] \cdot [B]$$

$$\frac{d[C]}{dt} = k_2[B]$$

$$\frac{d[D]}{dt} = k_1[L] \cdot [B]$$

All modeling was done in MATLAB R2018a. The parameters **R1_new** and **ratio_rxn_new** in the Supporting Information section "script for reaction rate and stabilization fraction analysis" represent k_1 and $\frac{k_2}{k1}$, the ratio of the second reaction rate to the first reaction rate respectively. **R1_new** and **ratio_rxn_new** were iteratively varied to match the relative reaction progress (from SCy5-alkyne quantitation) and relative SCy5.5-azide signal, represented in the code out by **completionnew** and **ratio_az_new** respectively.

Acknowledgements

The authors acknowledge the Flow Cytometry Core at the University of Michigan for assistance with sorting and the University of Michigan Advanced Genomics Core for useful discussions and technical support for NGS library preparation and sequencing.

This work was supported by an NSF CAREER Award CBET 1553860 (to G.M.T) and an NSF Graduate Fellowship to T.N. Additional support was provided by NIH Grant R35 GM128819 (to G.M.T).

Supporting information

MATLAB script for reaction rate and stabilization fraction analysis

```
R1_PE = 1.8 %dimensionalless rate of first reaction for propargyl ether

R1_new = 4.4 %dimensionless rate of first reaction for other molecule
%this is iteratively fit to satisfy completionnew ratio_new and ratio_new

ratio_PE = 3; %how much faster the second reaction is than the first for PE
R2_PE = R1_PE*ratio_PE; %second reaction rate

ratio_new = 0.0;  %how much faster the second reaction is than the first for other molecule
%this is iteratively fit to satisfy completionnew and ratio_new

R2_new = R1_new*ratio_new;
simtime = 1; %dimensionless time
```

```
[azide_signalPE,completionPE] = stab_rxn_ODE(0.5,R1_PE,R2_PE,simtime); %scaled signal from SCy5.5-azide rxn, completion of AHA rxn
[azide_signal_new,completionnew] = stab_rxn_ODE(0.5,R1_new,R2_new,simtime);

azide_signalPE %this was iteratively fit to find rxn rates for propargyl ether
completionPE

azide_signal_new
completionnew %this is output 1 and must match experiment

ratio_new = azide_signal_new/azide_signalPE %ratio of azide signal of other molecule to azide signal from PE,
%this is output 2 and must match experiment

function [totalsignal,completion] = stab_rxn_ODE(L,r1,r2,simtime)

close all;
options = odeset('Maxstep',10);

eqtime = [0, simtime]; %simulation length

x=zeros(4,1); % 4 species
%initialvalues:

z0=100*45.15/105.88;
x(1) = z0;

x(2) = 0;
x(3) = 0;
x(4) = 0;
```

```
%{
 unreacted pep
 single click
 stabilized
 two reacted pep
%}

L;%mM

[T , X] = ode45(@(t, x)odesystem(t, x), eqtime, x,options);

Time=T;

plot(T,X(:,1)/z0,T,X(:,2)/z0,T,X(:,3)/z0,T,X(:,4)/z0)
legend('unreacted','single click','stabilized','two reacted')

frac_non_stab = r1*L/(r1*L + r2);
%actual_frac_non_stab = X(length(T),4)/z0
completion = 1 - (2*X(length(T),1) + X(length(T),2))/(2*z0);
doublerxnsignal = 2*X(length(T),4)  ;
totalsignal = 2*X(length(T),4)+X(length(T),2);

frac_stab_total                                                                    =
X(length(T),3)/(X(length(T),1)+X(length(T),3)+X(length(T),2)+X(length(T),4))
frac_stab_rxn = X(length(T),3)/(X(length(T),3)+X(length(T),2)+X(length(T),4))

   function xdot = odesystem(t, x);
   xdot = [-x(1)*L*r1 ;...
         x(1)*L*r1 - x(2)*r2 - x(2)*L*r1;...
```

```
        x(2)*r2;...
        x(2)*L*r1];
    end
end
```

References

(1) Arkin, M. R.; Tang, Y.; Wells, J. A. Small-Molecule Inhibitors of Protein-Protein Interactions: Progressing toward the Reality. Chemistry and Biology. 2014. https://doi.org/10.1016/j.chembiol.2014.09.001.

(2) Böttger, A.; Böttger, V.; Garcia-Echeverria, C.; Chène, P.; Hochkeppel, H. K.; Sampson, W.; Ang, K.; Howard, S. F.; Picksley, S. M.; Lane, D. P. Molecular Characterization of the Hdm2-P53 Interaction. J. Mol. Biol. **1997**, 269 (5), 744–756. https://doi.org/10.1006/jmbi.1997.1078.

(3) Walensky, L. D.; Kung, A. L.; Escher, I.; Malia, T. J.; Barbuto, S.; Wright, R. D.; Wagner, G.; Verdine, G. L.; Korsmeyer, S. J. Activation of Apoptosis in Vivo by a Hydrocarbon-Stapled BH3 Helix. Science (80-.). **2004**. https://doi.org/10.1126/science.1099191.

(4) Leshchiner, E. S.; Parkhitko, A.; Bird, G. H.; Luccarelli, J.; Bellairs, J. A.; Escudero, S.; Opoku-Nsiah, K.; Godes, M.; Perrimon, N.; Walensky, L. D. Direct Inhibition of Oncogenic KRAS by Hydrocarbon-Stapled SOS1 Helices. Proc. Natl. Acad. Sci. **2015**, 112 (6), 1761–1766. https://doi.org/10.1073/pnas.1413185112.

(5) Cang, S.; Iragavarapu, C.; Savooji, J.; Song, Y.; Liu, D. ABT-199 (Venetoclax) and BCL-2 Inhibitors in Clinical Development. Journal of Hematology and Oncology. 2015. https://doi.org/10.1186/s13045-015-0224-3.

(6) Guo, K.; Li, J.; Tang, J. P.; Tan, C. P. B.; Hong, C. W.; Al-Aidaroos, A. Q. O.; Varghese, L.; Huang, C.; Zeng, Q. Targeting Intracellular Oncoproteins with Antibody Therapy or Vaccination. Sci. Transl. Med. **2011**. https://doi.org/10.1126/scitranslmed.3002296.

(7) Dao, T.; Yan, S.; Veomett, N.; Pankov, D.; Zhou, L.; Korontsvit, T.; Scott, A.; Whitten, J.; Maslak, P.; Casey, E.; et al. Targeting the Intracellular WT1 Oncogene Product with a Therapeutic Human Antibody. Sci. Transl. Med. **2013**. https://doi.org/10.1126/scitranslmed.3005661.

(8) Moellering, R. E.; Cornejo, M.; Davis, T. N.; Bianco, C. Del; Aster, J. C.; Blacklow, S. C.; Kung, A. L.; Gilliland, D. G.; Verdine, G. L.; Bradner, J. E. Direct Inhibition of the NOTCH Transcription Factor Complex. Nature **2009**, 462 (7270), 182–188.

https://doi.org/10.1038/nature08543.

(9) Diderich, P.; Bertoldo, D.; Dessen, P.; Khan, M. M.; Pizzitola, I.; Held, W.; Huelsken, J.; Heinis, C. Phage Selection of Chemically Stabilized α - Helical Peptide Ligands. ACS Chem. Biol. **2016**, 1–6. https://doi.org/10.1021/acschembio.5b00963.

(10) Heinis, C.; Rutherford, T.; Freund, S.; Winter, G. Phage-Encoded Combinatorial Chemical Libraries Based on Bicyclic Peptides. Nat. Chem. Biol. **2009**, 5 (7), 502–507. https://doi.org/10.1038/nchembio.184.

(11) Bernal, F.; Tyler, A. F.; Korsmeyer, S. J.; Walensky, L. D.; Verdine, G. L. Reactivation of the P53 Tumor Suppressor Pathway by a Stapled P53 Peptide. J. Am. Chem. Soc. **2007**, 129 (9), 2456–2457. https://doi.org/10.1021/ja0693587.

(12) Walensky, L. D.; Kung, A. L.; Escher, I.; Malia, T. J.; Barbuto, S.; Wright, R. D.; Wagner, G.; Verdine, G. L.; Korsmeyer, S. J. Activation of Apoptosis in Vivo by a Hydrocarbon-Stapled BH3 Helix. Science **2004**, 305 (5689), 1466–1470. https://doi.org/10.1126/science.1099191.

(13) Chu, Q.; Moellering, R. E.; Hilinski, G. J.; Kim, Y.; Grossmann, T. N.; Yeh, T.; Verdine, G. L. Towards Understanding Cell Penetration by Stapled Peptides. Medchemcomm **2014**, 6 (c), 111–119. https://doi.org/10.1039/C4MD00131A.

(14) Bird, G. H.; Mazzola, E.; Opoku-Nsiah, K.; Lammert, M. A.; Godes, M.; Neuberg, D. S.; Walensky, L. D. Biophysical Determinants for Cellular Uptake of Hydrocarbon-Stapled Peptide Helices. Nat. Chem. Biol. **2016**, 12 (10), 845–852. https://doi.org/10.1038/nchembio.2153.

(15) Wu, Y.; Kaur, A.; Fowler, E.; Wiedmann, M. M.; Young, R.; Galloway, W. R. J. D.; Olsen, L.; Sore, H. F.; Chattopadhyay, A.; Kwan, T. T. L.; et al. Toolbox of Diverse Linkers for Navigating the Cellular Efficacy Landscape of Stapled Peptides. ACS Chem. Biol. **2019**. https://doi.org/10.1021/acschembio.9b00063.

(16) Atangcho, L.; Navaratna, T.; Thurber, G. M. Hitting Undruggable Targets: Viewing Stabilized Peptide Development through the Lens of Quantitative Systems Pharmacology. Trends Biochem. Sci. **2018**. https://doi.org/10.1016/j.tibs.2018.11.008.

(17) Peraro, L.; Deprey, K. L.; Moser, M. K.; Zou, Z.; Ball, H. L.; Levine, B.; Kritzer, J. A. Cell Penetration Profiling Using the Chloroalkane Penetration Assay. J. Am. Chem. Soc. **2018**. https://doi.org/10.1021/jacs.8b06144.

(18) Jafari, R.; Almqvist, H.; Axelsson, H.; Ignatushchenko, M.; Lundbäck, T.; Nordlund, P.; Molina, D. M. The Cellular Thermal Shift Assay for Evaluating Drug Target Interactions in Cells. Nat. Protoc. **2014**. https://doi.org/10.1038/nprot.2014.138.

(19) LaRochelle, J. R.; Cobb, G. B.; Steinauer, A.; Rhoades, E.; Schepartz, A. Fluorescence Correlation Spectroscopy Reveals Highly Efficient Cytosolic Delivery of Certain Penta-Arg Proteins and Stapled Peptides. J. Am. Chem. Soc. **2015**, 3 (Figure 1), 150213085027009. https://doi.org/10.1021/ja510391n.

(20) Smith, G.; Petrenko, V. Phage Display. Chem. Rev. **1997**, 97 (2), 391–410. https://doi.org/10.1021/cr960065d.

(21) Daugherty, P. S.; Chen, G.; Olsen, M. J.; Iverson, B. L.; Georgiou, G. Antibody Affinity Maturation Using Bacterial Surface Display. Protein Eng. **1998**, 11 (9), 825–832. https://doi.org/10.1093/protein/11.9.825.

(22) Boder, E.; Wittrup, K. Yeast Surface Display for Screening Combinatorial Polypeptide Libraries. Nat. Biotechnol. **1997**, 15 (6), 553–557. https://doi.org/10.1038/nbt0697-553.

(23) Lipovsek, D.; Plückthun, A. In-Vitro Protein Evolution by Ribosome Display and MRNA Display. Journal of Immunological Methods. 2004. https://doi.org/10.1016/j.jim.2004.04.008.

(24) Chang, Y. S.; Graves, B.; Guerlavais, V.; Tovar, C.; Packman, K.; To, K.-H.; Olson, K. A.; Kesavan, K.; Gangurde, P.; Mukherjee, A.; et al. Stapled A–helical Peptide Drug Development: A Potent Dual Inhibitor of MDM2 and MDMX for P53-Dependent Cancer Therapy. Proc. Natl. Acad. Sci. **2013**, 110 (36), E3445–E3454. https://doi.org/10.1073/pnas.1303002110.

(25) Okamoto, T.; Zobel, K.; Fedorova, A.; Yang, H.; Fairbrother, W. J.; Huang, D. C. S.; Smith, B. J.; Deshayes, K.; Czabotar, P. E. Stabilizing the Pro-Apoptotic BimBH3 Helix (BimSAHB) Does Not Necessarily Enhance A Ffi Nity or Biological Activity. ACS Chem. Biol. **2013**, 14–19.

(26) Rezaei Araghi, R.; Ryan, J. A.; Letai, A.; Keating, A. E. Rapid Optimization of Mcl-1 Inhibitors Using Stapled Peptide Libraries Including Non-Natural Side Chains. ACS Chem. Biol. **2016**, 11 (5), 1238–1244. https://doi.org/10.1021/acschembio.5b01002.

(27) Navaratna, T.; Atangcho, L.; Mahajan, M.; Subramanian, V.; Case, M.; Min, A.; Tresnak, D.; Thurber, G. M. Directed Evolution Using Stabilized Bacterial Peptide Display. J. Am. Chem. Soc. **2020**. https://doi.org/10.1021/jacs.9b10716.

(28) Lau, Y. H.; de Andrade, P.; Sköld, N.; McKenzie, G. J.; Venkitaraman, A. R.; Verma, C.; Lane, D. P.; Spring, D. R. Investigating Peptide Sequence Variations for 'Double-Click' Stapled P53 Peptides. Org. Biomol. Chem. **2014**, 12 (24), 4074–4077. https://doi.org/10.1039/C4OB00742E.

(29) Zhang, L.; Navaratna, T.; Liao, J.; Thurber, G. M. Dual-Purpose Linker for Alpha

Helix Stabilization and Imaging Agent Conjugation to Glucagon-like Peptide-1 Receptor Ligands. Bioconjug. Chem. **2015**, 26 (2), 329–337. https://doi.org/10.1021/bc500584t.

(30) Lau, Y. H.; de Andrade, P.; McKenzie, G. J.; Venkitaraman, A. R.; Spring, D. R. Linear Aliphatic Dialkynes as Alternative Linkers for Double-Click Stapling of P53-Derived Peptides. ChemBioChem **2014**, 15 (18), 2680–2683. https://doi.org/10.1002/cbic.201402374.

(31) Lau, Y. H.; de Andrade, P.; Quah, S.-T.; Rossmann, M.; Laraia, L.; Skold, N.; Sum, T. J.; Rowling, P. J. E.; Joseph, T. L.; Verma, C.; et al. Functionalised Staple Linkages for Modulating the Cellular Activity of Stapled Peptides. Chem. Sci. **2014**, 5 (5), 1804–1809. https://doi.org/10.1039/C4SC00045E.

(32) Kale, S. S.; Villequey, C.; Kong, X.-D.; Zorzi, A.; Deyle, K.; Heinis, C. Cyclization of Peptides with Two Chemical Bridges Affords Large Scaffold Diversities. Nat. Chem. **2018**, 10 (7), 715–723. https://doi.org/10.1038/s41557-018-0042-7.

(33) Zhang, L.; Navaratna, T.; Thurber, G. M. A Helix-Stabilizing Linker Improves Subcutaneous Bioavailability of a Helical Peptide Independent of Linker Lipophilicity. Bioconjug. Chem. **2016**, 27 (7), 1663–1672. https://doi.org/10.1021/acs.bioconjchem.6b00209.

(34) Pazgier, M.; Liu, M.; Zou, G.; Yuan, W.; Li, C.; Li, C.; Li, J.; Monbo, J.; Zella, D.; Tarasov, S.; et al. Structural Basis for High-Affinity Peptide Inhibition of P53 Interactions with MDM2 and MDMX. Proc. Natl. Acad. Sci. U. S. A. **2009**, 106 (12), 4665–4670. https://doi.org/10.1073/pnas.0900947106.

(35) Foight, G. W.; Ryan, J. A.; Gullá, S. V.; Letai, A.; Keating, A. E. Designed BH3 Peptides with High Affinity and Specificity for Targeting Mcl-1 in Cells. ACS Chem. Biol. **2014**. https://doi.org/10.1021/cb500340w.

(36) Crooks, G. E.; Hon, G.; Chandonia, J. M.; Brenner, S. E. WebLogo: A Sequence Logo Generator. Genome Res. **2004**, 14 (6), 1188–1190. https://doi.org/10.1101/gr.849004.

(37) Rezaei Araghi, R.; Bird, G. H.; Ryan, J. A.; Jenson, J. M.; Godes, M.; Pritz, J. R.; Grant, R. A.; Letai, A.; Walensky, L. D.; Keating, A. E. Iterative Optimization Yields Mcl-1–Targeting Stapled Peptides with Selective Cytotoxicity to Mcl-1–Dependent Cancer Cells. Proc. Natl. Acad. Sci. **2018**, 115 (5), 201712952. https://doi.org/10.1073/pnas.1712952115.

(38) Bird, G.; Madani, N.; Perry, A.; Princiotto, A.; Supko, J.; He, X.; Gavathiotis, E.; Sodroski, J.; Walensky, L. Hydrocarbon Double-Stapling Remedies the Proteolytic Instability of a Lengthy Peptide Therapeutic. Proc. Natl. Acad. Sci. U. S. A. **2010**, 107 (32), 14093–14098. https://doi.org/10.1073/pnas.1002713107.

(39) Getz, J. A.; Schoep, T. D.; Daugherty, P. S. Peptide Discovery Using Bacterial Display and Flow Cytometry. Methods Enzymol. **2012**, 503, 75–97. https://doi.org/10.1016/B978-0-12-396962-0.00004-5.

(40) Zhang, Q.; Lu, H. Identification of Small Molecules Affecting P53-MDM2/MDMX Interaction by Fluorescence Polarization. Methods Mol. Biol. **2013**, 962, 95–111. https://doi.org/10.1007/978-1-62703-236-0-8.

(41) Getz, J. a.; Schoep, T. D.; Daugherty, P. S. Peptide Discovery Using Bacterial Display and Flow Cytometry. Methods Enzymol. **2012**, 503, 75–97. https://doi.org/10.1016/B978-0-12-396962-0.00004-5.

Chapter IV: A Tag-Free Two Color Approach to Sorting Displayed Libraries

Tejas A. Navaratna and Greg M. Thurber

Abstract

Cell surface display and selection techniques have revolutionized therapeutic molecule discovery with their ability to screen diverse libraries in a high-throughput fashion. In the simplest fluorescence-based screens (e.g. FACS), the desired binding target is typically labelled with a fluorophore and incubated with the randomized cell population, after which the brightest cells are collected, re-screened, and/or sequenced. While straightforward, this approach suffers from lack of discrimination between high displayers and good binders. The bacterial display scaffold, eCPX, permits dual display of N- and C- terminal peptides and display normalization is reported, but in a peptide-specific manner. We have previously reported screening p53-like stapled peptides for MDM2 binding with bacterial surface display but found that steric clashes between the N-terminal p53 peptide and C-terminal HA display tag were difficult to avoid and led to inconsistently decreased signal in both MDM2 and anti-HA channels. We report here a kinetic competition strategy between bound target of one color and a later-time same target of a second color. We conducted extensive modeling to determine important parameters, such as desired

dissociation constant (K_d), time between labelings, and final washout time. The resulting radial gating strategy, as computationally examined here will be used experimentally to isolate potent binders to various targets, including MDM2.

Introduction

Display techniques, including in phage, mRNA, bacteria, yeast, and mammalian cells have allowed the coupling of genotype to phenotype, and proteins with beneficial mutations can be selected and sequenced. Along with more general directed evolution techniques such as continual selection (e.g. PACE[1]), colony screens, growth rate competition in liquid media[2], and organismal survival[3], these methods have resulted in major advances in biomolecule design[4–6]. A confounding variable in protein design through directed evolution is the role of expression vs. molecular-level improvements. (However, it should be noted that sometimes selection of high expression is desirable, as mutations conferring high expression can be functionally equivalent to mutations conferring high activity for in-cell catalyst development[7] or when there is correlation between expression level and protein thermal stability as reported in several examples in yeast surface display[8]). The increased expression vs. molecular improvement conflict occurs because protein sequence can affect expression level, through amino acid epistatic interactions leading to varying levels of folding or cell surface localization, or through codon usage differences leading to varied translation rates. In the case of directed evolution of affinity reagents (e.g. antibodies, antibody fragments, affibodies, etc.), surface display is a convenient way to couple genotype to binding potency for easy sequence decoding, but the end goal is typically to express or synthesize hit compounds

in solution to evaluate biological activity[9–11]. Thus, merely measuring level of target engagement on the cell surface can fail to discriminate between expression and activity, that is, a single-channel sorting scheme may fail to differentiate between an efficient displayer and a potent binder, and only selecting the brightest cells means losing out on poor displayers that are strong binders.

Yeast surface methods have largely avoided this issue by using a separate display tag (typically c-myc) and labelling displayed proteins with a tag-specific fluorescent antibody in a different channel from the target protein[12]. Simultaneous detection of both signals allows discrimination based on display level and affinity, and an appropriate gating scheme can be drawn in FACS to select potent binders regardless of display level[13]. Wittrup and coworkers reported a 125-fold enrichment of a low-abundance mutant that had a modest 2-fold improved dissociation constant using an HA tag for measuring display level with yeast surface expression[14]. This was achieved with a single round of FACS at a low labeling concentration (0.25 nM) relative to the K_d (0.63 nM for the stronger binder vs. 1.37 nM). The labeling concentration was determined through a modeling analysis and was optimized by considering the signal-to-noise ratio in labeling and the relative K_d values of the desired strong binder vs. the background. More recently, Keating and coworkers went further and developed a scheme to rank yeast-displayed peptides by dissociation constants based on their coordinates in a two-dimensional target vs. expression tag FACS plot[15]. Their approach combined multi-gate sorting with deep sequencing over a broad range of affinities to understand BH3 peptides' binding to the

anti-apoptotic protein Bcl-xL and led to much better high-throughput assignments of affinity rankings than single-gate approaches.

Bacterial surface display is uniquely suited for the expression of non-canonical amino acid-containing peptides. A met replacement strategy was highly successful in quantitatively incorporating azidohomoalanine (AHA) into outer membrane proteins[16] and displayed scFvs[17]. Despite numerous other advantages for display, such as large library sizes and the potential of using continuous evolution[1], phage display cannot be sorted with quantitative FACS and sorting is difficult to monitor while in progress. In comparison, yeast, while having lower library sizes due to lower transformability (typically 10^5-10^7 members), can express a huge variety of proteins of sizes up to full antibodies[12]. This is suitable for large proteins, unlike E. coli and especially the eCPX scaffold, which is limited to the display of polypeptides of about 60 amino acids in length[18]. However, yeast is limited in its ability to incorporate the NCAAs required for most peptide stapling strategies[19]. We have previously developed SPEED (Stabilized Peptide Evolution by E. coli Display) to screen double click stapled peptides expressed with AHA incorporation using eCPX[10]. The display level of peptides by eCPX can range over an order of magnitude, making deconvoluting expression and activity challenging[18]. Although eCPX is a biterminal display scaffold that theoretically permits simultaneous display and normalization, we and others have observed steric clashes manifesting in reduced binding kinetics by the affinity peptide when labeling both termini peptides simultaneously[20]. This can be partially ameliorated by increasing linker length between the peptide and scaffold, but in a sequence and length-dependent manner[18]. The highest

affinity peptide isolated, SPD-M6-V1, also had very high display levels, despite several rounds of FACS employing a similar two-color pseudo-expression-normalized strategy as described here. The efficient selection could be due to the higher expression or the improved binding affinity of this clone. To understand the quantitative mechanisms of affinity normalization by two-color labeling of the same peptide, we developed a computational system to test the effects of incubation times, target affinity, and concentrations on FACS discrimination.

Results

Modeling

We hypothesized that by equilibrium labeling of the system with color 1 target, followed by kinetic labeling of the system with color 2 target, we could discriminate between tight binders that are low displayers and weak binders that are high displayers. Channel 1 records signal from color 1 according to the fraction of displayed peptides bound to color 1 based on its dissociation constant. This leads to coarse affinity and expression discrimination in the channel 1 axis (Figure III - 1). Addition of a high concentration (tight-binder-saturating) of color 2 probe should result in increased signal in channel 2 primarily for peptides with a lower equilibrium occupancy of color1 target, i.e. high displayers and moderate binders (Figure III - 1). Thus, cells can be discriminated and selected based on both affinity and display level. To test this hypothesis, we wrote a script (see methods) to capture peptide occupancy by each color.

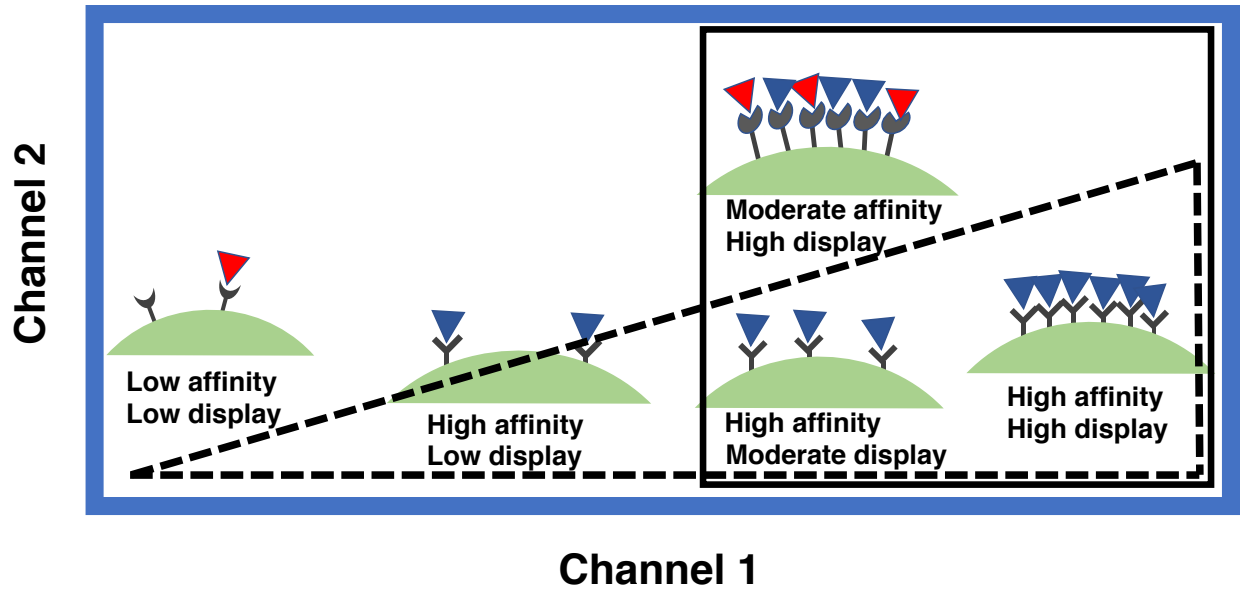

Figure IV - 1. Schematic of affinity and expression discrimination scheme.
Addition of color 1 target (blue triangles) and subsequent equilibration results in channel 1 (x-axis) detection, shown schematically by a solid gate, leading to separation between high affinity high displayers and high affinity low displayers. However, moderate affinity high displayers are likely not to be efficiently distinguished from high affinity displayers with moderate display, resulting in false-positives. Addition of excess color 2 (red triangles) to bind to cells expressing low-to-moderate affinity peptides results in y-axis channel 2 discrimination. Weaker binders (that have more peptide not bound to color 1 target) will bind to color 2 more efficiently due to its excess concentration, allowing for discrimination between moderate affinity high displayers and high affinity moderate displayers. The dashed line gate schematically represents the latter scheme.

For computational analysis, we conducted our simulation as follows:

Color1-target binds to displayed peptides and reaches an equilibrium fraction bound given by $f_{bound} = \frac{[color1]}{[color1] + K_d}$, where [color1] is the concentration of color 1-target and K_d is the equilibrium dissociation constant. In an experimental system, equilibrium would be reached by incubation with color1-target for several hours. Calculation of f_{bound} allows us to assign initial values for the peptide binding to color2-target differential equation system:

1. $\frac{d[unbound]}{dt} = -k_{on}\,[unbound][color2] + k_{off}\,[bound1] + k_{off}\,[bound2]$
2. $\frac{d[bound1]}{dt} = -k_{off}\,[bound1]$
3. $\frac{d[bound2]}{dt} = k_{on}\,[unbound][color2] - k_{off}\,[bound2]$

Here, [unbound] represents the number of unbound peptides on the cell surface and is equal to $(1 - f_{bound}) * [\text{peptide expression}]$, where [peptide expression] is the display level. [peptide expression] can be a normalized or crude value, as flow cytometer signal in channels for color1 or color2 will be proportional to [bound1] or [bound2] respectively. k_{on} and k_{off} are the kinetic parameters of binding, i.e, $K_d = \frac{k_{off}}{k_{on}}$. For this system, we assumed a typical k_{on} of 10^5 $M^{-1}s^{-1}$ and calculated k_{off} based on the K_d. [bound1] and [bound2] are the number of peptides bound to color1-target or color2-target respectively. This system of ordinary differential equations captures unbinding of color1-target and color2-target, and binding of color2-target, but due to washing out of color1-target during color2-target incubation, we assumed color1-target association, i.e. rebinding, to be negligible due to the high concentration of competitor.

Library flow cytometry simulations

We first simulated flow cytometry plots for libraries containing a range of K_d values from 500 pM to 10 nM and compared affinity and expression discrimination for one-color (Figure IV - 2A) and two-color schemes (Figure IV - 2B). This shows that a two color scheme can be used to successfully differentiate between high expressing moderate binders and low-to-moderate expression tight binders.

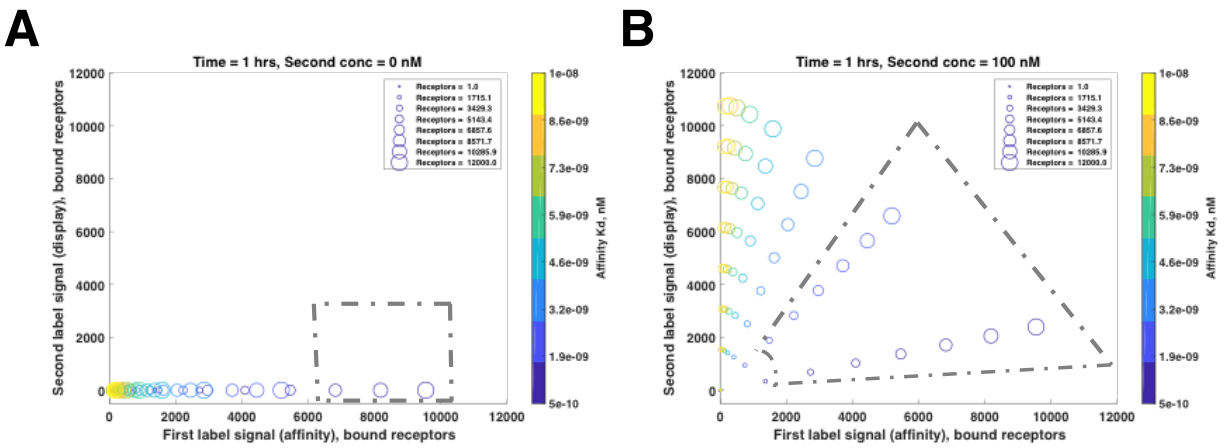

Figure IV - 2. Comparison of one-color and two-color sorting schemes.
(A) a one-color workflow results in all peptides in one axis with decent separation between the poorest affinity binders (10 nM, yellow) and the high affinity binders (500 pM, blue). This is a result of low equilibrium binding and dissociation during the one-hour washout period. However, moderate affinity binders with high expression (large circles) overlap and even surpass signal from high affinity binders with low to moderate expression. (B) the two-color workflow developed here allows for robust affinity-expression discrimination. Cells with similar affinity but different expression appear as a line with increasing slope, signaling worse affinity. A gate (gray dashed line) can be drawn to separate higher affinity variants regardless of display level.

Due to there being several free parameters in our system, that is, concentrations of color1-target and color2-target, library affinity range, receptor expression range, and importantly, time between color1-target washout and measurement, we first varied time to measurement (Figure IV - 3) to assess its importance.

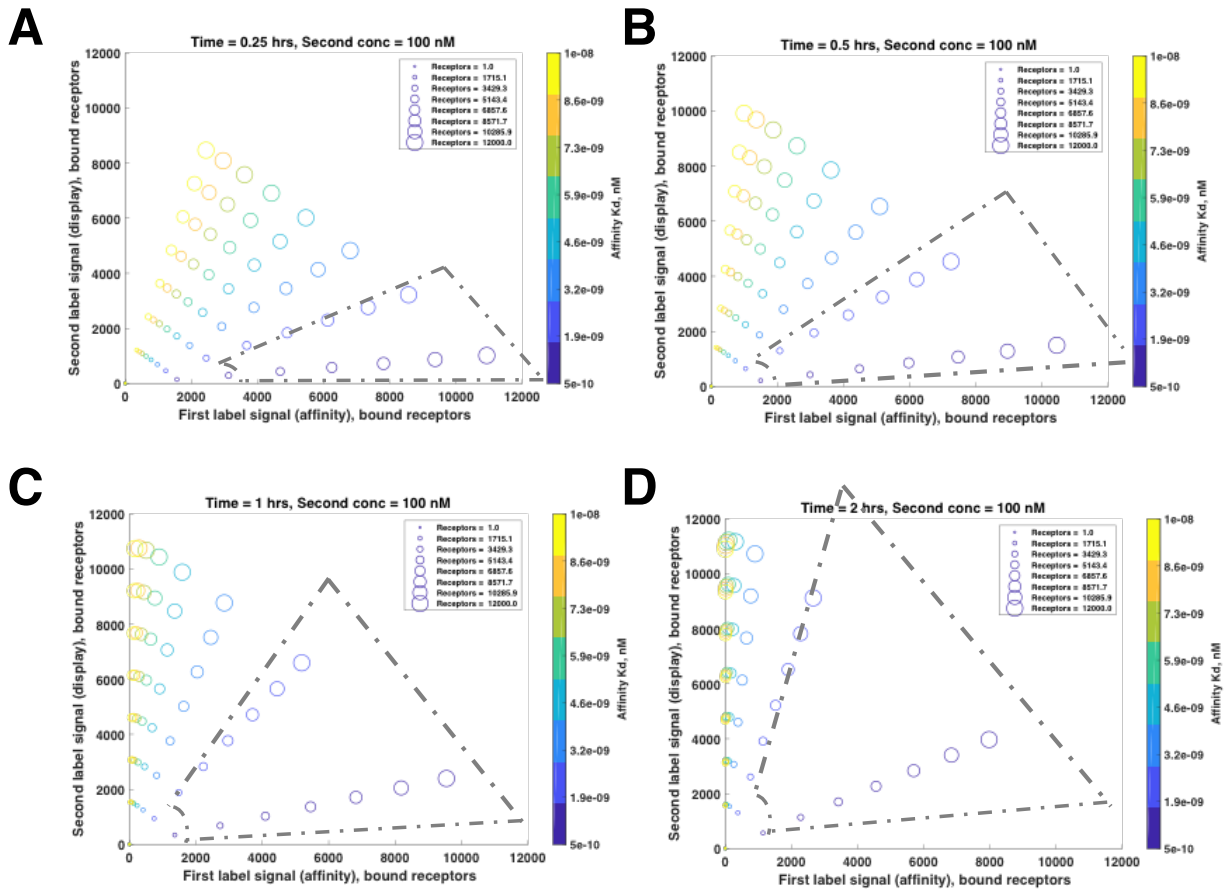

Figure IV - 3. Varying time of incubation with color2-target results in tunable sorting strategies.
(A) For a very short 15-minute incubation time, color 2 signal is suppressed and less discrimination is observed between similar high affinity clones. A short incubation time may be beneficial if the K_d of even the best binders is greater than 5 nM. (B)-(D) increasing incubation time from 30 minutes to 2 hours results in maintenance of color1 signal for only the highest affinity binders, enabling a stringent sorting strategy.

Experimental validation

To experimentally validate these computational studies, we examined clones obtained from successive sorts of a click-stabilized p53-based randomized peptide library with affinity for MDM2[10]. We have found a diverse collection of sequences with varying display levels and affinity (Table IV - I). Using the script detailed in the methods section, we simulated the expected coordinates for these sequences (Figure IV – 4) and included a

hypothetical sub-nM affinity binder (bottom right). These simulations suggest that the radial gated sort strategy, as elaborated above, would provide sufficient discrimination between affinity, regardless of display level.

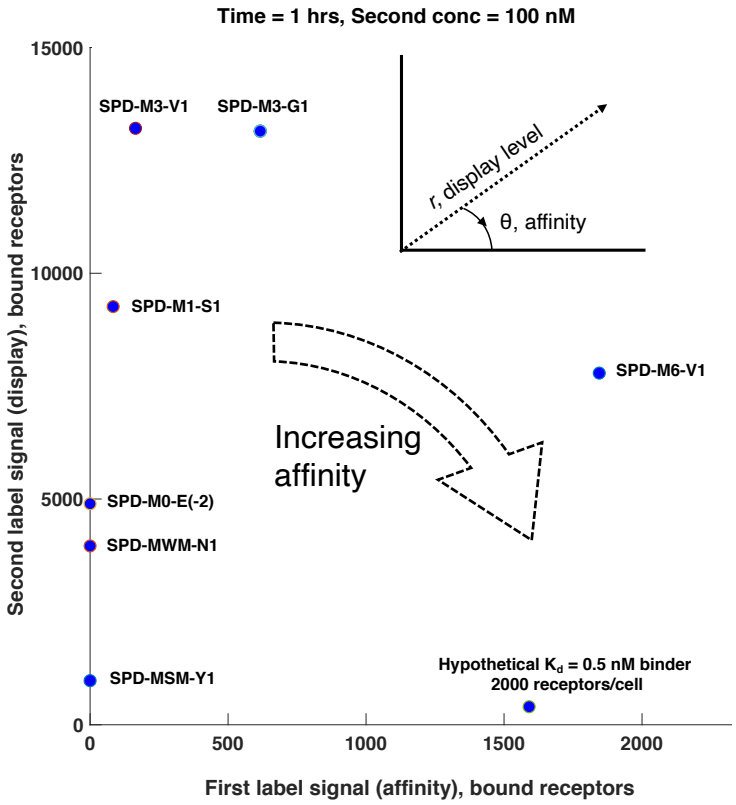

Figure IV - 4. Simulated flow cytometry coordinates of several sequences. Sequences were obtained by sorting a randomized library of stabilized peptides against MDM2. SPD-M0-E(-2) is the sequence closest to the native p53 sequence with small modifications and SPD-M6-V1 is the highest affinity candidate identified after one round of MACS and seven rounds of FACS, first detected by Sanger sequencing in round 6. as detailed in Chapter II[10].

Table IV - I. Potential experimental sequences for validation from rounds of MACS and FACS against MDM2.
SPD-M6-V1 is the highest affinity binder obtained from one round of MACS and 6 rounds of FACS, the number after the "M" refers to the sorting round. SPD-M0-E(-2) is the original p53-like sequence on which the library was based. WM is a weakly selectively round of MACS with 50 nM MDM2-GST-biotin incubation; SM is a stringent round of MACS with 2 nM MDM2-GST-biotin incubation. Display levels were obtained from extrapolation in the limit of high concentration using a one-site binding model in Prism 8. K_d values were obtained with the same model using a titration of 6-12 logarithmically spaced MDM2-GST-AF647 concentrations.

Name	Sequence	Relative Display (S_{max} / $S_{max,\ SPD\text{-}M6\text{-}V1}$)	Relative Affinity ($K_{d,\ SPD\text{-}M6\text{-}V1}$ / K_d)
SPD-M6-V1	VCDFXCYWNDLXGY	1.0	1.0
SPD-M3-G1	GGTFXGYWADLXAF	1.5	0.54
SPD-M3-V1	VLSFXDYWNLLXGS	1.5	0.38
SPD-M0-E(-2)	ETFXDLWRLLXEN	0.57	0.09
SPD-MWM-N1	NYDFXSGWVNLXCF	0.16	0.06
SPD-M1-S1	SCGFXCVWDSLXSD	1.0	0.35
SPD-MSM-Y1	YSCFXVYWCDLXGG	1.4	0.02

Even a genetically homogeneous population of bacteria will show a range of binding signal, spanning roughly an order of magnitude (Figure IV – 5A). This is not only due to heterogeneity in peptide display but also likely due to channel location in flow cytometry, as bacteria are much smaller than eukaryotic cells and will not necessarily be forced into a single stream at the detection point. This results in binding histograms of roughly Gaussian shape, and the median fluorescence level can be quantified in used in assays (ie. affinity determination). This signal spread does lead to overlap in signals when binding affinity is sufficient (for example, SPD-M6-V1 and SPD-M0-E(-2) overlap somewhat in the upper range of SPD-M0E(-2) and lower range of SPD-M6-V1). Therefore, when sorting

complex library mixtures, a more stringent cutoff would provide finer discrimination among clones with similar affinity and/or display level. Variations in binding signal for cells displaying the same peptide is captured by the two-color analysis (Figure IV – 5B) and a similar radial gating strategy as presented in Figure IV – 3 can be used even considering the inherent variability of the system.

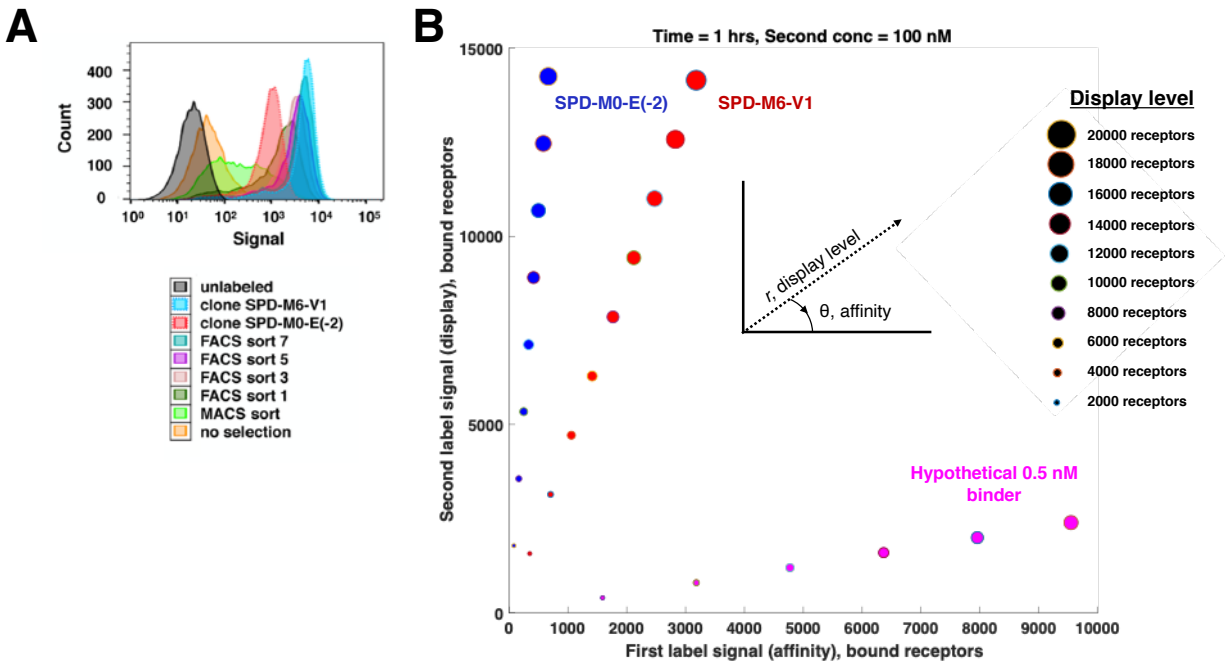

Figure IV - 5. Analysis of clonal variability in one color and two color sorting. (A) Histograms of one color single clone binding (SPD-M6-V1 and SPD-M0-E(-2)) and bulk unsorted and sorted libraries as evaluated with bacterial surface display. Figure adapted from Navaratna et al[10]. (B) The spread of signal for several example clones can be captured by varying the display level in simulations, and this simulation reveals that a radial gating scheme can be used even when considering expression variability.

Discussion

This work represents a computational investigation of a tag-free method to normalize protein displayers based on expression level. We show that we can discriminate between clones of modest affinity differences regardless of display level (Figure IV – 2B, Figure IV – 4.). Dissociation plays an important role in discrimination, with the k_{off} value controlling both the signal strength of the first color and the second (by allowing association). Therefore, control of time allowed for color 1 to dissociate (dissociation time, not to be confused with $t_{1/2,\ off}$) was also varied in simulations (Figure IV – 3). Analysis of dissociation time revealed that this parameter affected sort stringency and provided guidance towards the design of sorting campaigns: namely, early rounds and rounds aimed at isolating moderate-affinity binders should be conducted with a short, 10 to 30-minute-long dissociation time in order not to lose potential sequences that could be further affinity matured. Later rounds (or rounds known to contain high affinity, single digit nM K_d or better binders) should be conduct more stringently with longer dissociation times (1 to 2 hours long).

Additionally, we have chosen several candidate clones from sorting campaigns with a range of display level and affinity and these were modeled computationally, with the results showing that a radial gating strategy would be able to discriminate among binding affinities at varying display levels (Figure IV – 4, table IV – 1)

We also considered histogram spread and expression variability within several example clones that could be a result of flow cytometric conditions or inherent cell-to-cell variability. We show computationally that a two-color sorting scheme allows for the design

of gates that preserve clone selection regardless of cell or detection variability (Figure IV – 5). This platform therefore is a potentially powerful method of reducing noise and sampling bias in selections. Unlike variability in expression (length of r in Figure IV – 5B), affinity variability is more difficult to capture (variation in the angle θ in Figure IV – 5B) and work is ongoing to understand its impact on selections.

The two-color sorting approach presented here could also be used in systems that are not amenable to tag-based normalization, such as difficult to engineer natural protein displayers (e.g. mammalian cells), including immune cell populations (displaying the T-cell receptor and B-cell receptor) and MHC-peptide displayers. Future work will validate these computational methods to select specific clones based on affinity.

Methods

Clone selection

Sorted libraries were plated at high dilution to obtain single colonies that were characterized for display level and binding affinity as described in ref. 10. Promising variants for future experimental validation by sorting were Sanger sequenced at the University of Michigan Advanced Genomics Core.

Scripting

All scripting was done in MATLAB 2018a.

The annotated single .m file used to produce the plots in Figures IV - 2, IV - 3, IV - 4, and IV - 5B named dualcolorsort.m, is reproduced in its entirety below.

```
function dualcolorsort.m
close all;

kds = linspace(5e-10,10e-9,8); % affinity kd range in library (here, logspaced points between 500 pM and 10 nM)
expression = linspace(1,12000,8); %expression range in library (here, evenly spaced points between 1 and 12000 peptides)
time_at_measurement = 1; % time in hours after washing of 1st label and addition of 2 label
%time_at_measurement = logspace(-2,0.5,6);%hours, optional code if you

second_labeling_conc = 100e-9; %concentration of second color label [M]
first_labeling_conc = 10e-9;  %concentration of first color label [M]

cmap = parula(length(kds)); %color scheme used to display points


for times = 1:length(time_at_measurement) %if vector of time_at_measurement is given, this iterates through

for i = 1:length(kds) %interation over kds
   for j = 1:length(expression) %iteration over peptide expression
   [T,X]          =          dual_color_label_embed(kds(i),expression(j),first_labeling_conc, time_at_measurement(times), second_labeling_conc);
   sz = (20/length(expression))*j; %allows displayed data pointsize to scale with number of expression
         hold all;

%rest of this function is plot manipulation
plot(X(length(T),2),X(length(T),3),'o','MarkerSize',sz,'Color',cmap(i,:))
```

```
xlabel('First label signal (affinity), bound receptors')
ylabel('Second label signal (display), bound receptors')
set(gca,'FontSize',16)
set(gca,'FontWeight','Bold')
axis([0 max(expression) -500 max(expression)])
legendstring{j} = sprintf(' %s %0.1f ','Receptors = ',expression(j));
   end
end
delete(findall(gcf,'Tag','stream'));
set(gcf,'position',[0,0,1200,700])

str = ['Time = ' num2str(time_at_measurement(times)) ' hrs, Second conc = '
num2str(1e9*second_labeling_conc) ' nM'];
title(str,'Tag','stream');
A=reshape(legendstring,1,[]);

legend(A, 'Location','northeast','FontSize',10)
colormap(cmap);
roundkds = round(kds,2,'significant');
kdlabels = string(roundkds);
cbh=colorbar;
 cbh.Ticks = linspace(0, 1, length(kds)) ; %Create 8 ticks from zero to 1
 cbh.TickLabels = kdlabels ;    %Replace the labels of these 8 ticks with the numbers 1 to
8
 cbh.Label.String = 'Affinity Kd, nM';
set(gcf,'Position',[100 100 700 500])
end

end
```

```
function [T,X] = dual_color_label_embed(k_d,receptor_count, first_labeling_conc, time_at_measurement, second_labeling_conc)

k_on = 1e5; %M-1s-1
k_off = k_d*k_on; %s-1

number_bound = receptor_count * first_labeling_conc/(k_d + first_labeling_conc); %assumes equilibration of first labeling, standard because typically hours-overnight
number_unbound = receptor_count - number_bound; %initializes the system for second binding diff eq

eqtime = [0, time_at_measurement*3600];
options = odeset('Maxstep',10);

x=zeros(3,1); % 3 species, peptide unbound, peptide bound with 1, peptide bound with 2
%initialvalues:
x(1) = number_unbound;
x(2) = number_bound;
x(3) = 0;

[T,X] = ode23s(@(t, x)odesystem(t, x), eqtime, x,options);
%ODE assumes 1 is lost when 2 is added (washing assumption, so 1 cannot
%rebind the peptide)

function xdot = odesystem(t,x)

xdot = [-k_on*second_labeling_conc*x(1) + k_off*x(2) + k_off*x(3) ;...
      -k_off*x(2);...
      k_on*second_labeling_conc*x(1) - k_off*x(3)];
```

end

end

Acknowledgement

This work was supported by an NSF Graduate Fellowship to T.N.

References

(1) Esvelt, K. M.; Carlson, J. C.; Liu, D. R. A System for the Continuous Directed Evolution of Biomolecules. Nature **2011**. https://doi.org/10.1038/nature09929.

(2) Lee, S. M.; Jellison, T.; Alper, H. S. Directed Evolution of Xylose Isomerase for Improved Xylose Catabolism and Fermentation in the Yeast Saccharomyces Cerevisiae. Appl. Environ. Microbiol. **2012**. https://doi.org/10.1128/AEM.01419-12.

(3) Ngo, J. T.; Tirrell, D. A. Noncanonical Amino Acids in the Interrogation of Cellular Protein Synthesis. Acc. Chem. Res. **2011**. https://doi.org/10.1021/ar200144y.

(4) Chen, I.; Dorr, B. M.; Liu, D. R. A General Strategy for the Evolution of Bond-Forming Enzymes Using Yeast Display. Proc. Natl. Acad. Sci. U. S. A. **2011**. https://doi.org/10.1073/pnas.1101046108.

(5) Romero, P. A.; Arnold, F. H. Exploring Protein Fitness Landscapes by Directed Evolution. Nature Reviews Molecular Cell Biology. December 2009, pp 866–876. https://doi.org/10.1038/nrm2805.

(6) Hackel, B. J.; Kapila, A.; Dane Wittrup, K. Picomolar Affinity Fibronectin Domains Engineered Utilizing Loop Length Diversity, Recursive Mutagenesis, and Loop Shuffling. J. Mol. Biol. **2008**. https://doi.org/10.1016/j.jmb.2008.06.051.

(7) Broo, K.; Larsson, A. K.; Jemth, P.; Mannervik, B. An Ensemble of Theta Class Glutathione Transferases with Novel Catalytic Properties Generated by Stochastic Recombination of Fragments of Two Mammalian Enzymes. J. Mol. Biol. **2002**. https://doi.org/10.1016/S0022-2836(02)00032-3.

(8) Traxlmayr, M.; Obinger, C. Directed Evolution of Proteins for Increased Stability and Expression Using Yeast Display. Arch. Biochem. Biophys. **2012**, 526 (2), 174–180. https://doi.org/10.1016/j.abb.2012.04.022.

(9) Foight, G. W.; Ryan, J. A.; Gullá, S. V.; Letai, A.; Keating, A. E. Designed BH3 Peptides with High Affinity and Specificity for Targeting Mcl-1 in Cells. ACS Chem. Biol. **2014**. https://doi.org/10.1021/cb500340w.

(10) Navaratna, T.; Atangcho, L.; Mahajan, M.; Subramanian, V.; Case, M.; Min, A.; Tresnak, D.; Thurber, G. M. Directed Evolution Using Stabilized Bacterial Peptide Display. J. Am. Chem. Soc. **2020**. https://doi.org/10.1021/jacs.9b10716.

(11) Lahti, J. L.; Cochran, J. R. Yeast Surface Display. In Therapeutic Monoclonal Antibodies: From Bench to Clinic; 2009. https://doi.org/10.1002/9780470485408.ch9.

(12) Cherf, G. M.; Cochran, J. R. Applications of Yeast Surface Display for Protein Engineering. Methods Mol. Biol. **2015**. https://doi.org/10.1007/978-1-4939-2748-7_8.

(13) Boder, E.; Wittrup, K. Yeast Surface Display for Screening Combinatorial Polypeptide Libraries. Nat. Biotechnol. **1997**, 15 (6), 553–557. https://doi.org/10.1038/nbt0697-553.

(14) VanAntwerp, J. J.; Wittrup, K. D. Fine Affinity Discrimination by Yeast Surface Display and Flow Cytometry. Biotechnol. Prog. **2000**. https://doi.org/10.1021/bp990133s.

(15) Reich, L.; Dutta, S.; Keating, A. E. SORTCERY - A High-Throughput Method to Affinity Rank Peptide Ligands. J. Mol. Biol. **2015**. https://doi.org/10.1016/j.jmb.2014.09.025.

(16) Link, A. J.; Vink, M. K. S.; Tirrell, D. A. Presentation and Detection of Azide Functionality in Bacterial Cell Surface Proteins Presentation and Detection of Azide Functionality in Bacterial. J. Am. Chem. Soc. **2004**, 126 (34), 10598–10602. https://doi.org/10.1021/ja047629c.

(17) Van Deventer, J. a.; Yuet, K. P.; Yoo, T. H.; Tirrell, D. a. Cell Surface Display Yields Evolvable, Clickable Antibody Fragments. ChemBioChem **2014**, 15 (12), 1777–1781. https://doi.org/10.1002/cbic.201402184.

(18) Rice, J.; Daugherty, P. Directed Evolution of a Biterminal Bacterial Display Scaffold Enhances the Display of Diverse Peptides. Protein Eng. Des. Sel. **2008**, 21 (7), 435–442. https://doi.org/10.1093/protein/gzn020.

(19) Atangcho, L.; Navaratna, T.; Thurber, G. M. Hitting Undruggable Targets: Viewing Stabilized Peptide Development through the Lens of Quantitative Systems Pharmacology. Trends Biochem. Sci. **2018**. https://doi.org/10.1016/j.tibs.2018.11.008.

(20) Kenrick, S. a.; Daugherty, P. S. Bacterial Display Enables Efficient and Quantitative Peptide Affinity Maturation. Protein Eng. Des. Sel. **2010**, 23 (1), 9–17. https://doi.org/10.1093/protein/gzp065.

Chapter V: Concluding Remarks and Future Directions

Summary

This dissertation combines bio-orthogonal chemistry with non-natural amino acid incorporation to develop and apply a high-throughput method of engineering stapled alpha helical peptides. This bio-orthogonal chemistry, where the functional groups used do not cross-react with common biological chemical groups, enables cross-linking of non-natural amino acids, while preserving the native functions of standard amino acids. Combining the high transformability of E. coli and its ability to incorporate a variety of non-natural amino acids into induced proteins, we stabilized alpha helices on the surface of bacteria for directed evolution of semi-synthetic and chemically diverse biologically active molecules.

Chapter I provides a background description of peptide engineering and the importance of stabilized alpha helices for the development of novel therapeutics. Chapter II details the method development using non-canonical amino acid (NCAA) incorporation into cell surface-displayed peptides, stabilization, and screening of libraries. In this novel approach, SPEED (Stabilized Peptide Evolution with E. coli Display), we displayed NCAA-incorporated peptides on the surface of methionine auxotrophic E. coli as fusions to a variant of the previously reported eCPX scaffold. We optimized display by using different promoter-vector systems and double-click stabilization reactivity through

modulating stabilizing linker concentration as well as testing various copper chelator and reducing agent concentration combinations. This resulted in successful click-stabilization of the majority of surface displayed peptides and we applied this to evolve high affinity inhibitors of the p53-MDM2 interaction, due to its dysregulation in many cancers. Starting with a p53-like variant, we went through one cycle of randomization and eight rounds of screening for binding to MDM2. This resulted in a nearly 10-fold improved binder (starting from an already improved sequence with K_d = 15 nM affinity) that contained an unusual disulfide bond in addition to the click-stabilized structural element, so we decided to conduct solution nuclear magnetic resonance (NMR) studies to better understand the peptide's conformation. Together with MDM2-interaction transfer experiments, obtaining the solution structure led to new insights into helix preorganization for stapled peptide development. Specifically, even though disulfide bond appeared to mildly destabilize the alpha helix, the impact of the additional crosslink created a highly rigid peptide resulting in large affinity improvements.

Chapter III discusses an extension of SPEED to evolve binders in the context of a stabilizing agent's physicochemical properties. We found that a rigid staple, 1,3-diethynylbenzene, does not react well to stabilize peptides on the cell surface. Despite this, we found binding improvements in all libraries tested, including a hydrophobic all-hydrocarbon double-click staple, the aforementioned 1,3-diethynylbenzene, an amine-functionalizable linker, and no linker at all. Most interestingly, the staple context mattered, with libraries evolved with one linker and reacted with a different linker generally showing diminished binding relative to reaction with the evolved linker. We show that a high affinity

propargyl ether-evolved peptide loses significant binding when stabilized with other linkers instead. This suggests that picking a linker due to its properties (such as protease stability, fluorescence, or cell penetration) cannot merely be an afterthought following sequence evolution. Rather, the evolution of randomized libraries ought to be carried out with each specific linker instead of relying on the notion of linker modularity not to diminish binding.

In chapter IV, we describe the computational development of a tag-free expression normalization methodology for screening surface-displayed proteins. This was motivated by observed clashes between an anti-tag antibody and peptide-specific protein, leading to diminished signals in both channels. The eCPX scaffold is sluggish to display many highly charged tags and peptide display itself is highly sequence-dependent. This provided us with further impetus to develop a tag-free two-color fluorescence-based sorting strategy to screen libraries of surface displayed peptides. In summary, the library is incubated over hours (to reach binding equilibrium) with a limiting concentration of color1-target, after which it is washed and treated with a high concentration of color2-target. We showed that this simple workflow enables discrimination between moderate affinity-high displayers and high affinity-moderate displayers, which is important when display is peptide-dependent. Finally, we chose peptides identified from previous screens that possess diverse display levels and binding affinity values for future experimental validation of this technique, which will include a comparison experiment between the one-color, tag-free two-color, and display tag two-color methodologies to gauge efficiency in eliminating weak binders while enriching strong binders.

In Appendix I, we briefly discuss chemical synthesis, purification, and NMR characterization of the amine-functionalizable linker used in Chapter III. Appendix II details the alanine-scanning experiments for the p53-like sequence that informed the randomization strategy used in Chapter II. We elaborate in Appendix III on our attempts to sort for binders against other targets, specifically, the intracellular proteins KRAS and NOTCH1 as well as the extracellular CD8 protein. Finally, in Appendix IV, we discuss the engineering of double-click stabilized two-helix bundles for the molecular imaging of Her2.

Future directions

This dissertation is largely devoted to the development of methods for the screening of stabilized peptides. The applications for these techniques include development of chemical biology tools to understand cellular interactions, for novel therapeutic therapy, and for affinity-based bioseparations.

Still, there are many areas for potential improvement in this research. Although one round of randomization and extensive screening for MDM2 binding resulted in discovery of a potent K_d = 1.8 nM binder (SPD-M6-V1), additional re-diversification and selections can possibly improve affinity, particularly given the theoretical diversity of the original NNC library being 3.8 x 10^{10} sequences and our first library consisting of only 3 x 10^8 members. In reports, multiple rounds of randomization have been carried out for the discovery of strong binders from naïve libraries[1]. Most of this past work has used yeast and re-randomization is especially useful when library sizes are smaller. This is because

even a modest number of randomized sites results in an intractably large number of sequences to test with current display systems. For example, there are 4 x 10^{10} possible sequences for a peptide with 9 randomized amino acids and capturing this diversity requires a minimum of 10^{11} transformants for sufficient coverage. This is near the upper limit of bacterial techniques[2] and to the best of my knowledge, has not been accomplished in methionine auxotrophic cells. Because our original scheme encoded 9 randomized amino acids and we achieved a transformation yield of 3 x 10^{8} clones[3], we screened no more than 1% of possible sequences. Our alanine scan results (Appendix II) indicate that many amino acids tolerate substitution to alanine, which is evidence that the well of affinity is broad at the high affinity limit (there are likely many sequences that resemble SPD-M6-V1 that are equally potent binders). This is consistent with a report of solid phase peptide sequence modifications of MDM2 binders, where Partridge et al. found that single-residue substitutions of ATSP-7041 generally preserved high binding affinity[4]. To ensure that SPD-M6-V1 is representative of the most potent binding series of peptides discoverable by our SPEED technique, we have re-randomized an SPD-M6-V1-based sequence with NNN codons to encode any amino acid. This will inevitably encode undesired stop codons (premature termination) and methionine codons (inappropriate stabilization sites), but as this randomization is based on the already affinity-improved SPD-M6-V1, we hope that truncated sequences will be rapidly screened out.

Furthermore, we observed significant differences in display level for peptides of the same length (p53-like peptides, Chapter IV) and for peptides against other targets, such as KRAS and NOTCH1. We hypothesize that the highly charged nature of the

putative NOTCH1 binder did not allow for correct folding and translocation to the outer membrane. Because of these differences in display are inevitably present in the original randomized libraries and we did several one-color sorting rounds (including MACS) prior to implementing two color sorting, it is possible that we lost high affinity, low displaying binders early in the sorting workflow. This is an additional motivation for SPD-M6-V1 rerandomization and in the longer term, may benefit from other display strategies including in a yeast system. Additionally, while stabilization improved the correlation between affinities measured on the bacterial membrane and in solution, the two values diverged significantly in a small number of sequences (Chapter II). For example, SPD-M0-E(0) showed rather poor affinity in solution (K_d = 74 nM) but moderate affinity on the bacterial surface (K_d = 12 nM). Aga2-displayed peptides on yeast have better correlation between surface and solution binding[5,6], and we hypothesize that this is due to the greater distance away from the cell compared to eCPX (and potential for bacterial LPS to induce crowding, affinity-modifying effects at the surface). There have been strides made recently in NCAA incorporation in yeast[7] but additional strain and protein engineering may be necessary to achieve the near-complete NCAA replacement required for high fidelity stabilized peptide display.

Machine learning is another powerful avenue for designing better proteins. There have been several reported and impressive applications of machine learning to protein engineering, including the design of antimicrobial peptides and designer enzymes. Armed with flow cytometric data from thousands of clones (including binding isotherms from dozens of sequences) and next-generation sequencing data, we are starting to

understand evolutionary trends applied to several targets. I have great hope that in the years to come, deep learning with rich datasets will enable us to fill in the sequence and chemistry gaps that even the largest experimental peptide libraries are unable to meet, to design peptides that not only bind with high affinity but are also able to rapidly enter the cell and resist degradation.

As discussed previously, we have good reason to believe that there are a large number of chemically diverse SPD-M6-V1-based high affinity sequences. The NMR structure and docking (Chapter II) of SPD-M6-V1 showed that many side chains are not involved in significant inter- or intramolecular bonding, consistent with reported crystal structures of p53 and p53 analogues. This suggests that SPD-M6-V1 may be amenable to single site substitutions. While affinity is important for stapled peptide activity, intracellular delivery is generally considered to the roadblock in efficient modulation of protein-protein interactions[8]. In this dissertation, we discovered a high affinity MDM2 binder and further work can elucidate sequence-penetration relationships through single and multiple-site mutation to cationic or lipophilic amino acids without serious affinity loss. As shown by cell-surface affinity measurements and structural analysis, the disulfide bond of SPD-M6-V1 is important for high affinity binding. The intracellular environment is a reducing environment and we do not yet understand the stability of this specific disulfide bond in the presence of glutathione. Many protein toxins contain a rich network of disulfide bonds, with some being inert to cytosolic reducing conditions. Disulfide bonding as well as organized secondary structures are well appreciated to reduce protease degradation and we have found that protease resistance correlates well with in vitro anti-cancer

activity. Deep sequencing and re-randomization of the SPD-M6-V1 peptide can reveal peptides with similar binding properties but diverse protease stability, amphiphilicity, and therefore potentially cellular permeability. Exploration of this space will allow discovery of profound connections among sequence, structure, and function.

Finally, there are many more interesting targets to explore using SPEED. Immune checkpoint inhibitors against PD-1, PDL-1, and CTLA-4 have made tremendous strides in the oncology landscape, but these therapies come with serious side effects making it imperative that patients are chosen accurately. Identification of these receptors in tumors involves invasive biopsies[9] and high temporal resolution of receptor response to therapy (e.g. loss-of-expression mutations) is challenging to achieve. A tight binding peptide-based imaging agent (through NIR or MRI modalities) would bind in an expression-dependent manner and quickly clear, reducing contrast[10]. Such peptides also have possibilities in intraoperative imaging to identify tumor margins and metastases.

This work would not have been possible without major developments in chemistry and biology. Efforts to introduce non-canonical amino acids into proteins, combined with advances in stapled peptide development led us to develop a new technique to rapidly screen libraries against virtually any disease protein-protein interaction. This has led to the discovery of unusual disulfide bonded and double-clicked peptides that are potent binders of MDM2. There are efforts underway to understand the translatability of such molecules for cancer inhibition. I hope that expansion of this method to other targets will be highly fruitful and improve the drug and molecular imaging agent landscapes.

References

(1) Cherf, G. M.; Cochran, J. R. Applications of Yeast Surface Display for Protein Engineering. Methods Mol. Biol. **2015**. https://doi.org/10.1007/978-1-4939-2748-7_8.

(2) Getz, J. A.; Schoep, T. D.; Daugherty, P. S. Peptide Discovery Using Bacterial Display and Flow Cytometry. Methods Enzymol. **2012**, 503, 75–97. https://doi.org/10.1016/B978-0-12-396962-0.00004-5.

(3) Navaratna, T.; Atangcho, L.; Mahajan, M.; Subramanian, V.; Case, M.; Min, A.; Tresnak, D.; Thurber, G. M. Directed Evolution Using Stabilized Bacterial Peptide Display. J. Am. Chem. Soc. **2020**. https://doi.org/10.1021/jacs.9b10716.

(4) Partridge, A. W.; Kaan, H. Y. K.; Juang, Y. C.; Sadruddin, A.; Lim, S.; Brown, C. J.; Ng, S.; Thean, D.; Ferrer, F.; Johannes, C.; et al. Incorporation of Putative Helix-Breaking Amino Acids in the Design of Novel Stapled Peptides: Exploring Biophysical and Cellular Permeability Properties. Molecules **2019**. https://doi.org/10.3390/molecules24122292.

(5) Reich, L.; Dutta, S.; Keating, A. E. SORTCERY - A High-Throughput Method to Affinity Rank Peptide Ligands. J. Mol. Biol. **2015**. https://doi.org/10.1016/j.jmb.2014.09.025.

(6) Angelini, A.; Chen, T. F.; De Picciotto, S.; Yang, N. J.; Tzeng, A.; Santos, M. S.; Van Deventer, J. A.; Traxlmayr, M. W.; Dane Wittrup, K. Protein Engineering and Selection Using Yeast Surface Display. Methods Mol. Biol. **2015**. https://doi.org/10.1007/978-1-4939-2748-7_1.

(7) Stieglitz, J. T.; Kehoe, H. P.; Lei, M.; Van Deventer, J. A. A Robust and Quantitative Reporter System To Evaluate Noncanonical Amino Acid Incorporation in Yeast. ACS Synth. Biol. **2018**, 7 (9), 2256–2269. https://doi.org/10.1021/acssynbio.8b00260.

(8) Bird, G. H.; Mazzola, E.; Opoku-Nsiah, K.; Lammert, M. A.; Godes, M.; Neuberg, D. S.; Walensky, L. D. Biophysical Determinants for Cellular Uptake of Hydrocarbon-Stapled Peptide Helices. Nat. Chem. Biol. **2016**, 12 (10), 845–852. https://doi.org/10.1038/nchembio.2153.

(9) Yi, M.; Jiao, D.; Xu, H.; Liu, Q.; Zhao, W.; Han, X.; Wu, K. Biomarkers for Predicting Efficacy of PD-1/PD-L1 Inhibitors. Molecular Cancer. 2018. https://doi.org/10.1186/s12943-018-0864-3.

(10) Schmidt, M.; Wittrup, K. A Modeling Analysis of the Effects of Molecular Size and Binding Affinity on Tumor Targeting. Mol. Cancer Ther. **2009**, 8 (10), 2861–2871. https://doi.org/10.1158/1535-7163.MCT-09-0195.

Appendices

Appendix I: Synthesis and Characterization of a Functionalizable Stabilizing Linker

In Zhang et al. 2015 and Zhang et al. 2016, we developed and applied a bifunctional bis-alkyne containing linker to staple exendin-4 for imaging and protease stability characterization. We present directed evolution results with this linker in Chapter III of this thesis. The molecule was synthesized as follows: N-Boc-2,2′-(ethylenedioxy)diethylamine (805 µmol) was added to diisopropylethylamine (2.40 mmol) in 3.8 mL MeCN. Propargyl bromide in toluene was added dropwise (2.62 mmol). The reaction mixture was stirred overnight at room temperature before being concentrated under reduced pressure and then subjected to flash chromatography (80:7:1 $CHCl_3$: MeOH: NH_4OH). The desired fraction was concentrated, deprotected using 50% trifluoroacetic acid in dichloromethane, and purified using preparative RP-HPLC using a linear gradient of MeCN in H2O to yield 1 (475 µmol, 59%).1H NMR (400 MHz, CD3OD) δ 3.89 (4H, d), 3.77 (2H, t), 3.73 (2H, t), 3.70 (4H, s), 3.18 (2H, t), 3.15 (2H, t), 3.04 (2H, t). 13C NMR (400 MHz, CD_3OD) δ 76.8, 74.6, 69.9, 69.8, 66.5, 51.9, 42.2, 39.2. HRMS: m/z calculated for $C_{12}H_{20}N_2O_2$: 225.1603, found: 225.1600.

Appendix II: Alanine Scanning Mutagenesis of p53-Like Peptide

Prior to directed evolution experiments to discover potent inhibitors of MDM2 (Chapter II), we individually mutated each residue of a native p53-like sequence (ETFXDLWRLLXEN) to alanine using the primers in table A1, the template pQE80L-eCPX2-PLP from Navaratna et al.[1]. The protocol for point mutagenesis was adapted from ref. 2 and transformed into met auxotrophic TYJV2 E. coli for expression.

In this alanine scanning approach, we kept the stabilization sites fixed, and measured binding affinity in the context of bacterial surface display to evaluate the feasibility of the method and to inform the selection of residues to randomize for screening studies. Representative binding isotherms are shown in Figure A1.

Table A - 1. List of primers used in this alanine scanning study of a p53-like peptide.

Mutation	Sequence
E17A	TCCGTAGCTGGCCAGTCTGGCCAGGCAACCTTTATGGATCTGTGGCGCCTGC
T18A	GTAGCTGGCCAGTCTGGCCAGGAAGCCTTTATGGATCTGTGGCGCCTGCTGATG
F19A	GCTGGCCAGTCTGGCCAGGAAACCGCTATGGATCTGTGGCGCCTGCTGAT
D21A	GGCCAGTCTGGCCAGGAAACCTTTATGGCTCTGTGGCGCCTGCTGATGGAAAAC
L22A	GGCCAGTCTGGCCAGGAAACCTTTATGGATGCGTGGCGCCTGCTGATGGAAAAC
W23A	GCCAGTCTGGCCAGGAAACCTTTATGGATCTGGCGCGCCTGCTGATGGAAAACGGCGGT

R24A	AGTCTGGCCAGGAAACCTTTATGGATCTGTGGGCCCTGCTGATGGAAAACGGCGGTGGCA
L25A	GGCCAGGAAACCTTTATGGATCTGTGGCGCGCGCTGATGGAAAACGGCGGTGGCA
L26A	CAGGAAACCTTTATGGATCTGTGGCGCCTGGCGATGGAAAACGGCGGTGGCAGCGGA
E28A	ACCTTTATGGATCTGTGGCGCCTGCTGATGGCAAACGGCGGTGGCAGCGGAGGGCAGT
N29A	GGATCTGTGGCGCCTGCTGATGGAAGCCGGCGGTGGCAGCGGAGGGCAGTCT

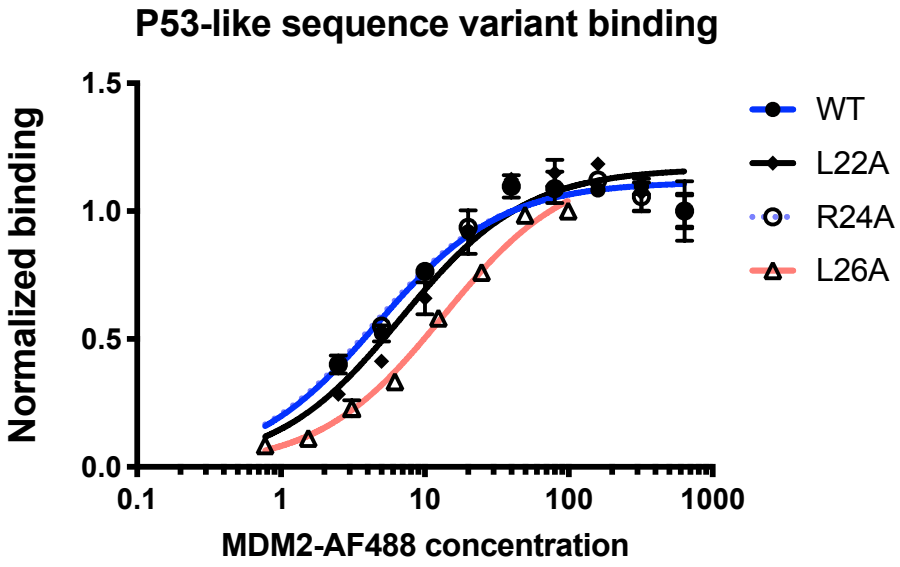

Figure A1. Several binding isotherms for p53-like sequence (WT) and single-aa alanine substituted mutants.
Of measurable alanine substituted constructs (F19A and W23A had no detectable signal), L26A had the lowest affinity, consistent with the binding structure and computational alanine scanning results.

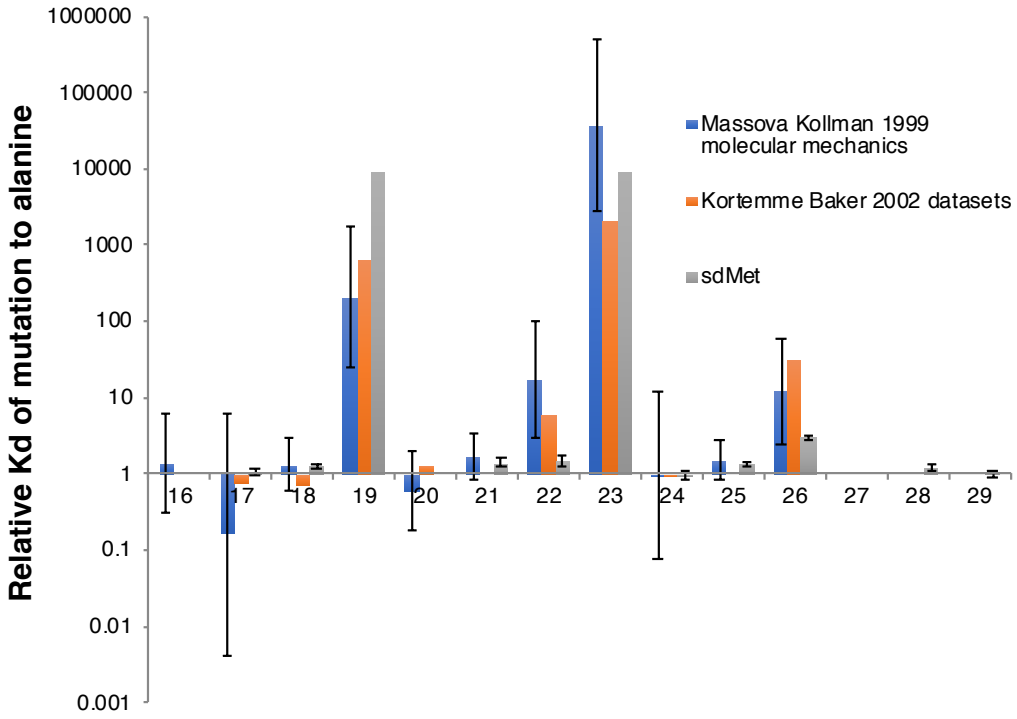

Figure A2. Comparison of experimental and computational alanine scans.
Bacterial surface alanine scanning (sdMet) was compared with molecular mechanics approaches[3] and statistical approaches[4] as validation for surface display of p53-like peptides. We were unable to measure binding signal for F19A and W23 mutants and thus report >10000 relative K_d for these constructs.

Appendix III: Sorting Campaigns Against Other Targets

We have also attempted to engineer potent stapled peptide binders to several other targets including the intracellular KRAS and NOTCH1 proteins and the extracellular portion of CD8. Recombinant expression of all three proteins was successful, but initial screens did not show convincing evidence of binding to KRAS and NOTCH1 for sequences reported in the literature. A very recent report by Ng and coworkers found that the reported all-hydrocarbon stapled SOS1-based sequence[5] did not exhibit KRAS-specific binding[6], consistent with our findings. As there were no reported peptide binders to CD8 at the beginning of the project, we constructed a naïve library and conducted several rounds of MACS and FACS to attempt to discovery consensus binding sequences. Because of anticipated weak affinity from a naïve library, a CD8 tetramer target was generated to boost avidity. Unfortunately, we did not observe significant binding to fluorescent CD8 and to tetramerized CD8 in our sorted populations.

KRAS

We based our double-click peptide sequence on the hydrocarbon stapled peptide mimic of SOS1 with sequence FFGIMLTNILKMEEGN[5] and cloned it into eCPX using the forward primer SOS1pep and reverse primer pQE80L rev. An HA sequence C-terminal of SOS1pep was inserted using SOS1pep-HA fwd and SOS1pep-HA rev for display

characterization. Soluble KRAS2B was produced as a GST fusion from Addgene plasmid #55655 (a gift from Julian Downward), Figure A4. Displayed SOS1pep showed significantly decreased display compared with p53-like peptide (Figure A5), but still was detectable above background. We did not detect KRAS-GST binding to SOS1pep (Figure A3) even with the addition of nucleotide triphosphates which can modulate the KRAS-SOS1 interaction[5]

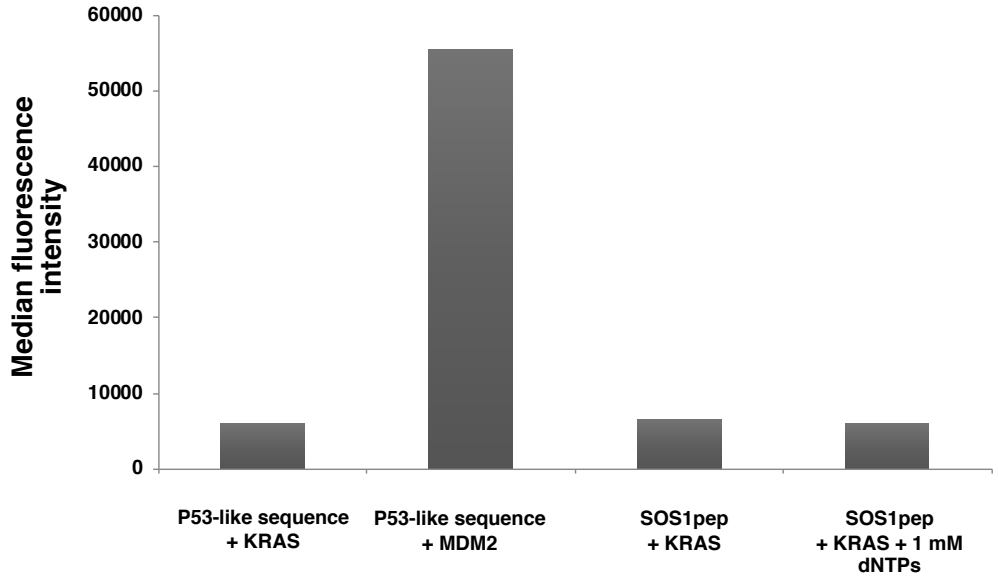

Figure A3. Flow cytometric analysis of peptide binding against various targets. P53-like sequence does not exhibit any binding to KRAS, as expected, but was included as positive control for binding to MDM2. SOS1pep does not exhibit binding to KRAS with and without the presence of 1 mM dNTPs at the concentrations tested (400 nM KRAS2B-GST).

NOTCH1

We based our double click peptide sequence on the hydrocarbon stapled peptide mimic of MAML with sequence ERLRRRIMLCRRHHMT[7] and cloned it into eCPX using the forward primer MAMLpep and reverse primer pQE80L rev. An HA sequence was inserted

C-terminal of MAMLpep using a similar SOE PCR strategy as for SOS1pep. Soluble GST-N1IC was produced from Addgene plasmid #47612 (a gift from Urban Lendahl), Figure A4. MAMLpep did not display to significant levels over background and non-induced controls (Figure A5), and we hypothesize that is due to the highly charged (5 arginine residues) nature of the peptide. It has been observed that the display of highly charged sequences is suppressed in bacterial outer membrane systems[8].

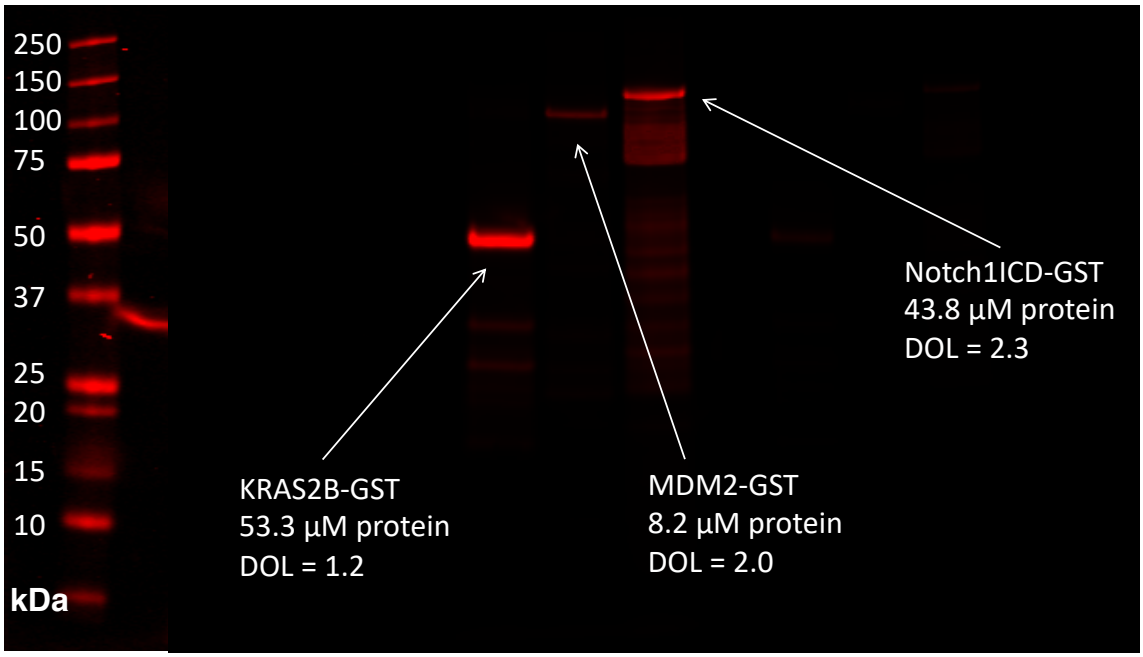

Figure A4. Reducing, denaturing SDS-PAGE gel of purified KRAS2B-GST, MDM2-GST, and Notch1ICD-GST.
All three have been labeled with AlexaFluor647 using nonspecific lysine chemistry. The gel was visualized on a Licor Odyssey NIR scanner.

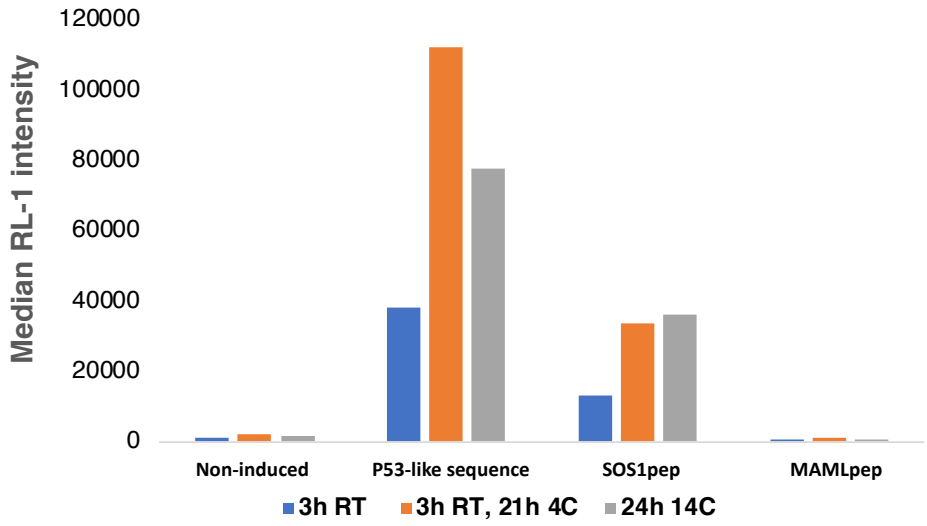

Figure A5. Detection of HA tag C-terminal of several peptides by flow cytometry. This revealed undetectable display for MAMLpep and diminished display of SOS1pep relative to the p53-like sequence for various induction times.

CD8

We expressed CD8a using procedures adapted from ref. 9 with the expression plasmid as a gift from K. Natarajan. The homodimer was purified in moderate yield from inclusion bodies after refolding (Figure A6).

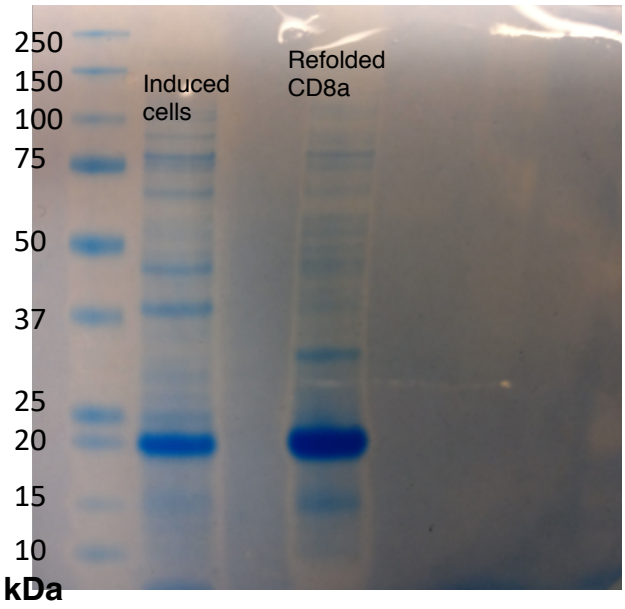

Figure A6. Reducing, denaturing SDS-PAGE gel of cells and purified recombinant CD8a.

A naïve 15-mer peptide library was generated using the naïve library fwd primer and pQE80L rev for screening to CD8 with two i,i+7 methionine sites fixed for click stabilization at sites 5 and 12. A library size of 2 x 10^9 members was generated according to the procedure described by Getz and Daugherty[10], but sequencing revealed that approximately 30% of these were non-peptide expressing eCPX plasmid background. Since we expected little interaction between eCPX and CD8, we were able to monitor fraction of non-peptide expressing clones to gauge sorting efficiency and success.

After 4 serial rounds of MACS with biotinylated CD8a and 1 round of FACS with AF647-labelled CD8a, we saw no change in the abundance of non-peptide expression clones and concluded that a larger search space needs to be accessed to find binders. Alternative approaches could include CD8 multimerization to increase the avidity of

surface-displayed peptide-CD8a interactions to pull out initially weak binders. This would be followed by affinity maturation through re-randomization and further screening.

Table A - 2. Primers used to display putative KRAS and NOTCH complex binding peptides and variants.

SOS1pep	ACTTCCGTAGCTGGCCAGTCTGGCCAGTTTTTCGGCATTATGCTGACCAACATCCTGAAAATGGAAGAAGGTAATGGCGGTGGCAGCGGAGGGCAGTCTGGGCAGTCTG
MAMLpep	ACTTCCGTAGCTGGCCAGTCTGGCCAGGAACGCCTGCGCCGCCGCATTATGCTGTGCCGCCGCCATCATATGACCGGAGGGCAGTCTGGGCAGTCTGGTGACTACAACAAAAACCAG
pQE80L rev	GAGGTCATTACTGGATCTATCAACAGGAGTCCAAGCTCAGC
SOS1pep-HA fwd	TATCCGTACGATGTGCCGGATTATGCGGGAGGGCAGTCTGGGCAGTCT
SOS1pep-HA rev	CGCATAATCCGGCACATCATACGGATAGCTGCCACCGCCATTACCTTCTTCCATTTTCAG
Naïve library fwd	ACTTCCGTAGCTGGCCAGTCTGGCCAG NNCNNCNNCNNCATGNNCNNCNNCNNCNNCNNCATGNNCNNCNNCGGCGGTGGCAGCGGAGGGCAGTCTGGGCAGTCTG

Appendix IV: Double-Click Stapled Two-Helix Bundles for Imaging Her2

The discovery of new cancer targets and a more detailed understanding of their contributions to cancer increases each year, but challenges remain in converting these scientific gains to clinically relevant therapeutic and imaging applications. Specifically, the HER2 gene has been implicated in many aggressive forms of breast cancer, as well as in some stomach and ovarian cancers. The overexpression of this gene results in promotion of proliferation and inhibition of apoptosis. As such, it has been an important target for drug discovery, and two monoclonal antibodies, trastuzumab and pertuzumab, have been developed for treatment of HER2-positive breast cancer. There is a clinical need to rapidly diagnose and monitor tumor response to treatment. Existing antibody-based HER2 binders take on the order of hours to days to target tumors and clear from healthy tissues, making them impractical as imaging agents[11]. Importantly, probe localization is independent of expression level, making these large molecules unsuitable for quantitatively imaging expression to determine the feasibility of treatment with a Her2 directed therapy. Orlova and colleagues developed a three-helix bundle containing ~7 kDa affibody that bound to Her2 with a 22 pM K_d and used it for radioimaging[12]. Because of ease of synthesis, handling, and potentially better pharmacokinetics, Webster and colleagues evolved a two-helix variant but were not able to recapitulate the high affinity of the three-helix affibody[13]. We have used bio-orthogonal chemistry to stabilize the secondary structure of a 35-amino acid sequence two-helix bundle. The method we have

developed allows facile attachment of a fluorophore or radiolabel for imaging applications. These molecules exhibit greater helicity than the original molecule, with concomitant increase in binding affinity to HER2 by three to four-fold.

Based on the crystal structure reported by Eigenbrot and colleagues of the three helix affibody bound to Her2 (Figure A7)[14], we rationally selected stabilization sites to avoid locations that would (1) remove intramolecular hydrogen bonding, (2) remove binding interactions with Her2, (3) remove hydrophilicity (to ensure solubility), or (4) introduce potential steric clashes especially upon stabilization with a bulky fluorophore. Thus, we selected sites 3-10 and 21-28 on helices 1 and 2 respectively to introduce azidohomoalanine residues to permit click stabilization (Figure A7).

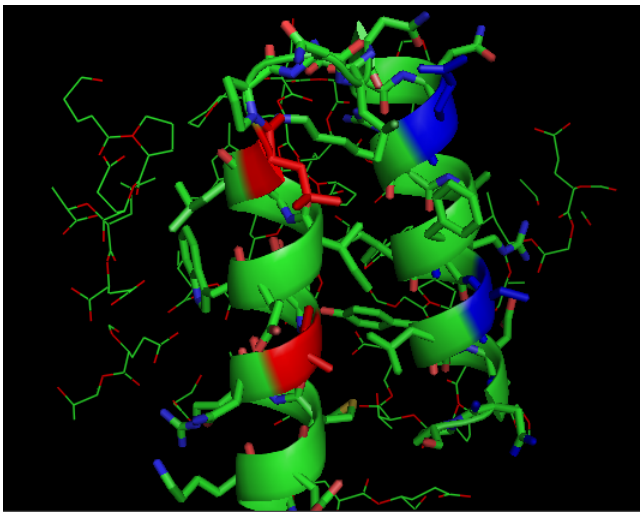

Figure A7. Crystal structure of the three-helix bundle bound to Her2 (PDB ID 3MZW).
The third helix, which is on the viewer's side of the structure, was removed for visual clarity. Residues E3 and E10 on the first helix are shown in red and Q21 and S28 on the second helix are shown in blue.

We obtained helix 1 (H1), helix 2 (H2), and single AHA (S1) variants of ZHer2 from Innopep (San Diego, CA).

Table A - 3. Sequences of 2-helix bundles tested.
Z = homocysteine, X = azidohomoalanine. The termini are disulfide bonded together.

Name	Amino acid sequence
Helix 1 (H1)	ZNK**X**MRNRYW**X**AALDPNLNNQQKRAKIRSIYDDPZ
Helix 2 (H2)	ZNK**X**MRNRYWEAALDPNLNNQQKRAKIRSIYDDPZ
Single AHA (S1)	ZNKEMRNRYWEAALDPNLNNQ**X**KRAKIR**X**IYDDPZ

Imaging extracellular receptors with near-infrared (NIR) dyes allows for deeper imaging than shorter wavelength fluorophores and offers advantages over other imaging techniques as well, including its non-ionizing nature, good contrast, and low cost[15]. Choice of dye matters: dyes with different physicochemical properties can affect clearance, cell residualization, and binding affinity[16,17]. We synthesized a panel of dye and helix variants (sequences in Table A - 1, dye structures in Figure A8) and characterized the affinity and helicity of select few variants. Products were purified by HPLC in high purity (representative MALDI spectra shown in Figure A9).

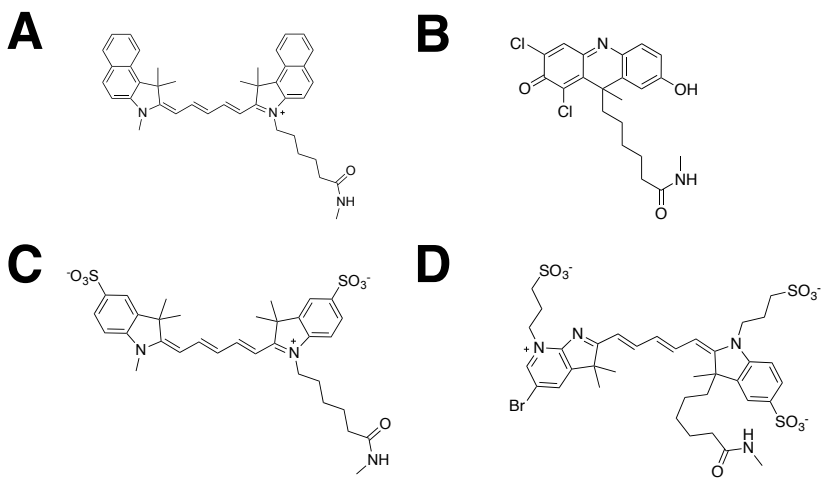

Figure A8. Chemical structures of four near-infrared (NIR) dyes used in this study. (A) Cyanine5.5 (Cy5.5), (B) DDAO (C) SulfoCyanine5 (SCy5) (D) AlexaFluor680 (AF680)

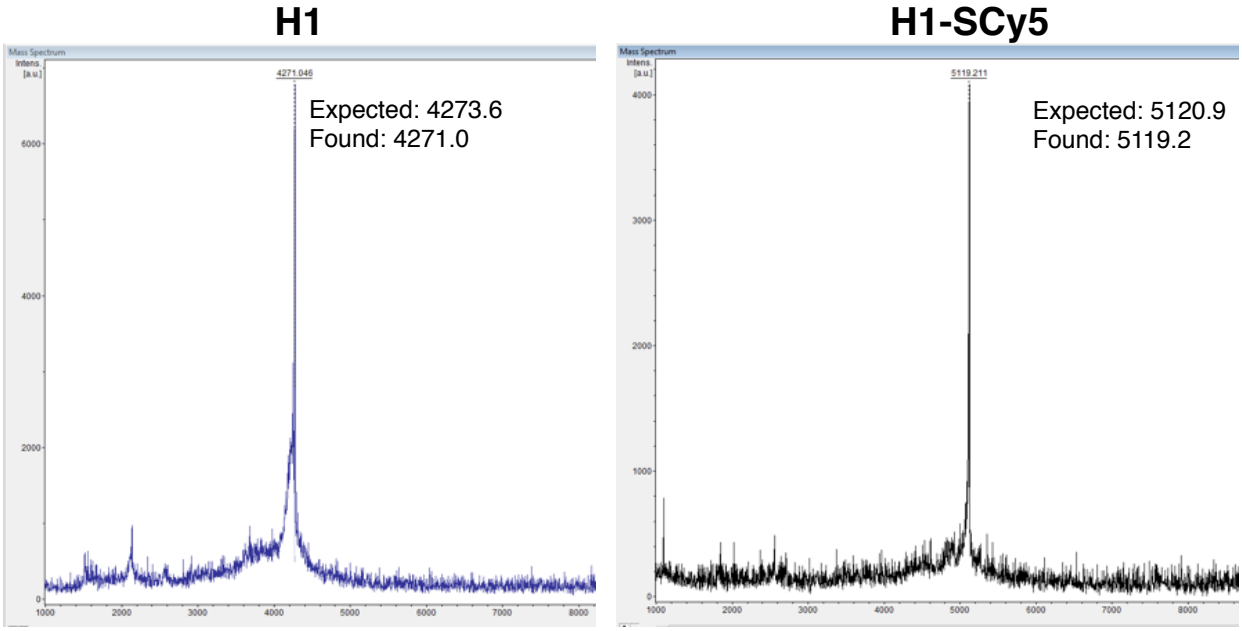

Figure A9. Reflectron positive MALDI spectra for H1 and H1-SCy5.

We first tested alpha helical character for non-stabilized and SCy5-stabilized versions of H1, given that pre-organization and increased helicity decreases the entropic cost of

binding and therefore can increase binding affinity[18–20]. SCy5-H1 was made by adapting the procedure developed by Zhang et al.[19] by first conjugating amine-reactive NHS ester dye to the functionalizable linker and then click-stabilizing the two-helix bundle in solution. We observed a modest increase in helicity from 22% to 38% (Figure A10).

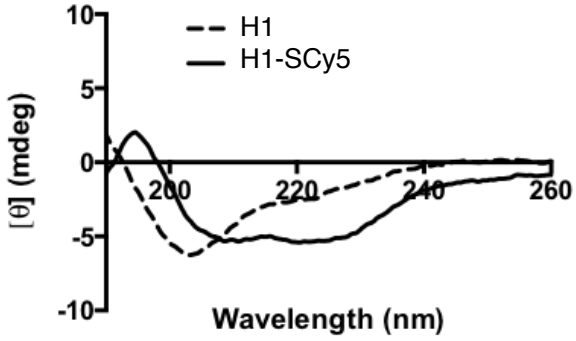

Figure A10. Circular dichroism spectrograms of H1 and H1 stabilized with SCy5. We observed improved alpha helicity values for the stabilized bundle (22% vs 38% helical), determined from molar ellipticity at 222 nm values.

To see if increased preorganization by stabilization translated to affinity improvements, we titrated H1-SCy5 against the Her2 overexpressing human gastric cancer NCI-N87 cell line (ATCC) and indeed observed increase in affinity from 12 nM to 2.8 nM. We also tested H2-SCy5 but there was no significant improvement in affinity (10 nM). Binding isotherms are shown in figure A11.

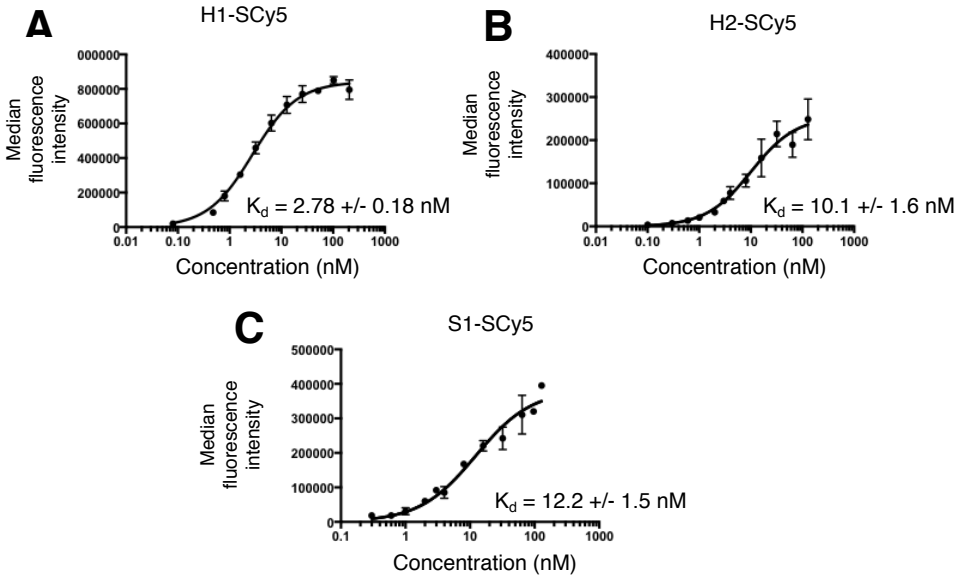

Figure A11. Titrations of fluorescent probes against Her2 on NCI-N87 cells.
(A) H1-Scy5 (B) H2-SCy5, and (C) non-stabilized S1-SCy5.

We tested the impact of dye physicochemical properties on Her2 binding using the four dyes Cy5.5, DDAO, SCy5, and AF680 (Figure A12). Cy5.5 is a bulky, hydrophobic dye with a +2 net charge, DDAO is relatively small and neutral, while SCy5 and AF680 share structural characteristics including size and negative charge. We synthesized helix 1 stabilized variants with all four dyes and observed significantly worse binding for Cy5.5 than the other 3 (K_d = 39 nM for Cy5.5, 2.1 nM for DDAO, 7.6 nM for AF680 (figure A12), and 2.8 nM for SCy5 (figure A11)).

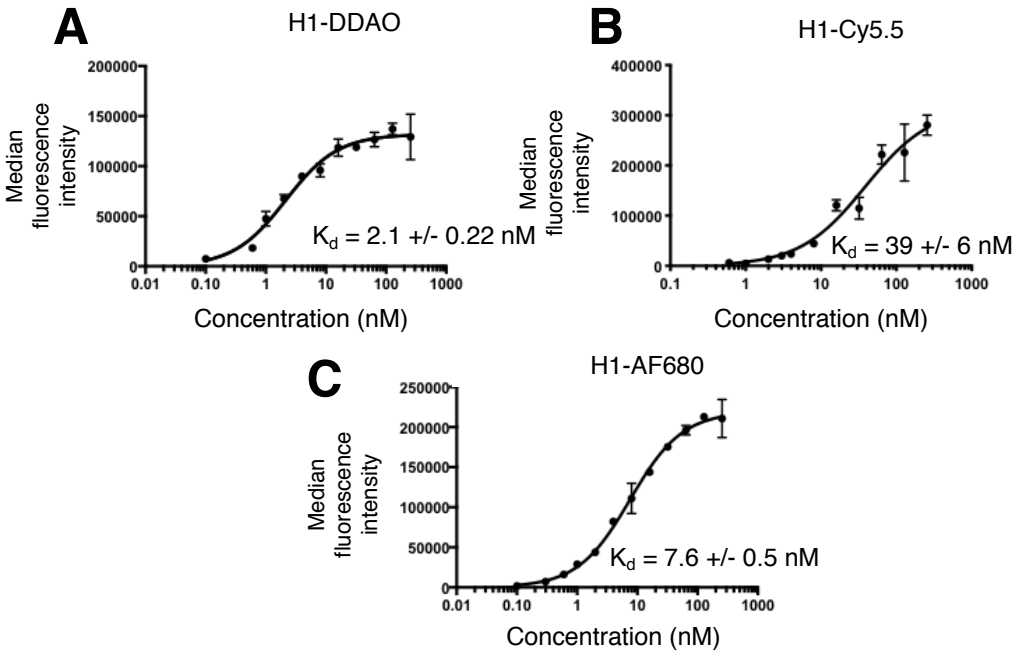

Figure A12. Titrations of NIR fluorophore-H1 stabilized bundles against Her2 expressed on NCI-N87 cells.
DDAO-conjugated bundles (A) were observed to have the lowest K_d, whereas Cy5.5 (B) showed relatively poor binding.

Finally, based on literature reports of protein functionalization through cysteine bridging via maleimide chemistry[21], we reacted and generated maleimide-bridged H1 (H1-mal) and double-click stabilized this to generate H1-mal-SCy5. Direct labeling of NCI-N87 cells with H1-mal-SCy5 revealed a much-reduced affinity of 67 nM (Figure A13, left) and to verify that this loss of binding was not a result of the click stabilization, we conducted a competition binding assay with known binder S1-SCy5 (K_d = 12.2 nM) to determine an further reduced affinity (K_d value of 93 nM, Figure A13, right). Stabilization, for maleimide-bridged two-helix bundles, appears to restore some affinity, but not close to the affinity of the original disulfide-bridged proteins.

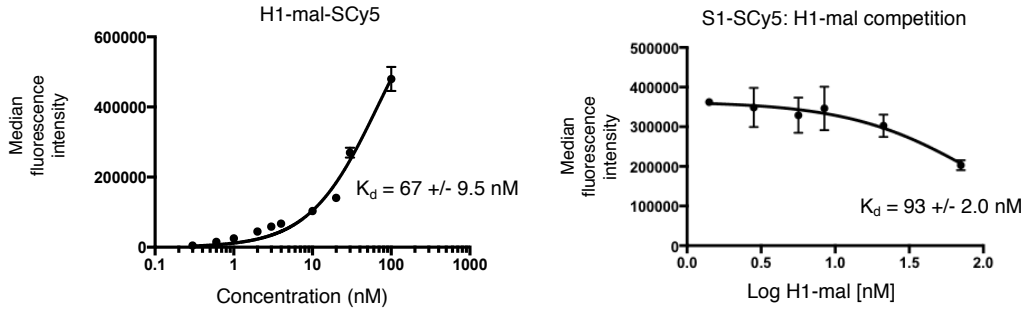

Figure A13. Titration experiments for maleimide-bridged H1.
Affinities were calculated with (direct binding, left) and without (competition, right) click stabilization.

Conclusions and future directions: This work combined rationally designing stabilization sites with peptide modification strategies to engineer high affinity imaging agents of Her2. It is apparent from these data that dye and stabilization location have outsized impacts of binding affinity, with DDAO and SCy5 providing the tightest binding, and helix 1 proving to the better location for stabilization. Future work will involve expanding this approach to other dye/linker combinations to generate even higher affinity binders, and in vivo imaging of Her2 expressing tumors to determine if Her2 downregulation in cancer resistance development can be imaged and to gauge chemotherapy response over time.

References

(1) Navaratna, T.; Atangcho, L.; Mahajan, M.; Subramanian, V.; Case, M.; Min, A.; Tresnak, D.; Thurber, G. M. Directed Evolution Using Stabilized Bacterial Peptide Display. J. Am. Chem. Soc. **2020**. https://doi.org/10.1021/jacs.9b10716.

(2) Liu, H.; Naismith, J. H. An Efficient One-Step Site-Directed Deletion, Insertion, Single and Multiple-Site Plasmid Mutagenesis Protocol. BMC Biotechnol. **2008**, 8 (1), 91. https://doi.org/10.1186/1472-6750-8-91.

(3) Massova, I.; Kollman, P. A. Computational Alanine Scanning to Probe Protein-Protein Interactions: A Novel Approach to Evaluate Binding Free Energies. J. Am. Chem. Soc. **1999**. https://doi.org/10.1021/ja990935j.

(4) Kortemme, T.; Baker, D. A Simple Physical Model for Binding Energy Hot Spots in Protein-Protein Complexes. Proc. Natl. Acad. Sci. U. S. A. **2002**. https://doi.org/10.1073/pnas.202485799.

(5) Leshchiner, E. S.; Parkhitko, A.; Bird, G. H.; Luccarelli, J.; Bellairs, J. A.; Escudero, S.; Opoku-Nsiah, K.; Godes, M.; Perrimon, N.; Walensky, L. D. Direct Inhibition of Oncogenic KRAS by Hydrocarbon-Stapled SOS1 Helices. Proc. Natl. Acad. Sci. **2015**, 112 (6), 1761–1766. https://doi.org/10.1073/pnas.1413185112.

(6) Ng, S.; Juang, Y.-C.; Chandramohan, A.; Kaan, H. Y. K.; Sadruddin, A.; Yuen, T. Y.; Ferrer-Gago, F. J.; Lee, X. C.; Liew, X.; Johannes, C. W.; et al. De-Risking Drug Discovery of Intracellular Targeting Peptides: Screening Strategies to Eliminate False-Positive Hits. ACS Med. Chem. Lett. **2020**. https://doi.org/10.1021/acsmedchemlett.0c00022.

(7) Moellering, R. E.; Cornejo, M.; Davis, T. N.; Bianco, C. Del; Aster, J. C.; Blacklow, S. C.; Kung, A. L.; Gilliland, D. G.; Verdine, G. L.; Bradner, J. E. Direct Inhibition of the NOTCH Transcription Factor Complex. Nature **2009**, 462 (7270), 182–188. https://doi.org/10.1038/nature08543.

(8) Verhoeven, G. S.; Alexeeva, S.; Dogterom, M.; den Blaauwen, T. Differential Bacterial Surface Display of Peptides by the Transmembrane Domain of OmpA. PLoS One **2009**. https://doi.org/10.1371/journal.pone.0006739.

(9) Wang, R.; Natarajan, K.; Margulies, D. H. Structural Basis of the CD8αβ/MHC Class I Interaction: Focused Recognition Orients CD8β to a T Cell Proximal Position. J. Immunol. **2009**. https://doi.org/10.4049/jimmunol.0901276.

(10) Getz, J. A.; Schoep, T. D.; Daugherty, P. S. Peptide Discovery Using Bacterial Display and Flow Cytometry. Methods Enzymol. **2012**, 503, 75–97. https://doi.org/10.1016/B978-0-12-396962-0.00004-5.

(11) Thurber, G. M.; Schmidt, M. M.; Wittrup, K. D. Antibody Tumor Penetration: Transport Opposed by Systemic and Antigen-Mediated Clearance. Advanced Drug Delivery Reviews. 2008. https://doi.org/10.1016/j.addr.2008.04.012.

(12) Orlova, A.; Magnusson, M.; Eriksson, T. L. J.; Nilsson, M.; Larsson, B.; Höiden-Guthenberg, I.; Widström, C.; Carlsson, J.; Tolmachev, V.; Ståhl, S.; et al. Tumor Imaging Using a Picomolar Affinity HER2 Binding Affibody Molecule. Cancer Res. **2006**, 66 (8), 4339–4348. https://doi.org/10.1158/0008-5472.CAN-05-3521.

(13) Webster, J. M.; Zhang, R.; Gambhir, S. S.; Cheng, Z.; Syud, F. a. Engineered Two-

Helix Small Proteins for Molecular Recognition. ChemBioChem **2009**, 10 (8), 1293–1296. https://doi.org/10.1002/cbic.200900062.

(14) Eigenbrot, C.; Ultsch, M.; Dubnovitsky, A.; Abrahmsén, L.; Härd, T. Structural Basis for High-Affinity HER2 Receptor Binding by an Engineered Protein. Proc. Natl. Acad. Sci. U. S. A. **2010**, 107 (34), 15039–15044. https://doi.org/10.1073/pnas.1005025107.

(15) Bhatnagar, S.; Verma, K. D.; Hu, Y.; Khera, E.; Priluck, A.; Smith, D. E.; Thurber, G. M. Oral Administration and Detection of a Near-Infrared Molecular Imaging Agent in an Orthotopic Mouse Model for Breast Cancer Screening. Mol. Pharm. **2018**. https://doi.org/10.1021/acs.molpharmaceut.7b00994.

(16) Zhang, L.; Bhatnagar, S.; Deschenes, E.; Thurber, G. M. Mechanistic and Quantitative Insight into Cell Surface Targeted Molecular Imaging Agent Design. Sci. Rep. **2016**. https://doi.org/10.1038/srep25424.

(17) Cilliers, C.; Liao, J.; Atangcho, L.; Thurber, G. M. Residualization Rates of Near-Infrared Dyes for the Rational Design of Molecular Imaging Agents. Mol. Imaging Biol. **2015**. https://doi.org/10.1007/s11307-015-0851-7.

(18) Sia, S. K.; Carr, P. a; Cochran, A. G.; Malashkevich, V. N.; Kim, P. S. Short Constrained Peptides That Inhibit HIV-1 Entry. Proc. Natl. Acad. Sci. **2002**, 99 (23), 14664–14669. https://doi.org/10.1073/pnas.232566599.

(19) Zhang, L.; Navaratna, T.; Liao, J.; Thurber, G. M. Dual-Purpose Linker for Alpha Helix Stabilization and Imaging Agent Conjugation to Glucagon-like Peptide-1 Receptor Ligands. Bioconjug. Chem. **2015**, 26 (2), 329–337. https://doi.org/10.1021/bc500584t.

(20) Bird, G. H.; Gavathiotis, E.; Labelle, J. L.; Katz, S. G.; Walensky, L. D. Distinct BimBH3 (BimSAHB) Stapled Peptides for Structural and Cellular Studies. ACS Chem. Biol. **2014**, 9 (3), 831–837. https://doi.org/10.1021/cb4003305.

(21) Smith, M. E. B.; Schumacher, F. F.; Ryan, C. P.; Tedaldi, L. M.; Papaioannou, D.; Waksman, G.; Caddick, S.; Baker, J. R. Protein Modification, Bioconjugation, and Disulfide Bridging Using Bromomaleimides. J. Am. Chem. Soc. **2010**, 132 (6), 1960–1965. https://doi.org/10.1021/ja908610s.